Molecular Dynamics Simulations of Polymers and Micelles at Interfaces

Dissertation

zur Erlangung des akademischen Grades

doctor rerum naturalium

(Dr. rer. nat.)

im Fach Physik

eingereicht an der

Mathematisch-Naturwissenschaftlichen Fakultät I

der Humboldt-Universität zu Berlin

von

(Diplom-Physiker) Nikolai Severin

geb. 4.1.1971 in Moskau

Präsident der Humboldt-Universität zu Berlin

Prof. Dr. Dr. h.c. H.Meyer

Dekan der Mathematisch-Naturwissenschaftlichen Fakultät I

Prof. Dr. J.P.Rabe

Gutachter/innen
1. Prof. Dr. J.P. Rabe
2. Prof. Dr. E.W. Knapp
3. Prof. Dr. L. Schimansky-Geier

Tag der mündlichen Prüfung: 8.7.99

Abstract

Molecular Dynamic (MD) simulation of two different systems was performed: 1) Polyethylene- isotactic Polypropylene (PE-iPP) interfaces and 2) cylindrical micelles formed by tetradecyl trimethylammonium bromide (C_{14}TAB) molecules in aqueous solution and at solid liquid interfaces.

The general difficulties of simulation of polymer crystalline interfaces were discussed and one method was proposed for such simulations. Thise method was used to simulate epitaxial crystallisation of PE on iPP. The experimental results on epitaxial crystallisation were confirmed by MD simulation and in addition epitaxial crystallisation of PE on iPP surface with high dencity of methyl groups was predicted. MD simulation also predicted that PE should change at the interfacial region from the orthorhombic to monoclinic crystalline structure.

Several nanoseconds of life of cylindrical micelles were simulated. The simulation results for the micelle in aqueous solution were favourably compared with experimental results. In contradiction to the standard picture of an ionic micelle the simulated micelle formed hole in its centre and the density of the hydrophobic micelle core was inhomogeneous. This effect partially was explained by the inhomogeneous distribution of the terminal methyl groups in the micelle core. Cylindrical and half cylindrical micelles of C_{14}TAB molecules were simulated at the paraffin- and gold-aqueous interfaces.

Keywords: molecular dynamic simulation, polymer interfaces, micelles.

Abstrakt

Molekulardynamik (MD) Simulationen wurden an zwei verschiedenen Systemen durchgeführt: 1. Grenzfläche zwischen Polyethylen und isotaktischem Polypropylen (PE-iPP) und 2. Zylindrische Mizellen, bestehend aus Tetradecyltrimethylammoniumbromid (C_{14}TAB), in wässriger Lösung und an Fest-Flüssig-Grenzflächen.

Die allgemeinen Schwierigkeiten bei der Simulation von Grenzflächen kristalliner Polymere wurden diskutiert und eine Methode für solche Simulationen vorgeschlagen. Diese Methode wurde zur epitaxialen Kristallisation von PE auf iPP benutzt. Experimentelle Ergebnisse der epitaxialen Kristallisation konnten durch die Simulation bestätigt werden. Ferner konnte vorhergesagt werden, dass PE bevorzugt auf einer iPP-Oberfläche mit hoher Methylgruppenkonzentration kristallisiert. Ebenso wurde durch die MD Simulation vorhergesagt, dass PE in der Grenzflächenregion von einer orthorhombischen zur monoklinischen Kristallstruktur wechselt.

Die Simulationsdauer für die Mizellen betrug einige Nanosekunden. Die Ergebnisse für die Mizellen in wässriger Lösung stehen hierbei in guter Übereinstimmung mit experimentellen Werten. Im Widerspruch zur allgemein üblichen Vorstellung führte die Simulation der Mizellen zur Ausbildung eines Hohlraums in ihrer Mitte sowie zu einer inhomogenen Dichte des hydrophoben Mizellkerns. Dies wurde zum Teil der inhomogenen Verteilung der terminalen Methylgruppen im Mizellkern zugeschrieben. Zylindrische und halbzylindrische Mizellen wurden an den Paraffin/Wasser- und Gold/Wasser-Grenzflächen simuliert.

Schlagworte: Molekulardynamik Simulation, Polymer Grenzfläche, Mizellen.

Molecular Dynamics Simulations of polymers and micelles at interfaces

Table of contents:

1. General introduction

The aim of this work is the atomistic molecular dynamics (MD) simulation of (1) polyethylene - isotactic polypropylene interfaces and (2) cylindrical and half-cylindrical micelles of amphiphilic molecules at solid-liquid interfaces.

Molecular dynamics solves the classical equations of motions for a system of N particles interacting according to a potential energy field. In general the particles may represent different physical objects like satellites in the gravitation field of earth or atoms of a molecular system. The most important capability of MD is that during the dynamics simulation a system undergoes conformational and momentum changes so that different parts of the phase space accessible to the simulated molecular system can be explored. By providing mechanisms for controlling the temperature and pressure of the simulated systems, molecular dynamics also allows to generate statistical ensembles from which various energetic, thermodynamic, structural and dynamic properties can be calculated.

The drawback of MD simulation is the limitation in the time span which can be simulated and on the system size i.e. the number of particles and interactions involved in the calculation. The fast progress in the development of computers allows to simulate larger systems with a more detailed description of inter-particle interactions. However for the detailed description of atomic interactions the number of atoms included in a simulation is still restricted to several tens of thousands. Simulated times of atomistic molecular systems are limited by several nanoseconds, which is related to the fast vibrations of chemical bonds. These are very severe restrictions, on the other hand many molecular systems of particular interest can be simulated. For example it is possible to simulate the dynamics behaviour of small bio-molecules, which is important to understand processes in the cell. A proper simulation of the environment of a molecular system allows to increase greatly the range of applications for MD simulations.

It is possible to simplify molecular system in order to increase the time span of MD simulation. The simplifications may range from simple unification of group of atoms to more general simplifications. For example the methyl group is replaced by single particle with potentials and dipole moment that should represent the methyl group. This simplification allows to increase the number of particles involved in the simulation and increase a little bit the simulation time step. But the information about the coordinates of all atoms is important for the short range interactions. The example of more general simplification is representation of a polymer molecule as a flexible rubber rod, without detailed consideration of atomic structure. This simplification allows to increase greatly the time span of MD simulation, it allows even to simulate some

long time processes like adsorption of molecules on a solid-liquid interface or process of micro/macro phase separation.

In addition to MD method there are several other computer simulation methods that allow simulation of molecular systems. In the Brownian Dynamic (BD) method the solvent for example is represented as a random forces on atoms. It is also important to mention the Monte Carlo (MC) simulation method. In general it was developed to predict equilibrium distribution of a system. It has several advantages and disadvantages. In many cases MC method samples conformational space faster than MD method but in general it is not designed to provide dynamic information on the system.

The restriction to several nanoseconds of the simulated time renders atomistic MD simulations dependent on the starting configuration of a system. Hence, atomistic MD simulations are bounded to experimentally established structures. On the other hand many experiments provide just a general picture of the molecular conformation and do not provide atomic coordinates and in its turn MD simulation may provide information on the atomic coordinates of a molecular system. That is why MD simulations are a powerful means for the investigation of structure and short time dynamics of molecular systems in combination with experimental techniques.

2. **Molecular dynamics (MD) Simulation**

Molecular Dynamics (MD) simulations solve Newton's equation of motion for a system of *i* particles.

$$\vec{f}_i = m_i \vec{a}_i$$

where $\vec{f}_i$ is the force, acting on the *i*-th particle, m_i is the mass and $\vec{a}_i$ is the acceleration of the *i*-th particle. The force can be computed directly from the derivative of the potential energy *U*:

$$-\frac{dU}{d\vec{r}_i} = m_i \frac{d^2\vec{r}_i}{dt^2} \qquad \text{(Eq. 1)}$$

With the known expression for the potential energy, known masses and known initial positions in coordinate-momentum space it is possible to solve this equation, i.e. to find the trajectory of the system. Analytically only systems of 1 or 2 independent particles can be solved. The numerical solution of Newton's equation using an empirical fit to the potential energy surface is called molecular dynamics simulations.

A standard method of solving an ordinary differential equation such as Eq.1 numerically is the finite-difference method. The general idea is as follows. Given the initial coordinates and velocities and other dynamic information at time t, the positions and velocities at time $t = t + \Delta t$ are calculated. The time-step Δt depends on the integration method as well as the system itself.

The basic criteria for a good integrator are: it should be fast, it should require little computer memory, it should permit the use of a relatively long time step and it must conserve the total energy.

For the MD calculations two different integration algorithms were applied, which are described below.

Verlet leap frog integrator

The advantages of the Verlet algorithm is that it requires only one energy evaluation per time step, modest memory, and it also allows a relatively large time-step to be used. The Verlet leapfrog algorithm function as follows:

$$\vec{v}(t+1/2\Delta t) = \vec{v}(t-1/2\Delta t) + \Delta t\vec{a}(t)$$
$$\vec{r}(t+\Delta t) = \vec{r}(t) + \Delta t\vec{v}(t+1/2\Delta t)$$
$$\vec{a}(t+\Delta t) = \frac{\vec{f}(t+\Delta t)}{m}$$

Where $\vec{r}$ are coordinates, $\vec{v}$ is the velocity and $\vec{a}$ is an acceleration of an atom. The force $\vec{f}(t+\Delta t)$ is evaluated from $-dU/d\vec{r}$ at $\vec{r}(t+\Delta t)$.

The Verlet leapfrog method has one major disadvantage: positions and velocities calculated are displaced by half a time-step out of synchrony.

Verlet velocity integrator

The algorithm is as follows:

$$\vec{r}(t+\Delta t) = \vec{r}(t) + \Delta t\vec{v}(t) + \frac{\Delta t^2\vec{a}(t)}{2}$$
$$\vec{a}(t+\Delta t) = \frac{\vec{f}(t+\Delta t)}{m}$$
$$\vec{v}(t+\Delta t) = \vec{v}(t) + \frac{1}{2}\Delta t[\vec{a}(t) + \vec{a}(t+\Delta t)]$$

A key parameter in the integration algorithms is the integration time step Δt. In order to use computational time more efficiently, as large as possible time-step should be used. However, a too large time-step causes instability in the integration process.

The time-step used depends both on the system as well as on the integration algorithm. The main limitation to the time-step is a high frequency motion which should be taken into account. The vibrational period should be splitted into at least 8-10 segments to satisfy the Verlet integrator. In most molecular systems, the highest vibrational frequency is the one of C-H bond vibrations, whose period is on the order of 10^{-14} s. The integration time-step should therefor be about 1 fs, which was used during all simulations.

Forcefield

A forcefield is a set of potential energy functions of inter-atomic distances and of molecular internal coordinates, which represents the energy of molecules and of assemblies of molecules normally in the electronic ground state. From the knowledge of the force-field one can calculate all molecular properties which are determined by the energy of the system. The calculation of the potential energy, along with its first and second derivatives with respect to the atomic coordinates, yields the information necessary for minimisation, harmonic vibrational analysis and dynamics simulations.

The pcff force-field supplied with the InsightII package (MSI) was used in all MD simulations. The pcff force-field is adopted to use for the simulation of polymers. The exact form of the pcff force-field is presented below[18].

$$E_{pot} = \sum_b \left[K\left(b - b_0\right)^2 \right] + \sum_q H\left(q - q_0\right)^2$$

(1) (2)

$$+ \sum_j V\left[1 + \cos\left(j - j_1^0\right)\right] + \sum_c K_c c^2$$

(3) (4)

$$+ \sum_b \sum_{b'} F_{bb'}(b - b_0)(b' - b_0') + \sum_q \sum_{q'} F_{qq'}(q - q_0)(q' - q_0')$$

(5) (6)

$$+ \sum_b \sum_q F_{bq}(b - b_0)(q - q_0) + \sum_b \sum_j (b - b_0)\left[V_1 \cos j + V_2 \cos 2j + V_3 \cos 3j\right]$$

(7) (8)

$$+ \sum_{b'} \sum_j (b' - b'_0)\left[V_1 \cos j + V_2 \cos 2j + V_3 \cos 3j\right]$$

(9)

$$+ \sum_q \sum_j (q - q_0)\left[V_1 \cos j + V_2 \cos 2j + V_3 \cos 3j\right]$$

(10)

$$+ \sum_j \sum_q \sum_q K_{j\,qq'} \cos j\,(q - q_0)(q' - q'_0)$$

(11)

$$+\sum_{i>j}\frac{q_i q_j}{er_{ij}}+\sum_{i>j}\left[\frac{A_{ij}}{r_{ij}^{9}}-\frac{B_{ij}}{r_{ij}^{6}}\right]$$

Figure 1 presents graphic illustrations for the force-field terms.

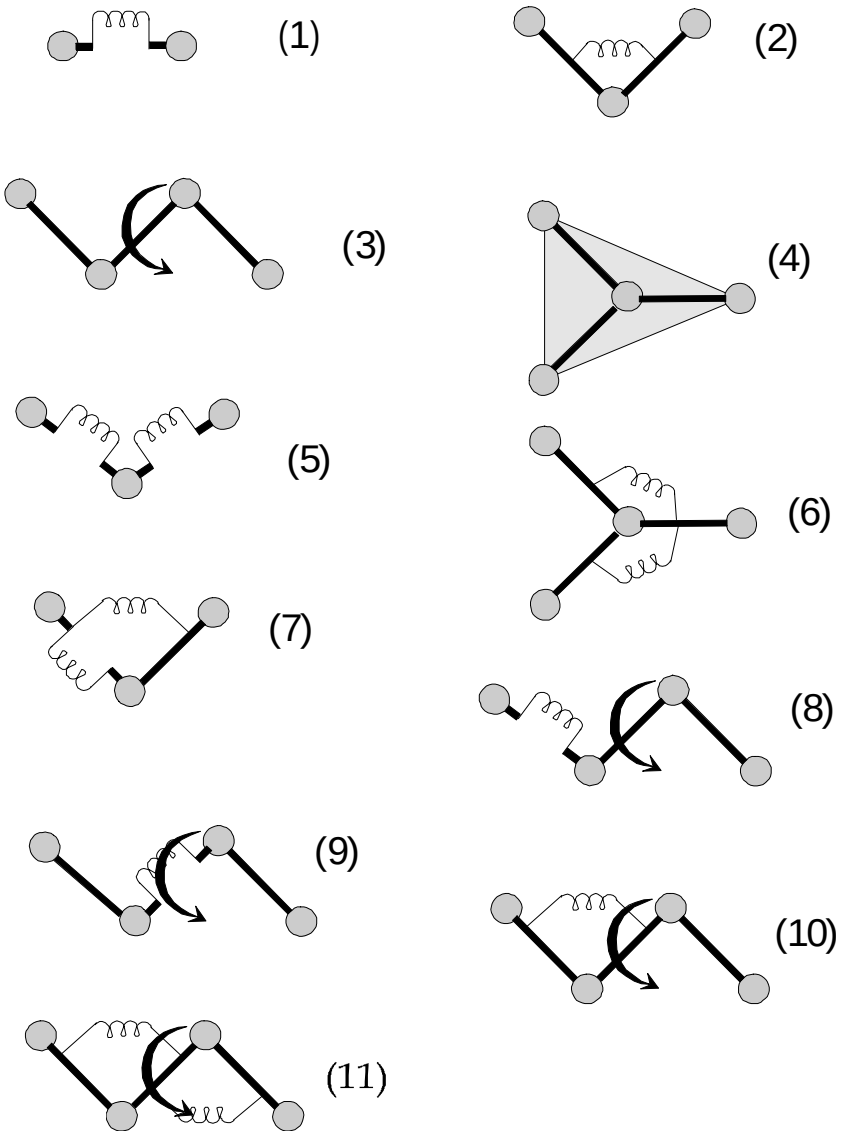

Figure 1. Graphic illustration of the pcff force-filed terms.

Periodic boundary conditions

The size of the systems treated by MD simulation is limited to several tens of thousand particles. This limitation is governed by the limitation of computer power. Thus if one particle represents one atom, the size of a simulated cell is limited to several nanomiters. A simulation carried out on a isolated system is a poor approximation of what would happen in a true bulk, because of the influence of boundaries. To remedy this, the cell is replicated in three

dimensions, thus the simulated cell should have translational periodicity. This is a much better representation of a bulk system, because the molecules near the surface now interact with molecules in adjacent cells. The image atoms are used to calculate energies and forces on the real atoms.

Cut-off

The periodic boundary conditions method allows to simulate a virtually infinite system which consist of a base cell and its images. The energies and forces on the imaged atoms are not calculated because their motions are computed as symmetry operations on the real atoms. It is now important to define long range interactions in the system. The simplest way is to allow molecules to interact with the molecule or molecular image closest to it. This method is called minimum image model. Each molecule interacts only with molecules and images within a distance of half the cell size. The disadvantage of this method is that computational time has a cubic dependence on the number of atoms in the system. Therefore it is common to introduce a non-bond cut-off, i.e. to neglect the non-bond interactions for pairs of atoms separated by distances greater than a cut-off value. The use of cut-off with a van der Waals interaction potential is quite reasonable, since the van der Waals potential is relatively short range and dies out as $1/r^6$. At r=8-10 Å the energies and forces are quite small compared to k_bT at room temperature. Thus, it is reasonable to set the cut off length to about 10 Å for van der Waals interactions. The Coulombic interactions on the other hand die off as 1/r, so at much longer distances Coulombic interactions are not negligible. However for most of cases polymeric systems are composed of neutral groups with electric dipoles or higher multipoles. The dipole-dipole interaction dies off as $1/r^3$. The interaction energy of two monopols of one elementary charge at r=1 nm is about 33 kcal mol^{-1}, while the interaction energy of two dipoles formed from elementary monopols at the distance r=1 nm is 0.3 kcal mol^{-1}. It is clear that cutting off monopole-monopole interaction at r=1 nm would be misleading, while cutting off dipole-dipole interaction at r=1 nm is only a modest approximation.

If periodic boundary conditions are applied to a molecular system, volume and pressure can be defined. Different statistical ensembles can be generated, depending on which thermodynamic variables are kept fixed. In the present simulations the following ensembles were used: 1. NVT: number of particles, volume and temperature are constant, and 2. NPT: number of particles, pressure and temperature are constant.

Temperature

The temperature is a macroscopic quantity, which is related to the microscopic description of molecular simulations through the kinetic energy, which is calculated from the atomic velocities. The temperature and the distribution of atomic velocities in a system are related by the Maxwell-Boltzman equation:

$$g(\vec{v})d\vec{v} = \left(\frac{m}{2pk_BT} \right)^{1/2} \exp\left(-\frac{m\vec{v}^2}{2k_BT} \right) d\vec{v} \qquad (2)$$

In the initial stage the velocities are generated according to Eq. 2, and the gaussian distribution is generated by a random number generator.

During MD simulation the temperature is related to the average kinetic energy of the system through the equipartition principle. This principle states that every degree of freedom has an average energy of $\frac{kT}{2}$ associated with it:

$$T = \frac{2E_{kin}}{N_f k_B}$$

where T is the instantaneous temperature, E_{kin} is the total kinetic energy of the system and N_f is the number of degrees of freedom. For a nonperiodic isolated molecular system N_f is equal to 3N-6 (six degrees of freedom are subtracted because both the translation and rotation of the centre of mass are ignored). For a periodic system N_f is 3N-3 (only the three degrees of freedom corresponding to translational motion can be ignored, since the rotation of a central cell imposes a torque on its neighbouring cells).

The direct Velocity scaling method was used for temperature scaling. Velocities of all atoms were uniformly scaled as follows:

$$v_{new} = v_{old} \sqrt{\frac{T_{new}}{T_{old}}}$$

where T_{new} is the desired temperature and T_{old} is the current temperature[18].

Pressure

The pressure may be calculated using the virial theorem, which is written in the form of generalised equipartition:

$$\left\langle p_k \, \P\mathrm{H} / \P p_k \right\rangle = k_b T$$

$$\left\langle q_k \, \P\mathrm{H} / \P q_k \right\rangle = k_b T$$

where p_k and q_k are generalised momentums and coordinates and H is the hamiltonian of the system. If we choose cartesian coordinates the second equation can be rewritten in terms of cartesians coordinates of atoms r_i and forces f_i on the atoms:

$$-\frac{1}{3}\left\langle \sum_{i=1}^{N} \vec{r}_i \cdot \vec{\nabla}_{r_i} U \right\rangle = \frac{1}{3}\left\langle \sum_{i=1}^{N} \vec{r}_i \cdot \vec{f}_i^{\,tot} \right\rangle = -Nk_b T$$

The symbol f_i^{tot} is used because it represents the sum of intermolecular forces and external forces. The external forces are related to the pressure:

$$\frac{1}{3}\left\langle \sum_{i=1}^{N} \vec{r}_i \cdot \vec{f}_i^{\,ext} \right\rangle = -PV$$

If we define the internal virial W

$$-\frac{1}{3}\sum_{i=1}^{N} \vec{r}_i \cdot \vec{f}_i^{\,\mathrm{int}} = W$$

where we now restrict attention to intermolecular forces, then

$$PV = Nk_b T + \langle W \rangle$$

For pairwise interactions it is more convenient to express W in a form, which is independent of the origin of coordinates:

$$\sum_i \vec{r}_i \cdot \vec{f}_i = \sum_i \sum_{j \neq i} \vec{r}_i \vec{f}_{ij} = \frac{1}{2}\sum_i \sum_{j \neq i} \left(\vec{r}_i \vec{f}_{ij} + \vec{r}_j \vec{f}_{ji} \right)$$

The first equality follows from writing f_i as the sum of forces f_{ij} on atom i due to atom j. The second equality follows because the indices i and j are equivalent. Using Newton's third law this expression may be rewritten in the form:

$$\frac{1}{2}\sum_i \sum_{j \neq i} \vec{r}_{ij} \vec{f}_{ij}$$

where $\vec{r}_{ij} = \vec{r}_i - \vec{r}_j$. This form is independent on the origin of coordinates[9].

In general pressure is a tensor P_{ij} where *i* and *j* subscripts run over x,y and z coordinates. The first subscript *i* refers to the direction normal to the plane on which the force acts and the second refers to the direction of the applied force.

Two methods of pressure control were used during MD simulation: the isotropic Berendsen[21] and the Parinello-Rahman[22] method. With the Berendsen method there is no change in the shape of the system, and only the pressure is controlled. At each time step, the x, y and z coordinates of each atom are scaled by the factor:

$$m = \left(1 + \frac{\Delta t}{t}\, g[P - P_0]\right)^{1/3}$$

where Δt is the time step, P is the instantaneous pressure, and P_0 is the target pressure. The cartesian components of the unit cell vectors are scaled by the same factor m.

With the Parrinello-Rahman method, the system's shape can change, and therefore both pressure and stress can be controlled.

Energy minimisation

Energy minimisation is the important method for potential energy surface investigations. The minimisation finds configurations that are stable points on the potential surface. This means finding a point in the configuration space where the total force acting on each atom vanishes. By simply minimising the energy, stable conformations can be identified. The advantage of the minimisation technique is that it is very fast in comparison with MD simulations, but it minimises the system with respect to potential energy and does not take into account entropy effects. Second it does not give any information about the evolution of the system in time. It is very useful to combine both minimisation and MD simulations techniques. In the initial structure some atoms may experience strong forces from neighbouring atoms which would lead to a high acceleration of these atoms during the first steps of MD simulations. That is why it is necessary to run a minimisation before a MD simulation.

3. MD simulation of Polyethylene/isotactic Polypropylene (PE/iPP) interfaces.

3.1 Introduction to the simulation of PE - iPP interfaces

Plastic waste has become one of the main issues of environmental concerns. Major polymeric components of plastic waste are polyethylene (PE) and polypropylene (PP). Separation of the plastic waste into individual polymers is costly and complete sorting is sometimes impossible. Thus it is important to study blends of PE and PP in order to put recycled blends into effective and efficient use.

It is well known that PE and PP are immiscible polymers. The term 'immiscible' means that the Gibbs energy of mixing is positive, thus two immiscible components tend to macroseparate from their mixture. The immiscibility of PE and PP was established by directly visualising macroseparation in the blend of molten PE and PP. A thin film of blended PE and PP was placed between two heated glass slides and observed with light microscopy. It was shown that initially small domains of PE and PP tend to merge leading finally to macroseparation of both polymers. Despite of the immiscibility of many polymers it is possible to produce their blends. Because of the high viscosity of bulk polymers the process of macroseparation takes place on a long time scale. By extrusion of two immiscible molten components and following fast cooling below crystallisation or glass transition points of both components it is possible to prevent them from macroseparation. It is clear that properties of a blend of two immiscible components would strongly depend on the preparation conditions like, for example on the mixing and cooling rates. In general, immiscible polymers are also incompatible. The term 'incompatible' means that the mechanical properties such as impact strength, Youngs modulus, strain and elongation at the stretching limit of the blend are inferior to the mechanical properties of the pure components.

Despite the immiscible nature of PE and PP it was recently found that it is possible to process blends of PE and iPP (isotactic polypropylene) with an impact strength of the blend which is two times higher than the impact strengths of the pure components. It is very important for industrial applications that by blending of common and cheap polymers one can obtain blends with improved impact strength. The blend of PE and iPP with improved impact strength was processed by extrusion of both molten components, followed by fast cooling. Transmission electron microscopy (TEM) images of the blend show that these preparation conditions lead to a fine micro-separation of PE and iPP, hence to an increased total interfacial area between PE and iPP in their blend. It was

suggested that the properties of PE - iPP interfaces help to dissipate a sufficient amount of energy in the blend, hence enhanced total interfacial area improves the impact performance of the blend. The suggestion of the important role that interfaces play in the impact performance of the blend was the starting point of this work.

In general one may subdivide the investigation of interfaces on the macroscopic and microscopic level. On the microscopic level the interface is characterised on atomistic length scales with changes of the structure of both components in the interfacial region. When one considers properties of interfaces on the macroscopic scale, the roughness of the surfaces of both components should be taken into account. It is hard to establish micro structure of the interfaces in a real blend, since one finds too many randomly oriented interfaces. In addition, because of the semi-crystalline nature of polymers one should expect four types of interfaces in the PE - iPP blend: amorphous-amorphous, crystallin-crystalline and amorphous-crystalline, crystalline-amorphous interfaces. The model experiment of epitaxial crystallisation of PE and iPP may help to resolve the structure of their interface. In epitaxial crystallisation one polymer is crystallised in the form of a thin layer on a thin layer of another polymer. The polymer sandwich is then investigated by X-ray scattering. But the structure of the interface is then difficult to discriminate from the structure of the polymers in the films, hence one expects that the material at the interface has exactly the same structure as in the film. It is obvious that this method may not reveal the fine structure of the interface. Molecular dynamics (MD) simulations may help to solve this problem since it allows to simulate the interface on the atomistic length scales, hence to investigate the fine structure of interfaces. That is why it was decided to perform MD simulations of PE and iPP interfaces in order to establish their exact microscopic structure.

3.2.1 Polyethylene, Polypropylene and their blends

Polyethylene macromolecules have the chemical formula: $CH_3 - \left[CH_2\right]_n - CH_3$ where *n* typically is in the range of 10^3-10^6. In the technical literature the term high density polyethylene is used for this linear polyethylene while the term low density polyethylene is used for branched polyethylene. I will focus in the following on the investigation of high density polyethylene and will use the abbreviation PE also for high density polypropylene instead of HDPE. The melting point of PE is at 138° C and its glass transition[4] is between -128° and -30° C, depending on the history of the sample and the experimental method which is used to determine the glass transition temperature.

The all trans conformation (zigzag) (Fig. 1) of the PE macromolecule is the form with the lowest potential energy. Crystals are composed of PE macromolecules in the all trans conformation.

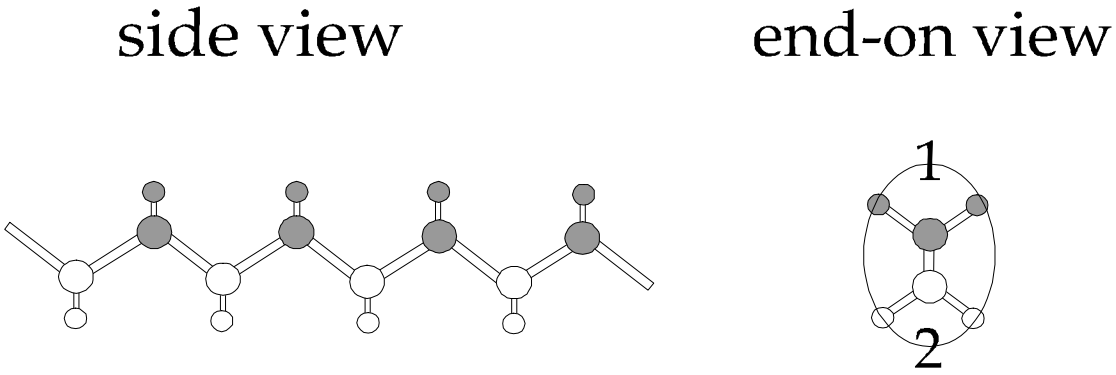

Figure 1. The all trans conformation (zigzag) of PE. Side and end-on view. The carbon atoms are large and hydrogen atoms are small. The ellipse is drawn to facilitate the display of PE crystalline forms shown in the figure 2. The shading is chosen in agreement with Figure 2 in order to outline the difference in height between sides 1 and 2.

Normally PE crystallises in the orthorhombic crystalline form (Fig. 2a). The orthorhombic PE crystalline unit cell has the following cell dimensions: a=7.40 Å, b=4.94 Å and c=2.534 Å. It was found that under extreme conditions, like for example crystallisation with extreme cooling rates or crystallisation under stress, PE can crystallise also in the monoclinic form (Fig. 2b). The monoclinic PE crystalline unit cell has the following cell dimensions: a=8.09 Å, b=2.53 Å, c=4.79 Å and β=107.9°.

Polyethylene crystalline modifications

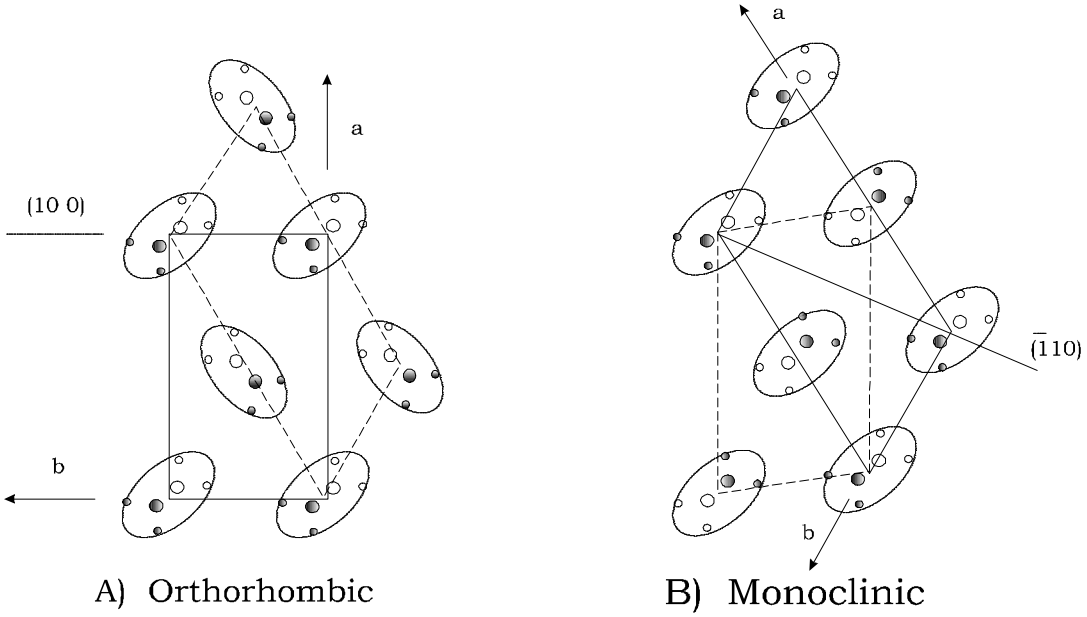

Figure 2. Orthorhombic and monoclinic crystalline forms of polyethylene. Cut through *ab* - plane with macromolecular long axes perpendicular to it. The ellipses are just a guide for the eyes and show the orientation of PE zigzags. It is important to notice that in the monoclinic form all ellipses have the same orientation while in the orthorhombic cell they have different orientation. The shading is consistent with Figure 1.

Polypropylene has the chemical formula:

$$CH_3 - \left[CH_2 - \underset{\displaystyle CH_3}{\underset{|}{CH}}\right]_n - CH_3$$ with a large *n*.

Tacticity of polypropylene is defined by the stereo-chemistry of the pending methyl group (CH_3). Polypropylene may be synthesised in three different forms: isotactic, syndiotactic and atactic. I will focus on the isotactic polypropylene (iPP). By definition all repeat units of isotactic polypropylene are geometrically identical. The melting point of isotactic polypropylene is at 171° C and the glass transition point[4] between -30°and 20° C, depending on sample history and experimental method which is used to determine the glass transition point.

It is known that iPP may crystallise in three different crystalline forms: α (monoclinic) , β (hexagonal) and γ (triclinic). In the present work just the

α crystalline form of iPP will be investigated. Crystalline forms of iPP are composed of iPP 3_1 helices (Fig. 3).

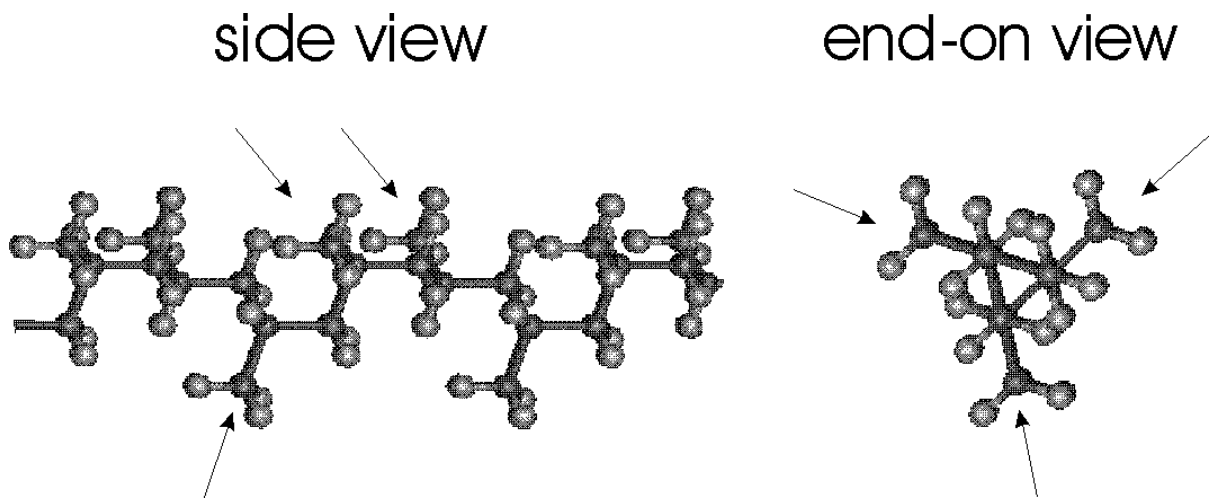

Figure 3. The helical form of iPP macromolecule. On the side view two helical turns are presented. Arrows show three methyl groups along one helix.

The α-form of crystalline iPP is composed of both right- and left-handed helices. Cell parameters of the α crystalline form are: a=6.65 Å, b=20.78 Å, c=6.50 Å and β=99.6°.

PE and iPP are known as immiscible polymers. The term 'immiscible' means that the Gibbs energy of mixing of two components is positive or by another words that they tend to macro-separate from their mixture. It is known that most blends of immiscible polymers exhibit lower mechanical properties for example stretching limit or impact strength. Materials whose blends has lower mechanical properties are called also incompatible materials. Since PE and iPP are immiscible polymers they are also expected to be incompatible. However, it was found recently that PE and iPP can be considered technically compatible materials. It was reported that it is possible to make a blend of PE and iPP with a higher Young modulus than the Young modulus of the pure components. It was also found that the impact strength of PE and iPP blend is about two times as high as the impact strength of the pure components.

Impact strength

The impact strength is an important factor for the commercial value of polymers or polymer blends. It is defined as the energy, which leads to the destruction of the sample, normalised to the area of the sample cut, perpendicular to the sample surface. The shape and the size of a sample is defined according to technical standards. The measurement of the energy,

leading to sample destruction is also defined by technical standards. For example: a hammer is dropped on a sample from different heights. The minimum height, which leads to a sample destruction allows to estimate the impact strength of a sample. It is important to distinguish notched and unnotched impact strength, i.e. whether the sample was notched before impact strength measurements or not.

Two types of materials with respect to impact strength measurements can be distinguished: brittle and ductile materials. Brittle materials have usually low impact strength. The unnotched impact strength of an ideal brittle material consists of the energy for crack formation and the surface energies of surfaces formed by crack propagation. For notched impact strength it is just the second component. Ductile materials which are also called tough materials, have usually higher impact strength. The impact strength of ductile materials includes in addition to brittle materials the energy of polymer matrix plastic deformation.

The toughness of polymeric systems has been studied intensively. It was established that a substantial increase in toughness of brittle polymers can be achieved by blending them with rubber particles. The mechanisms which are responsible for the increasing impact strength are multiple crazing, shear yielding, crazing with shear yielding and rubbery particles stretching and tearing. A common accepted view on the role of rubber particles is that this particles alter the stress in the material and induce plastic deformation of the polymer matrix. In general it is accepted that the plastic deformation in the polymer matrix, such as multiple crazing and shear yielding or both, absorb a major part of the total fracture energy.

It was proposed that blends with rubber particles larger than 1 μm prefer crazing, whereas shear deformation in a ductile polymer matrix is favoured by particles[3] smaller than 1 μm.

The multiple crazing mechanism

It was noticed that the fracture of rubber-toughened polystyrene is usually preceded by an opaque whitening of the stress area. It was also concluded that whitening is associated with the absorption of a large amount of energy[11]. Later it was established that polymer matrix crazing is responsible for stress whitening and therefore for the absorption of energy. Transmission electron microscopy shows that extensive crazing occurs in a nylon matrix within the whitening zone. Crazes are micro-cracks filled by voids and fibrils which are formed by yielding[12]. The energy dissipated by crazing consists of two components: 1. energy dissipated by yielding in fibril formation, and 2. energy stored as surface energy in the craze matter.

The mechanism for shear yielding

It was found that by blending of brittle polymer with rubber particles it is possible to obtain material with ductile characteristics thus improving its impact performance. It was further supposed that dilation which should occur in certain regions near the rubber particles aids in the lowering of T_g. The rubber particles are subjected to combined tensile stresses which prevent catastrophic crack propagation in the matrix[14].

On the other hand it was established that the sharp brittle to ductile transition occurs when surface-to-surface inter-particle distances become lower than a critical value R_c, which depends on the type of polymer matrix and rubber particles[15]. R_c was established to be independent of particle size and rubber volume fraction. This is in agreement with the results on stress-strain behaviour of PS (polystyrene) thin films. It was found that with decreasing PS film thickness, the material undergo a brittle to ductile transition[16]. A lattice of holes, which can represent non-adhering rubber particles, creates thin ligaments of polymeric material, i.e. potential initiation places of deformation. Brittle fracture of this ligaments can only occur if the stored elastic energy per ligament overcomes the surface energy of this ligament. It was shown that for thin ligaments (small inter-particle distances) brittle fracture does not occur, however complete deformation of the ligament takes place, eventually ductile macroscopic fracture behaviour is observed[17].

On the basis of this work it should be possible to explain the improved impact strength of PE/PP blends. It was clearly shown that PE is a ductile material. On the other hand PP shows semibrittle characteristics. Most of experimental work considered improving of impact performance of brittle polymers by blending them with rubber particles. Therefore let us consider improving of PP impact performance by blending it with PE. a) at low concentrations of PE in PP one can suppose large distances between PE inclusions, thus multiple crazing mechanism of impact strength improvement. b) at high concentration of PE in PP it is reasonable to suppose shear yelding mechanism of improving impact performance, moreover it was found that the better dispersion of PE in PP (thinner ligaments of PP) leads to a better impact performance of PE/PP blends. Therefore interfacial properties play an important role in the determination of the impact performance of polymer blends. The ‘strong’ interfaces would favour the multiple crazing mechanism while a polymer matrix plastification mechanism would be favoured by ‘weak’ interfaces. That is why it is important to investigate PE/PP interfaces in blends.

Up to now there is no experimental method which would allow to investigate polymer interfaces on a molecular scale directly in a blend. A polymer blend contains too many randomly oriented interfaces, therefore it

becomes impossible to focus with experimental method on the structure of a single interface. In addition both PE and PP are semicrystalline polymers at room temperature both in the pure state and in the blend. That is why one may suppose the existence of three types of interfaces: amorphous-amorphous, crystalline-crystalline and amorphous-crystalline, crystalline-amorphous. The semicrystalline nature of PE and iPP below their crystallisation temperatures is common for all polymers.

The so called crystals formed by polymer molecules are different from those formed by small molecules as the unit cell of the crystal contains part of a molecule rather than the hole molecule. The single crystals composed of flexible polymer molecules usually have one face with a much larger area than the other two and hence one dimension of the crystal is smaller than the other two and much smaller than the molecular length of the polymer. A single polymer crystal of this type is called lamella crystal. It was found that polymer molecules are packed in the lamella crystal perpendicular to the surface with the large area. This leads to the conclusion that the chains should fold back in the crystal. The detailed picture of chain folding as well as the crystal size depends on many parameters such as chemical structure of a polymer chain, crystallisation temperature and crystallisation procedure.

When polymers are crystallised from the melt, they form aggregates composed of lamella crystals. The most common shape of such aggregates is a spherulite (Fig. 4). Voids in between lamellae are filled with chains folding back to the lamellae from which they emerged or going to the neighbouring lamella. The material in-between lamellae is not crystalline and it is not also fully amorphous because chain orientation is induced by the presence of crystalline lamellae. The chain folding is not so obvious when lamellae form superstructures like spherulites. The usual argument for the polymer chains folding in spherulites formed from melt is that amorphous material between lamellae is less dense than the crystal and that if all the chains emerge from the crystal, adopt random conformations and do not fold back into the same crystal, then the density at the surface will be significantly higher than in the crystal. The co-existence of crystalline lamellae and amourohuse material in-between lamellae is the origin of the semicrystalline nature of melt crystallised polymers.

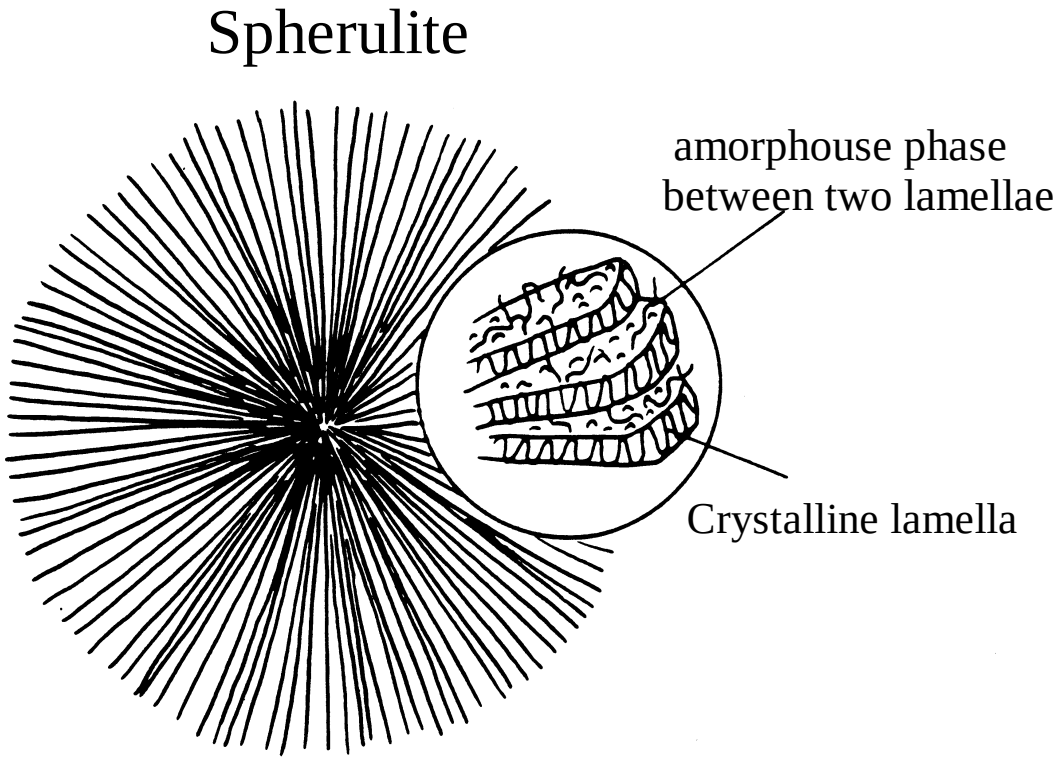

Figure 4. Schematic structure of a spherulite. Lamella crystals grow from the centre of the spherulite. The enlarged part shows several lamellae and an amorphous regions in-between lamellae. The amorphous part is formed by chains that fold back to the same lamella where they emerged from or by chains that reach into the neighbouring lamella.

As it was discussed above that a direct investigation of PE-iPP interfaces in a blend is quite difficult. However it is possible to perform a model experiment by epitaxial crystallisation of PE and iPP. In this case PE and iPP form a single interface and it is possible to establish a relationship of PE and iPP crystals. Several examples of epitaxial crystallisation of PE and iPP are listed below.

It was supposed in the literature that the ‘cross hatched’ morphology of PE and iPP established by epitaxial crystallisation of PE on iPP is responsible for the improved mechanical properties of PE and iPP blends. Lamellae of PE grow epitaxially at about 50° with respect to the orientation of PP lamellae. Hence a PE lamella epitaxially crystallised on iPP bridges many lamellae of iPP and vice versa. It was supposed that the bridging leads to hardening of the PE/iPP blend (Fig. 2).

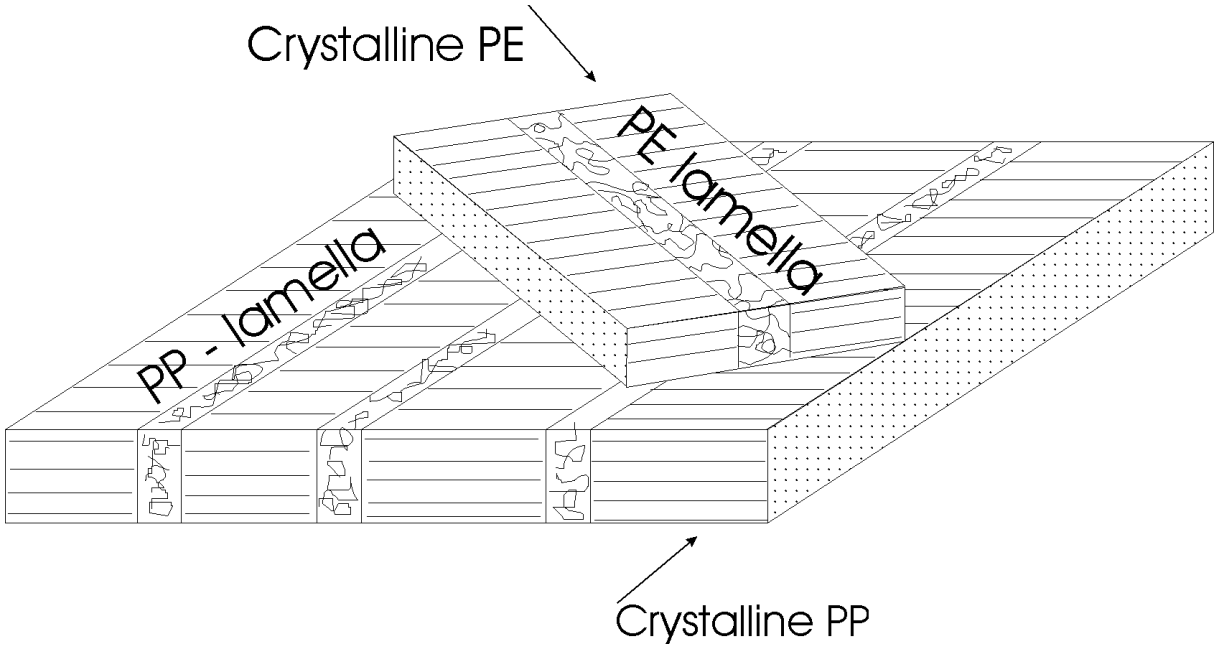

Figure 2. Bridging mechanism established by epitaxial crystallisation. It was found that lamellae of PE form an angle of about 50° with iPP lamellae. This figure shows the bridging of several iPP lamellae by PE lamellae.

Epitaxial crystallisation was carried out by two methods: 1. annealing of sandwiched films of PE/iPP; and 2. vacuum deposition or cast film crystallisation of PE or iPP onto single crystals or oriented films of iPP or PE respectively[1-2].

1. A thin film of highly oriented iPP was sandwiched with a thin film of PE the following way: Solution of 0.5% PP and PE, respectively in xylene were poured on two separately heated glass slides. After evaporation of the solvent, a motor driven cylinder was brought into contact with the two glass slides, lifted up and to allowed to wind up very thin PP and PE-films simultaneously. The films were 50 nm thick and highly oriented. The film of compressed PE and iPP was annealed at a temperature above the melting point of PE but below the melting point of iPP. After cooling down the film to room temperature, PE crystallised epitxially on iPP[1].

2. Polymer films are produced by melting the polymer and a solvent which can crystallise, between two with PE and iPP covered slides. On cooling, the solvent crystallises first and the polymer crystallises next in the form of a thin epitaxially oriented film if the substrate is appropriate. The crystallised solvent substrates are then dissolved. A vapour (of molecular weight 1300 for

PE and 3000 for iPP) condenses and crystallises on the substrate surface held at room temperature[2].

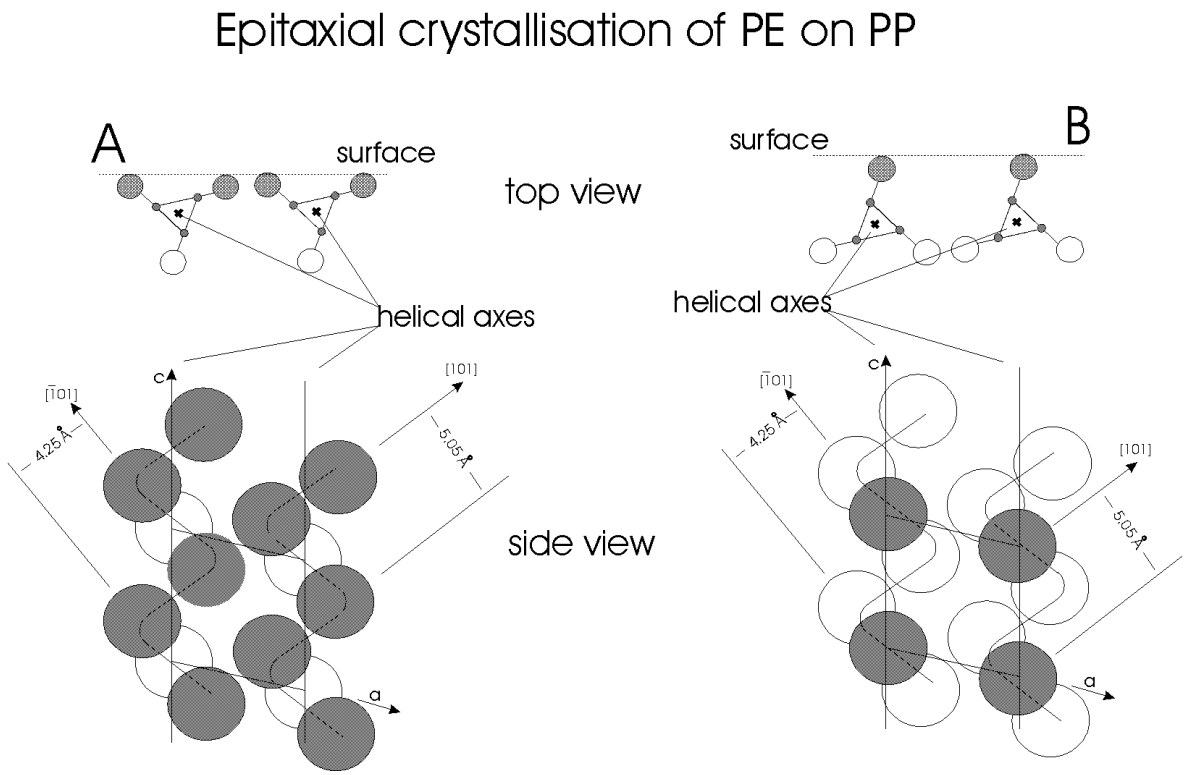

Figure 4 The two (010) faces of iPP (α–modification). The face with the higher density of methyl groups (surface of type A) results in rows of methyl groups parallel to $[101]$ and $[\bar{1}01]$ with inter-row distances of 5.05 Å and 4.25 Å respectively. Faces with the lower density of methyl groups (surface of type B) have less pronounced rows of methyl groups but exhibit the same symmetry as the faces with the higher density of methyl groups.

PE crystallises in the orthorhombic crystalline form on the α-modification of iPP, such that molecules of PE are inclined at an angle of about 50° with respect to the substrate chain axes. The contacting planes are (100) for PE and (010) iPP respectively. It was postulated, that epitaxially grown PE chains interact with rows of methyl groups that populate the (010) plane of the iPP α-modification. The distance between PE chains in the (100) crystallographic plane is 4.95 Å, while the distance between neighbouring rows of methyl groups in the (010) plane of iPP is 5.05 Å. There are two (010) crystallographic planes of iPP, which differ just by the density of methyl groups. It is not possible to find experimentally, whether PE crystallise on the (010) plane of iPP with the high density of methyl groups or with the low density of methyl groups (Fig. 4 adopted from the work of Lotz and Witmann[2]).

It is important to notice that methyl groups on the (010) crystallographic plane of iPP form patterns of the ‘four’ or ‘five’ faces of a dice[3], for the low or

high density of methyl groups, respectively. Diagonals of the dice elements form rows with inter-row distance 5.05 A and 4.25 A.

The advantage of the epitaxial crystallisation method is that it allows to investigate the relationship between PE and iPP lamellae. However it does not allow to investigate the detailed structure of the interface. In particular, it does not allow to look into structural changes that may occur in a layer of several angstroms thickness. MD simulations may help to resolve this problem, as it can yield a detailed picture of the interface structure. But MD simulations have other disadvantages: while they allow to simulate an interface of very thin layers of two components, the properties of an interface between two very thin layers could be different from the properties of an experimentally investigated of microscopically thick interfaces. That is why it is important to combine results of MD simulations with experimental results.

3.2.2 **Model for the PE/iPP interface**

As explained above it was decided to model three types of interfaces: amorphous/amorphous, crystalline/crystalline and amorphous/crystalline interfaces of PE and iPP. In order to model these interfaces first amorphous and crystalline PE and iPP were simulated separately.

Amorphous bulk systems were created by packing 18 molecules in the case of PE and 16 molecules in the case of iPP into a box with periodic boundary conditions. The densities of amorphous iPP and PE were set to fulfil the experimental value of the density 0.85 g/cm^3 for both iPP and PE. During the packing procedure the neighbourhood of each atom is checked by the distance criteria such that the distance between two nonbonded atoms are longer than the sum of the corresponding Van der Waals radii.

The structures of amorphous PE and iPP were then prerelaxed by energy minimisation. In order to optimise the sample further the system was subjected to annealing cycles of 20 ps duration where the temperature was increased linearly from 300 K to 800 K with a 100 K temperature step. After annealing the system was cooled down to 300 K with 100 K temperature steps in 20 ps time intervals. After another 200 ps at constant temperature of 300 K no further decrease of the potential energy could be observed.

The crystalline cells were constructed by adopting the orthorhombic unit cell of PE and the α crystalline form unit cell of iPP. The orthorhombic unit cell

of PE has cell dimensions a=7.26 Å, b=4.8 Å, c=2.57 Å, α=β=γ=90°, and consists of two methylene units (C_2H_4) (fig.1 and fig.2). The α–modification of iPP has cell dimensions: a=6.43 Å, b=20.86 Å, c=6.1 Å, α=γ=90° β=83.2°. All crystalline iPP modifications are formed by helixes. Each helix consist of three repeat units $(C_3H_6)^5$ of iPP (fig.3). The unit cell of α crystalline form of iPP consists of four helices having the following sequence: 1. Left Up, 2. Right Up, 3. Left Down, 4. Right Down, where Left = left handed helix, right = right handed helix, Up = helix points upwards, Down = helix points downwards.

The structures of crystalline PE and iPP were prerelaxed by energy minimisation, and then subjected to MD simulation with constant pressure. Two pressure control methods were tested to keep constant pressure: 1. isotropic Berendsen and 2. Parinello-Rahman methods. 1. We had to rise the pressure to 1.4 GPa in order to keep the crystalline systems stable and with correct density. 2. Systems showed good agreement with experimental parameters under a pressure 1 Bar. That is why Parinello-Rahman method of pressure control was used for the simulation of systems containing crystalline PE or iPP. The systems with crystalline PE or iPP were annealed for 50 ps at the temperatures 400 K, 350 K. Heating over 500 K caused gauche defects in PE and a higher potential energy of the crystalline system, respectively.

1. amorphous PE - amorphous iPP

Amorphous iPP and PE systems were created with exact matching of *a* and *b* cell sizes and with molecules of iPP and PE not crossing *ab* cell faces. The interface of amorphous iPP and PE was created by layering of *ab* cell faces of these systems of amorphous iPP and PE. The combined system was subjected to energy minimisation and then treated by MD simulation at 300 K for 500 ps.

2. crystalline PE - amorphous iPP, amorphous PE - crystalline iPP.

Crystalline iPP was constructed with matching of its (010) crystallographic plane, (low density of methyl groups on the surface), with *ab* cell face. The amorphous cell of PE was constructed with matching of *a* and *b* cell sizes with *a* and *b* cell sizes of the iPP crystalline cell. The interface of crystalline iPP and amorphous PE was created by layering of this ensembles by *ab* faces.

Crystalline PE was constructed with matching of its (100) crystallographic plane with *ab* cell face. The amorphous cell of iPP was constructed with matching of *a* and *b* cell sizes with *a* and *b* sizes of the PE crystalline cell. The

interface of crystalline PE and iPP was created by layering of these ensembles by *ab* cell faces. Crystalline - amorphouse interfaces were subjected to energy minimisation and then treated by MD simulation at 300 K for 500 ps.

3. crystalline PE - crystalline iPP

Direct layering of the iPP crystalline ensemble with the PE crystalline ensemble is not a good strategy: due to the periodic boundary conditions, chains of PE would not be able to rotate during MD simulation with respect to the orientation of iPP chains, and therefore MD simulation of one PE/PP crystalline-crystalline interface would not allow to investigate all possible PE/PP crystalline-crystalline interfaces. On the other hand the direct simulation of epitaxial crystallisation of PE on the PP substrate is also not possible, since the characteristic times of epitaxial crystallisation are much longer than times accessible in the MD simulation. Therefore we decided to create ensembles of crystalline PE with different orientations of PE chains inside the cell. This method allows to investigate properties of crystalline-crystalline PE/PP interface with a particular orientation of PE molecules with respect to the orientations of PP chains. The experiments predict several possible orientations of PE molecules with respect to the orientation of PP molecules, as has been described above.

It was decided to restrict the investigation of crystalline-crystalline interfaces to those established in epitaxial crystallisation and to several reference interfaces. Crystalline iPP was constructed with matching of the (010) crystallographic plane, both low and high density of methyl groups, with the *ab* cell face. Crystalline PE was constructed with matching of the (100) crystallographic plane with the *ab* cell face, and matching of *a* and *b* cell sizes as close as possible to *a* and *b* cell sizes of crystalline iPP. The exact matching was of course impossible and the cell sizes mismatched by 6%-8% of their cell sizes. Initial orientations of crystalline PE chains inside the cell were set to 0°, 90°, 47°, -47°, where the angle 47° denotes an interface where PE molecules are parallel to rows formed by methyl groups on the iPP surface with an 5.05 Å inter-row distance.

Ensembles of pure crystalline PE with polyethylene chains initially rotated in the cells were treated by MD simulation in order to check whether they have the same structural and energy properties as an unrotated PE crystalline ensemble. The potential energy terms like bond stretching, changing of angle and e.i. of rotated PE ensembles fitted to energetically parameters of unrotated PE within 5%. The rotated ensembles of crystalline PE preserved the orthorhombic crystalline structure. Since the cell sizes of crystalline PE and crystalline iPP did not match exactly, the cells sizes were adjusted. The *a* and *b* cell sizes of PE and iPP were scaled in order to fit to each other and the *c* cell

sizes were scaled in order to keep the volume constant. For example, for the layering of the iPP (010) plane with the low density of methyl groups on the surface and the (100) plane of PE, iPP had a=28.12 Å, b=26.41 Å and a=25.7 Å, b=24.64 Å, which gives 9% and 7% mismatch of the cell sizes, respectively.

Crystalline PE - crystalline iPP interfaces were subjected to energy minimisation and then treated by MD simulation at 300 K. In total they were treated by 200-500 ps of MD simulation, but since molecules at crystalline-crystalline interfaces do not have much freedom, no further decrease of the potential energy could be observed after the first 50 ps of MD run.

3.2.3 Results

Energy calculations

In order to compare crystalline - crystalline interfaces with different initial orientation of PE molecules with respect to the orientation of iPP chains, adhesion energies were calculated. Adhesion energies were calculated as the sum of the energy of mixing and surface energies.

$$E_{adhesion} = E_{mixing} + E_{PE\_surface} + E_{PP\_surface}$$

The energy of mixing was calculated for each particular orientation of PE molecules with respect to the orientation of iPP chains, as a difference in energy of the combined system and the energies of bulk crystalline PE and iPP.

$$E_{mixing} = E_{PE+PP\_\text{int}erface} - E_{PE\_bulk} - E_{PP\_bulk}$$

Surface energies of crystalline PE and PP were calculated in the environment of benzene. The calculation of surface energies with vacuum as environment caused melting of crystalline surfaces of iPP and PE. Therefore we had to apply pressure on the surfaces of iPP and PE. We considered benzene as a better environment. Benzene is a non-polar solvent and should cause less perturbation of PE and PP surfaces.

$$E_{PE\_surface} = E_{PE+benzene} - E_{PE} - E_{benzene}$$

$$E_{PP\_surface} = E_{PP+benzene} - E_{PP} - E_{benzene}$$

Energies of PE and iPP ensembles as well as combined systems were extracted from MD trajectories of this systems. Adhesion energies and surface energies were normalised to the interfacial (or surface) area.

Energies of bulk PE and iPP or combined systems were determined from the MD trajectories of these systems. Potential energies of the systems were stored every 0.5 ps and then averaged over least 50 ps. It is important to notice that the potential energy determined for two last runs of 50 ps duration differ less than the error bar of the potential energy determination. It is also important that the difference between the potential energy of the combined system and the sum of the potential energies of bulk PE and PP was much higher than the error bar of the potential energy determination.

Computation of crystalline PE and iPP surface energies in benzene environment were carried out for the (100) and (010) crystallographic planes respectively: 29 $\frac{J}{m^2}\cdot 10^{-3}$ for PE and 14 $\frac{J}{m^2}\cdot 10^{-3}$ for iPP. Adhesion energies for different orientations of PE chains with respect to the orientation of iPP chains are summarised in table 1:

angles	energies in $\frac{J}{m^2}\cdot 10^{-3}$			
	E_{mix} high	E_{mix} low	E_{adh} high	E_{adh} low
90°	43	39	-1	-5
0°	55		11	
47°	36	27	-8	-17
-47°	55	49	11	5

Here '**high'** means high density of methyl groups on the (010) crystallographic surface of iPP at the interface with PE, and '**low'** means low density of methyl groups on the (010) crystallographic surface of iPP at the interface with PE. Both energy of mixing and adhesion energies are presented since it is important to notify that the energy of mixing is always positive, while the adhesion energies vary from positive to negative values.

The calculated surface energies for amorphous PE and iPP in benzene environment are 0.26 $\frac{J}{m^2}$ and 0.13 $\frac{J}{m^2}$ respectively. The adhesion energy for crystalline iPP and amorphous PE interface is -0.18 $\frac{J}{m^2}$, while for the interface of crystalline PE and amorphous iPP it is 0.17 $\frac{J}{m^2}$.

Structural changing at the interface

The structure of crystalline PE and iPP did not change when PE and iPP were layered with amorphous PE and iPP.

Rotation 47° of PE molecules with respect to the orientation of PP chains, low density of methyl groups on the PP contacting surface

The ensemble consisting of two layers of PE and PP has two PE/PP interfaces due to the periodic boundary conditions. In order to avoid possible interference of two interfaces we constructed model systems, consisting of three layers - PE layer, PP layer and layer of benzene. It should be mentioned that no significant structural difference of PE and iPP between the three layer and the two layer systems were observed after MD simulation.

The structure of PE changed from orthorhombic to monoclinic for the entire layer of PE. We could not detect the interfacial depth of PE: increasing the thickness of PE layer from 20 Å to 40 Å did not help to resolve an interfacial depth of PE. The $(\bar{1}10)$ face of monoclinic PE interacts with the iPP surface (Fig. 4).

The structure of iPP did not change drastically in the entire layer of iPP, only one layer of PP helices closest to the PE has changed: every second methyl group along the PP helix has a bit rotated, these methyl groups are indicated on the figure 4 with arrows.

PE:(monoclinic) a=8.7 Å, b=2.54 Å and c=4.5 Å, α=89°, β=95.5° and γ=91°

PP: a=6.7 Å, b=21 A and c=6.6 Å, α=90°, β=94° and γ=91°

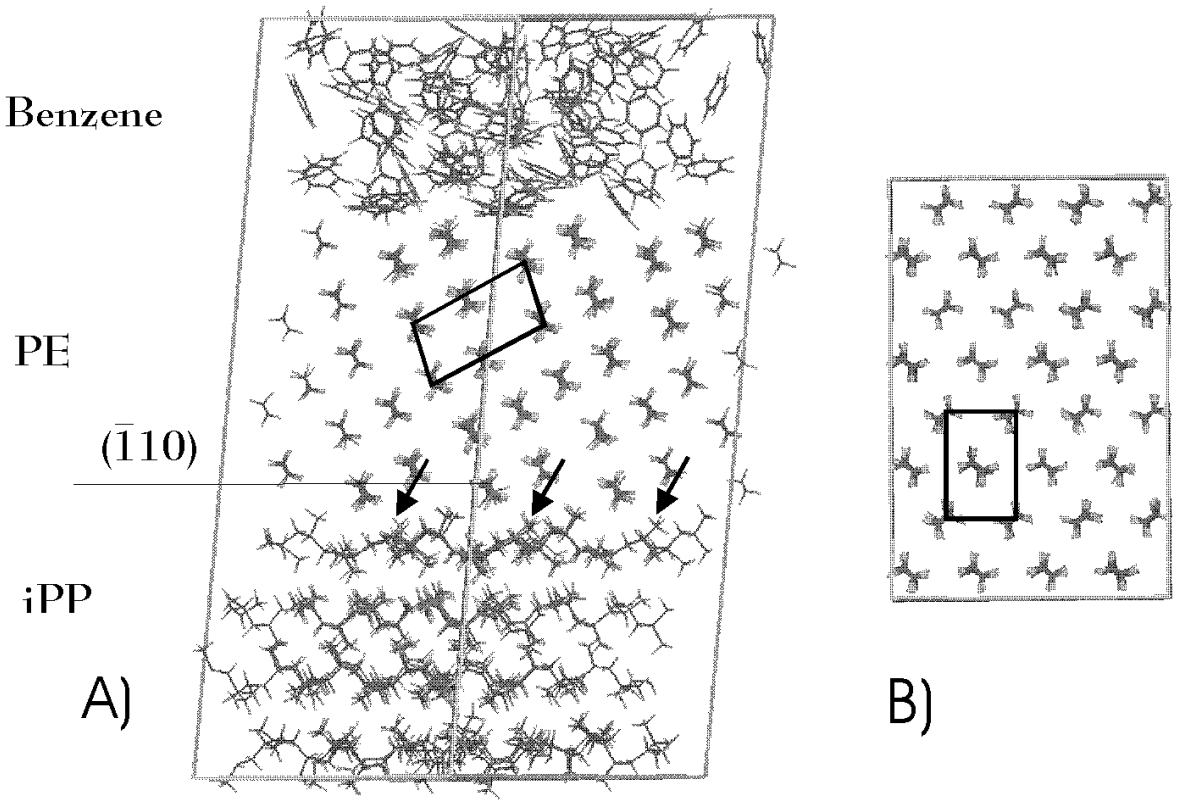

Figure 4 A) Interface of crystalline iPP and crystalline PE with low density of methyl groups on the PP contacting surface. End on view on PE molecules, iPP molecules are rotated about 47° to the point of view. Arrows point out the methyl groups on the surface of iPP which were initially oriented upwards. B) Top view on orthorhombic crystalline polyethylene.

Rotation 47° of PE molecules with respect to the orientation of PP chains, high density of methyl groups on the PP contacting surface

The structure of PE and iPP crystalline unit cells did not change significantly.

PE:(orthorhombic) a=7.85 Å, b=4.8 Å and c=2.55, $\alpha=\beta=\gamma=90°$

iPP: a=6.7 Å, b=20 Å and c=6.6 Å, $\alpha=89°$, $\beta=93°$ and $\gamma=92°$

Figure 5 shows the snapshot of the MD equilibrated structure of the PE/iPP interface.

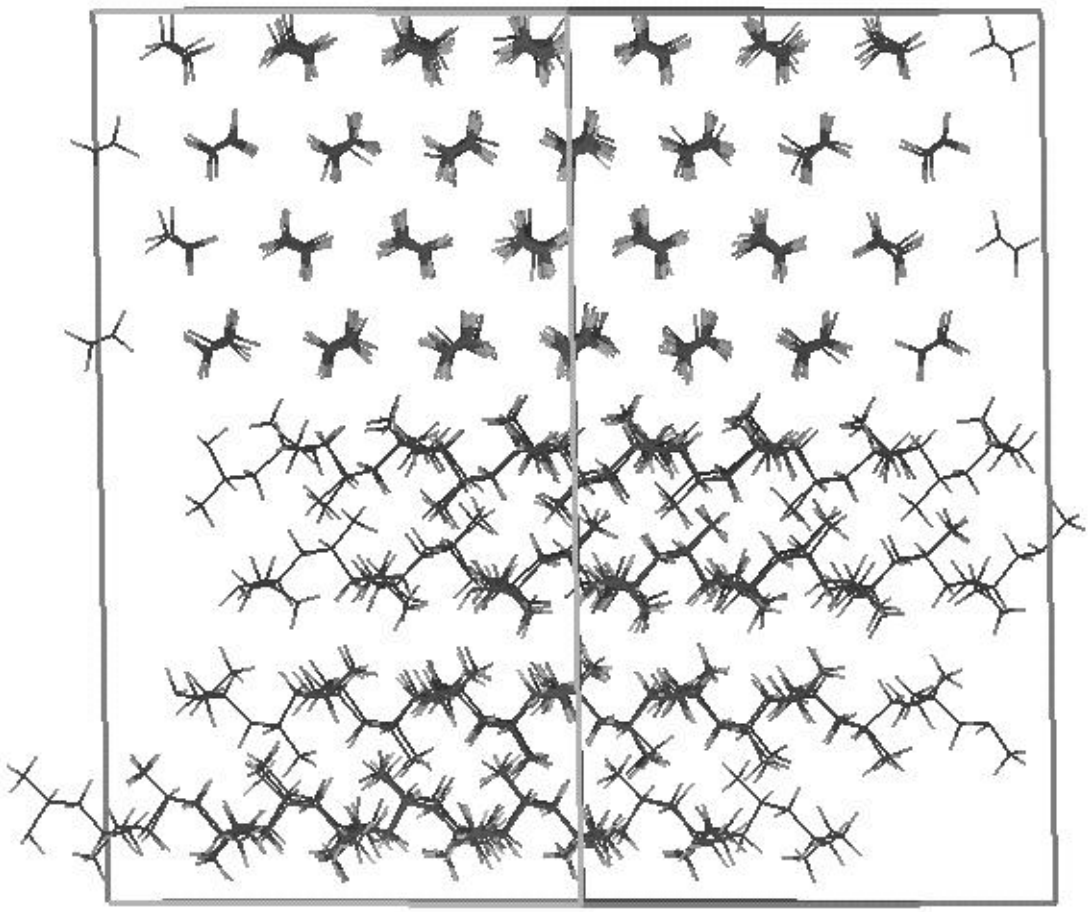

Figure 5 Interface of crystalline iPP and crystalline PE with high density of methyl groups on the crystalline iPP contacting surface. End on view on PE molecules, iPP molecules are rotated about 47° with respect to the point of view.

3.3.4 Discussion

Possible shortcomings:

Amorphous - amorphous and amorphous - crystalline interfaces

One of the present limitations of the MD simulation method is that we can simulate just several nanoseconds, while all processes which we are interested in this work e.g. (crystallisation and epitaxial crystallisation) take place on much longer time scales than several nanoseconds. If we choose a starting structure far from its equilibrium, we cannot expect that during MD simulation it would converge to its equilibrium state. This disadvantage should be taken into account during simulation of amorphous polymers at temperatures below the temperature of their crystallisation. If we perform MD simulations long enough we should see partial crystallisation of amorphous polymers.

The fact, that PE and PP are semicrystalline polymers both as neat materials and in the blend suggest amorphous - amorphous and crystalline - amorphous interfaces. It should be pointed out that amorphous parts, which give an amorphous halo in X-ray scattering experiments, are not purely amorphous, but are just parts of polymer chains in-between crystalline lamellae, which are forced to stay in a non crystalline state. This state can even not be called amorphous because the chain orientation is induced by the presence of the crystalline lamellae as it was mentioned in the introduction. In computer simulation nothing prevents polymers from crystallisation at temperatures below temperature of crystallisation.

From the statements made above one can conclude that even when we do not see any further decrease of potential energy with time, this does not mean that amorphous ensembles are already equilibrated. This is true for the bulk amorphous systems and as well as for the interfaces of two amorphous polymers or for the interfaces of semi-crystalline polymers. If we simulate amorphous systems for a very long time, we should see crystallisation of bulk amorphous PE and PP and epitaxial crystallisation of layered system.

Crystalline-crystalline interfaces

On the other hand crystalline-crystalline interfaces do not have much freedom – e.g. PE macromolecules can not rotate laterally on top of iPP chains. If we assume that the crystalline structures of both PE and iPP do not differ very much from bulk crystalline PE and iPP (orthorhombic and α–modification respectively), then the system of combined PE and iPP should not undergo large conformational changes during MD. Therefore, MD trajectories should not be very long to minimise the energy of crystalline-crystalline ensembles. Experimental investigations of structures, formed by PE during epitaxial crystallisation show that PE crystallises epitaxially either in the orthorhombic structure or in the monoclinic depending on substrate and environmental conditions. iPP can crystallise in three different crystalline forms: α–, β–, and γ–modifications. On the other hand it was established that just the α crystalline modification of iPP induces epitaxial crystallisation of PE, and iPP crystallises epitaxially in the α–modification on the PE substrate. Based on the assumptions made above one can conclude that it could be possible to investigate by means of computer simulations crystalline-crystalline interfaces of PE and iPP.

The algorithm of layering of crystalline-crystalline interfaces could cause artificial structural changes. As it was mentioned above ensembles of crystalline PE and PP had a mismatch in cell sizes in the a and b axes. During layering this mismatch was corrected by scaling of the PE and PP cell sizes, which means

that bond lengths and angles were scaled as well. For example in the case of layering of a PE ensemble with PP, when PE molecules were oriented at 47° with respect to the orientation of PP chains, bonds and angles were scaled as follows:

1. PE: C-C bond length was changed from 1.54 Å to 1.50 Å.

2. PP: C-C bond lengths were changed from 1.54 Å to 1.42,1.59,1.60,1.53 Å.

This artificial scaling of bond length and angles could cause several shortcomings:

Changing bond lengths without a correlated scaling of the force field leads to storing of a considerable amount of energy in the system. There could be several ways leading to structural changes in the system due to the stored energy. a) If we assume that energy minimisation does not relax the molecular system to the global minimum but stops at a local minimum, then the difference of energy between global and local minima should be stored in all degrees of freedom. This means that for example the energy stored in bond lengths could be distributed to torsion potentials, and this could lead to the appearance of gauge defects in the PE structure and the changing the helical structure of PP. b) Releasing of a large amount of energy during MD simulation could be also dangerous: for example it may lead to local heating provoking local structural changing.

Analysing crystalline - crystalline interfaces shows that bond lengths and angles relax to their normal values. For example in the case of a crystalline - crystalline interface while, PE molecules are oriented at 47° with respect to the orientation of PP chains, low density of methyl groups on the PP surface, bonds and angles have converged to the following values (after energy minimisation and 50 ps of MD simulation):

1. PE: C-C bond length has converged to 1.544 (1.54 before layering).

2. PP: C-C bond length has converged to 1.545 (1.54 before layering).

Analysing of the crystalline - crystalline interface after minimisation and 50 ps of MD simulation does not reveal the appearance of gauge defects or destroying of the helical structure of PP.

Adjusting of cell sizes causes that one part of the combined system wants to increase the cell size while the second part of these molecular system wants to decrease the cell size. In the case of layering of PE and PP this could be relieved by small rotations of PE molecules with respect to PP molecules or by structural changes of PP and PE layers. I do not know how to argue that either structural changes of PE and PP in the combined systems were caused by cell size mismatches or induced by the interaction of PE and PP at the interface. The

answer could probably be found by comparing of results of computer simulation with experimental results.

Comparing of experimental results with results of computer simulation

Computer simulated structures of pure crystalline PE and iPP α–modification slightly differ from experimentally measured structures of PE and iPP α-modification.

PE:

MD simulated: a=7.66 Å, b=5.06 Å and c=2.58 Å, α=β=γ=90°

experiment: a=7.4 Å, b=4.94 Å and c=2.534 Å, α=β=γ=90°

PP:

MD simulated: a=6.57 Å, b=21.5 Å and c=6.01 Å, α=γ=90°, β=97°

experiment: a=6.65 Å, b= 20.78 Å and c=6.50 Å, α=β=90°, β=99.6°

It is also important to compare distances between rows of methyl groups: 5.05 A, 4.25 Å from experiment and 4.9 A, 4.28 Å from computer simulation. The model of epitaxial crystallisation was based on lattice matching of 5.05 A of iPP with 4.94 A of PE. Structures of computer simulated crystalline PE and iPP do not match exactly with experimentally established structures. On the other hand computer simulated crystalline PE and iPP exhibit a lattice matching within the same error bar.

The calculation of adhesion energies by means of computer simulation allows to establish the structure with the lowest adhesion energy, hence to predict epitaxial crystallisation of PE on PP substrate and vice versa epitaxial crystallisation of PP on a PE substrate. Adhesion energies for PE - PP interfaces are summarised in the table 1. It is hard to compare the computer calculated adhesion energy with the experimentally measured energy needed to split an interface into parts. The computer calculated adhesion energy corresponds to the energy of an ideal interface - a flat surface of PE interacting with a flat surface of PP. In a real experiment the surfaces of both samples are not flat any more, with some interpenetration of one polymer material into another. Depending on the preparation conditions mixing on the molecular level in the interfacial region should be also taken into account. In the particular case of the PE - iPP interface it is known that PE forms tongues which penetrate into iPP. The experimentally measured adhesion energy includes the energy of yielding of these tongues and consist mostly of this tongue yielding energy.

The calculated adhesion energies and energies of mixing could be compared effectively with experiments. The calculated energy of mixing is always positive, which means that the computer simulation predicts immisciblity of PP and PE. It was clearly proven experimentally that PE and PP are immiscible in the melt. Most of the experimental works indicate also immisciblity of PE and PP in the solid form - 'weak' PE/iPP interfaces, but it was supposed as well that improved mechanical properties of PE/iPP blends could be explained by 'strong' PE/iPP interfaces.

The lowest calculated adhesion energy (table 1) corresponds to the case of 47° orientation of PE molecules with respect to iPP chains and the low density of methyl groups on the iPP surface. PE molecules have the same orientation with rows formed by methyl groups on the iPP surface with an inter-row distance of 5.05 Å. The adhesion energy is higher when the PE molecules are oriented 47° with respect to the orientation of iPP chains, and the PE molecules have the same orientation with rows formed by methyl groups on the iPP surface with an inter-row distance of 4.25 Å. We did not consider by the computer simulation all orientations of PE molecules with respect to the orientation of iPP chains. In addition we did not investigate the interaction of different crystallographic planes of both PE and iPP. Within the range of simulated ensembles, from calculated adhesion energies we may conclude that PE molecules should crystallise epitaxially on iPP at 47° with respect to the orientation of PP chains, and with low density of methyl groups at the surface.

The model of epitaxial crystallisation of PE on the iPP substrate is still in debate in the literature. It was supposed that the 'cross-hatched' morphology of epitaxially crystallised PE on the iPP substrate, is driven by the 'cross hatched' morphology of the iPP substrate. Due to the lattice matching of crystalline PE and iPP, PE molecules crystallise at about 50° with respect to the orientation of iPP chains. iPP substrates crystallised under normal conditions, have two chain orientations at 100° to each other. This 'cross hatched' nature of iPP substrates induces the 'cross hatched' morphology of epitaxially crystallised PE. This model does not fit to the experimental work[1] of epitaxially crystallised PE on the highly oriented iPP substrate. By drawing, highly oriented films of iPP were obtained, where molecules of iPP were oriented just in one direction in this film. Epitaxially crystallised PE on this substrate also shows a 'cross hatched' morphology. In this experiment 'cross hatched' morphology of epitaxially crystallised PE can not be explained by the 'cross hatched' morphology of the substrate.

In order to explain the 'cross hatched' morphology one should take into account that the probability to find left and right handed helices on the surface of

iPP is equal. This leads to the conclusion that the surfaces of different domains of iPP could be composed of left handed or right handed helices. If the rows of methyl groups with an interrow distance of 5.05 Å formed by right handed helices have the angle 47° with the helical axes then rows of methyl groups with 5.05 Å interrow distance formed by left handed helixes have the angle -47° with the helical axes. The 'cross hatched' morphology of epitaxially crystallised PE on iPP could be explained by the presence of both left and right handed helices on the surface of iPP.

It is not possible to distinguish by X-ray scattering whether PE crystallises on the (010) crystallographic surface of iPP with high a density of methyl groups or with a low density of methyl groups. On the other hand it was established[3] that the (010) surface of iPP, produced for epitaxial crystallisation of PE, contains low density of methyl groups. To produce a (010) crystallographic surface of iPP for epitaxial crystallisation, iPP is crystallised on a crystalline low molecular weight substrate, which induces the (010) crystallographic plane of iPP. After removing of the low molecular weight substrate, the (010) crystallographic plane of iPP is ready. This result shows that the (010) crystallographic surface of iPP with the low density of methyl groups is energetically more favourable in contact with a low molecular weight solvent. It also indicates that the (010) crystallographic plane of iPP with low density of methyl groups could be energetically more favourable in contact with epitaxially crystallised PE.

The energetically most favourable combined ensemble is the ensemble with PE chains oriented at 47° with respect to the orientation of iPP molecules with the low density of methyl groups on the iPP contacting plane (table 1.). The analysis of the structural changes shows that the PE structure has changed entirely from orthorhombic to monoclinic. Energetically the orthorhombic structure is more favourable, but the energy difference between orthorhombic and monoclinic crystalline form is very low, as shown by computer simulation[7,8]. As it was described above structural changes in the combined system could be induced by additional energy introduced into the system or by tension induced through adjusting cell sizes, especially when the energy of orthorhombic and monoclinic structures does not differ very much. On the other hand it was found that some substrates do induce epitaxial growth of PE with the monoclinic structure. The observed monoclinic phase is spatially transient: it does not go beyond 3 or 5 nm from the substrate surface[6]. The computer simulation does not allow to go beyond 5 nm thickness of PE layer, so we just cannot see the transition from the monoclinic to the orthorhombic crystalline phase.

3.3 Conclusions.

MD simulation of PE - iPP interfaces was performed. Amorphous – amorphous, crystalline - amorphous and crystalline - crystalline interfaces were simulated. Due to the drawback of the periodic boundary conditions which does not allow lateral rotation of one crystalline phase on top of the second one, the simulations of crystalline-crystalline interfaces were restricted to that adopted from the experiments on epitaxial crystallisation of PE and iPP and to several reference interfaces.

Adhesion energies in the benzene environment were calculated in order to compare different types of interfaces. It was found that the strongest adhesion for crystalline-crystalline interfaces corresponds to the rotation of PE macromolecules of about 47° with respect to the orientation of iPP helixes with low density of methyl groups on the iPP surface. At this particular orientation PE molecules fit exactly in the rows formed by methyl groups on the surface of iPP. Hence the structure model for epitaxial crystallisation of PE and iPP has been proven. Experimental methods do not provide information whether PE crystallises epitaxially on the surface of iPP with high or low density of methyl groups. Strong adhesion for the case PE-iPP interface with low concentration of methyl groups allow to predict epitaxial crystallisation of PE molecules on the surface of iPP with low surface concentration of methyl groups.

The unexpected transition of crystalline PE from orthorhombic to monoclinic crystalline form is observed for the interface with the strongest adhesion energy. It is possible that this phenomena is caused by the artefacts of the building of a super-cell with an interface of PE and iPP. On the other hand it is also possible that the transition from orthorhombic to monoclinic crystalline form happens just in a very thin layer of PE at the interface, while bulk PE is still in the orthorhombic crystalline form. Therefore the monoclinic crystalline form can be space transient and was not observed in the experiment on the epitaxial crystallisation because the layer of PE in the monoclinic form was too thin to be detected without special preparation conditions of the experiment.

3.4 Literature

1. J. Peterman, G. Broza, U. Rieck, A. Kawagushi, J. of Material Science, **22,** (1987), 1477-1481.

2. B. Lotz and J.C. Wittmann, J. of Polym. Sci., Part B, **24,** (1986), 1559-1575

3. W. Stocker, S.N. Magonov, and H.-J. Cantow, J.C. Wittmann and B. Lotz, Macromolecules, Vol. 26, **22**, (1993), 5915-5923.

4. J. Brandrup, E.H. Immergut, "Polymer Handbook", third edition, John Willey and Sons.

5. G. Natta and P. Gorradini, Supplemento al Nuovo Cimento, **15**, N10, (1960) 40-51.

6. J.C. Wittmann and B. Lotz, Polymer, **30**, (1989), 27-34.

7. Masymichi Kobayashi and Hiroyuki Tadokoro, Macromolecules, **8**, N6, (1975), 897-903.

8. T. Yemni and L.McCullough, J.Polym.Sci., Polym. Phys. Ed., **11**, (1973), 1385.

9. M.P. Allen, D.J. Tildsley, 'Computer simulation of liquids', Clarendon press, Oxford, Science Publications (1987).

10. H. J. C. Berendsen, J. P. M. Postma, W. F. van Gunsteren, A. DiNola, J. R. Haak, 'Molecular dynamics with coupling to an external bath', J. Chem. Phys., **81,** (1984), 3684-3690.

11. C.B. Bucknall and R.R. Smith. Polymer **6** (1965) 437.

12. E.I. Souheng Wu, J. Polym. Sci. **21** (1983) 699-716.

13. Jingshen Wu, Yiu-Wing Mai, J. Mater. Sci. **28** (1993) 6167-6177.

14. S. Strella, J. Polym. Sci. **4** (1996) 527-528.

15. Souheng Wu, Polymer, **26** (1985) 1855-1863.

16. M.C.M. van der Sanden, H.E.H. Meijer and P.J. Lemstra, Polymer **34** N10 (1993) 2149-2154.

17. M.C.M. van der Sanden, H.E.H. Meijer and T.A. Tervoot, Polymer **34** N14 (1993) 2961-2970.

18. InsightII version 4.0.0 manual

19. B. Gross, J. Petermann, J. of Material Sci., **19** (1984) 105-112.

20. B.L. Schürman, U.Niebergall, N.Severin, Ch.Burger, W.Stocker and J.P.Rabe, Polymer **39,** (1998) 5283-5291.

21. H.J.C. Berendsen, J.P.M. Postma, W.F. van Gunsteren, A. DiNola, and J.R. Haak, J.Chem.Phys. **81** (8), (1984) 3684-3690.

22. M. Parinello, A. Rahman, J.Appl.Phys., **52**, (1981) 7182-7190

4. MD simulation of cylindrical and half-cylindrical micelles in water and at solid liquid interfaces.

4.1 Introductory remarks.

In the second part of this work MD calculations of aggregates of amphiphilic molecules at sold-liquid interfaces are presented. Amphiphilic molecules by definition are composed of two parts, hydrophobic and hydrophilic. These opposing properties in the same molecule are the origin of micro-phase separation of amphiphilic molecules and solvent when dissolved in a polar solvent like water. It is well known that amphiphilic molecules form a wide variety of different aggregates like spherical micelles, bilayers or even more complicated structures of interpenetrating networks of amphiphilic molecules and solvent[18]. As amphiphilic molecules are very important in industry and biology, self aggregation of amphiphilic molecules and the structure of their aggregates was investigated intensively. Most of experimental data lead to a qualitative picture of a micelle. A few experimental techniques give as well structure of a micelle quantitatively. But due to a limited resolution some aspects of the structure of micelles are not clear.

While the self aggregation of amphiphilic molecules in aqueous solution is fairly well understood, it is not clear how these aggregates are affected by the presence of a solid surface. The surface force apparatus provide quantitative measures of adsorption, but little information on the aggregate structure. Neutron reflection is a very powerful tool to probe the structure of adsorbed aggregates. Substituting of hydrogens from different parts of amphihpilic molecule by deuteriums allows to obtain high resolution in the direction perpendicular to the substrate surface. The drawback of neutron reflection is that it does not resolve the adsorbed structure in the plane parallel to the surface. Another powerful tool for the investigation of structures formed by amphiphilic molecules on different substrates is scanning force microscopy (SFM). In contradiction to the neutron reflection SFM provides good resolution in the plane parallel to the surface and relatively poor resolution in the direction normal to the substrate surface. A combination of these two experimental methods allows to propose a picture of the adsorbed structure.

MD simulation is another powerful mean to obtain detailed insight into the structure and molecular behaviour of amphiphilic aggregates. The advantage of the MD method is that it allows to track the position of each atom in the system with time, so that it allows to simulate and predict the exact picture of micelles. At present time MD simulation has several limitations. First, the MD method allows to simulate the evolution of a micelle on a very short time period, usually several nanoseconds. Second, MD allows to simulate only relatively

small molecular systems, consisting of thousands of atoms. In order to simulate the evolution of micelles on longer time scales some simplifications could be made. Starting from the models with a unification of atom groups like CH_2 or H_2O and ending with the models that simulate just main properties of amphiphilic molecules - hydrophobic and hydrophilic parts. Simplifications allow to simulate larger amphiphilic systems on much longer times scales, even selfaggregation of amphiphilic molecules form aqueous media. But, of course, each simplification leads to the loss of some information about a simulated molecular system. That is why in order to get a detailed picture of an amphiphilic aggregate one should use an atomistic MD simulation.

Neutron magnetic resonance (NMR) measurements of correlation times in the micelles show that fast correlation times are in the picosecond range. That is why it is supposed that a micelle should equilibrate its structure during the MD simulation on several nanoseconds. But as the characteristic times of self aggregation are much longer, it is clear that the simulated structure would depend highly on the starting configuration.

Atomistic MD simulation was performed in order to obtain the detailed structure of the aggregates formed by trimethyl ammonium bromide (TAB) molecules on different substrates. Structures of TAB aggregates on hydrophobic and hydrophilic substrates suggested by SFM were adopted to use as the starting structures for MD simulation. Half cylindrical micelles on gold and paraffin and cylindrical micelle on gold was simulated. Cylindrical micelle in water environment was also simulated for two reasons: first to compare the simulation data with experimental data in order to establish the reliability of the simulation, and second to compare the structure of the cylindrical micelle in water with adsorbed aggregates in order to find out how the presence of the substrate affects their structure.

4.2.1 Amphiphilic molecules

The separation of two immiscible molecular components from their liquid mixture is described by the fundamental thermodynamic equations of self-assembly[8]. Equilibrium thermodynamics requires that in a system of molecules forming aggregated structures in solution like micelles the chemical potential of all identical molecules in different aggregates should be the same. For aggregates of the same type but with a different total number M of molecules this may be expressed as:

$$m_M = m_M^0 + \frac{kT}{M}\log\left(\frac{X_M}{M}\right) \qquad M=1,2,3...N... \qquad \text{eq.1}$$

where μ_M is the mean chemical potential of a molecule in an aggregate of aggregation number M and X_M is the concentration of these molecules in the aggregate. The first term of this formula m_m^0 is the standard value of the chemical potential (the mean interaction energy per molecule), the second term is the loss of entropy by aggregation. Combining of these equations for M=1 and M=N yields:

$$X_N = N\left\{X_1 \exp\left[\left(m_1^0 - m_N^0\right)/kT\right]\right\}^N \qquad \text{eq.2}$$

This equation together with the conservation relation for the total concentration in the solution $C = \sum_{N=1}^{\infty} X_N$ defines the system totally.

When m_N^0 remains constant for aggregates of different size ($m_N^0 = m_1^0$) equation 2 becomes $X_N = NX_1^N$. Since $X_1<1$ we must have $X_N<<X_1$. Hence most molecules will be in the monomer state. Aggregates will be formed when there is a difference of cohesive energy for the molecule in the dispersed phase and in the aggregated structures. For sufficiently low monomer concentration X_1 such that $X_1 \exp\left[\left(m_1^0 - m_N^0\right)/kT\right]$ is less than unity we have essentially the dispersed phase of molecules. With increasing monomer concentration micelle formation becomes more favourable. The monomer concentration $(X_1)_{crit}$ at which this occurs is called the critical micelle concentration (CMC).

$$\left(X_1\right)_{crit} \approx \exp\left[-(m_1^0 - m_N^0)/kT\right]$$

The self aggregation of amphiphilic molecules is also described by the fundamental thermodynamic equations of self-assembly. The fundamental

thermodynamic equations of self-assembly describe the equilibrium of all types of aggregates including phase separation. On the other hand the dual nature of amphiphilic molecules does not allow macroscopic phase separation. The head groups prefer to stay in contact with a polar solvent, while tail groups tend to minimise contact with solvent. This leads to the formation of aggregates where head groups are mostly concentrated on the surfaces of aggregates and tails pack in the aggregate's core.

It is well known that amphiphilic molecules may aggregate in a wide variety of different aggregate types like spherical micelles, lamellas, bilayers or even more complicated structures of interpenetrating networks of solvent and amphiphilic aggregates (Fig. 1, the figure is adopted from the book of Israelachvili[8]).

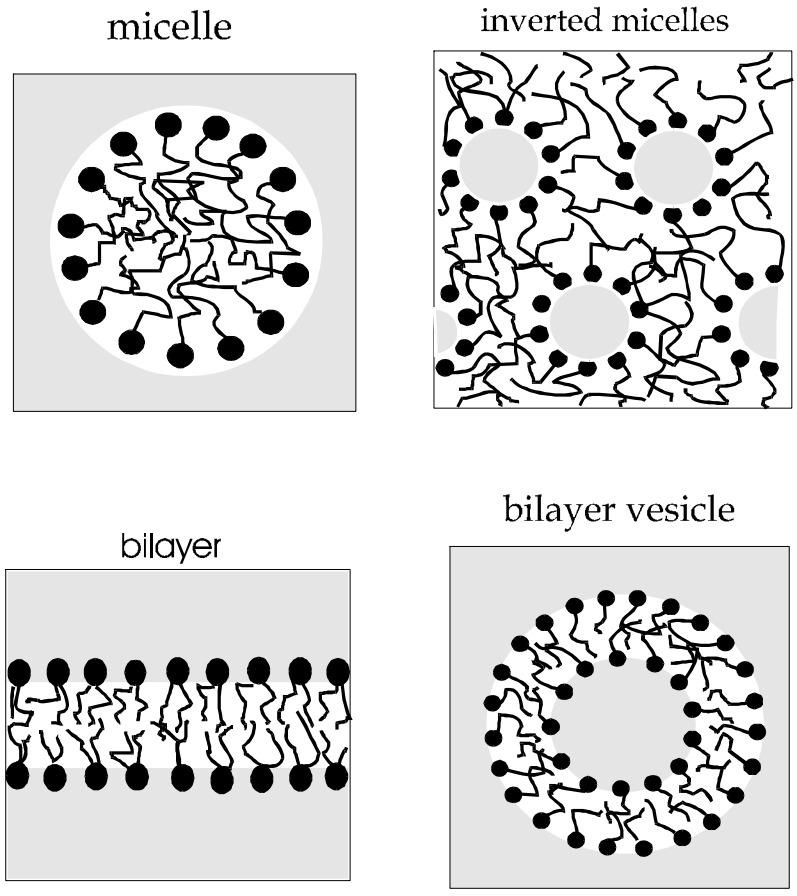

Figure 1. Examples of structures formed by amphiphilic molecules.

In most amphiphilic molecules an alkyl chain is used as hydrophobic tail. Fully saturated alkyl chains are very flexible. Each C-C bond in a fully extended alkyl chain adopts a trans state but each bond can also exist in two other conformations, the gauche$^+$ and gauche$^-$ states, which can be formed with the amount of 0.8 - 1.0 kT energy at room temperature. Therefore, a fully saturated alkyl chain possesses a large number of accessible states. On the other hand n-

alkanes are found to be in a crystalline state at room temperature. One may consider that in an aggregate the chains could also pack in an array of parallel all-trans chains, and the head groups are concentrated on two of six faces of a crystalline block and on four faces hydrocarbon chains would contact with water. Hence, it is impossible to form such an array without energetically expensive hydrocarbon-water contact. Therefore we should expect that the alkyl chains in the interior of a micelle are conformationally disordered (liquid like). This expectation is supported by NMR measurements of fast correlation times and order parameters for alkyl chains in micelles[4]. The motions of alkyl chains in a micelle can be classified by two types: fast local motions in the alkyl chain and slow motions, ascribed to tumbling of the whole aggregate and/or diffusion of the amphiphilic molecules in the micelle. The measurements reveal fast intra-chain motions with correlation times around 10^{-11} s, a value in close agreement with the correlation times calculated from similar measurements on liquid n-alkanes.

It is important to describe more detailed NMR experiments, by comparing results of MD simulations with the correlation times measured by NMR. NMR measures spin relaxation of the nuclei in the external magnetic field and provides information on the rotational motion of the atoms. In MD simulations it is better to express atom rotation in terms of rotations of the bonds, for example rotation of C-H bond in the alkyl chain. This rotation is characterised by the auto-correlation function of bond orientation: $C(t) = \langle \bar{b}(0) \cdot \bar{b}(t) \rangle / \langle \bar{b}^2(0) \rangle$, where $\bar{b}$ is the bond vector. In general a time relaxation function *C(t)* can be represented as a sum of exponentials: $\sum_i A_i \exp(-t / t_i)$, where each decay term represents different types of motion. For example in the case of amphiphilic molecules in a micelle orientation changes of C-H bonds can be due to transition between trans and gauche conformations in the alkyl chain (fast modes) or due to rotational motions of the micelle as a whole and diffusion of the heads of the amphiphilic molecules on the micelle surface (slow modes). Fast modes are in the range 1-100 ps and slow modes are in the nanosecond time regime. It is also interesting that it is possible to distinguish whether carbon atoms in the methyl group or in the alkyl chain. It is even more important that it is possible to distinguish carbon atoms in alkyl chain i.e. how far they are from the terminal group. Measurements of fast correlation times in amphiphilic micelles show that correlation times for the terminal head groups of alkyl chains are almost the same as the correlation times for the head groups of the same amphiphilic molecules in the dispersed state. The values of the fast correlation times are increasing considering carbons closer to the amphiphilic head group. The alkyl chains are anchored to the bulky head groups and therefore carbon atoms closer to the head groups loose their mobility.

The very low solubility of water in the bulk n-alkane phase (about one water molecule for each $2x10^4$ CH_2 groups[5]) allows to predict a negligible water penetration into the aggregated micelle hydrophobic core. Indeed this point of view was supported by NMR relaxation measurements[6]. Claims of experimental evidence for extensive water penetration in the core were shown to be unfounded[7]. NMR may distinguish between CH_2 group in contact with water molecules and CH_2 group in the hydrophobic core composed of alkyl chains. It was shown that there is extensive contact between CH_2 groups and water molecules, that is why it was concluded that there is extensive water penetration in the micelle core. On the other hand it was shown later that NMR results may be explained by fact that water molecules should contact with CH_2 groups from the amphiphilic molecules in dispersed phase and in addition CH_2 groups on the edge on the micelle contact with water molecules. It was shown on the basis of NMR experiments that water does not mix with alkyl chains, but there is no evidence that water can not be found in the centre of the micelle. However neutron diffraction studies[8] give the evidence that water is totally excluded from the micelle core.

Accepting the above arguments, lead to the picture that the micelle core can be considered as a non-polar liquid droplet consisting (almost exclusively) of fully saturated alkyl chains. The packing density of the chains is determined by the Van der Waals forces and chain etropy. As the chains are chemically identical to n-alkane chains, we should expect a packing density almost identical to that found for bulk n-alkane.

The standard picture of amphiphilic micelles now may be summarised in three simple points[9]:

(i) on average, each amphiphil molecule associated with a micelle has almost all of its hydrocarbon chains in the micelle core;

(ii) the ionic head-groups, ions and water are almost completely excluded from the micelle core;

(iii) the amphiphil chains are conformationally disordered (liquid like) and fill the core at approximately liquid n-alkane density throughout.

The standard picture implies that the chain-water interface is sharply defined (with an average roughness in the order of a few Å) and that the head-groups are just outside the micellar core in a layer, again with a roughness of a few Å.

While self aggregation of amphiphilic molecules in free solution is well understood. It is not clear how these aggregates are affected by the presence of a solid boundary surface. Recently the pioneering work of scanning force microscopy (SFM) imaging of surface aggregates formed by tetradecyl trimethylammonium bromide (TAB) molecules was performed[2]:

$$Br^{-}\left[\left(CH_3\right)_3 N^{+}\right]-\left(CH_2\right)_{13}-CH_3$$

The SFM method gives detailed resolution in the plan e parallel to the surface but can not resolve the thickness of an adsorbed layer. The surface force apparatus[8] allows to determine the thickness of the adsorbed layer with 0.5 Å accuracy. Hence combination of SFM imaging with surface force apparatus measurements allowed to define the shape of the structures formed by TAB molecules on different substrates. It was suggested that TAB molecules self-assemble in aggregates like spherical micelles, half cylindrical micelles or cylindrical micelles depending on the substrate.

The SMF images of the structures formed by TAB molecules on the hydrophobic substrates (graphite) showed parallel stripes, whose widths are 4.7±0.3 nm - roughly twice the length of an amphiphilic molecule and oriented perpendicular to the substrate symmetry axis. Hence alkyl tails that are supposed to be packed perpendicular to the half-cylinder symmetry axe are oriented parallel to substrate symmetry axes. The height of this structures is roughly the length of TAB molecule. These results are in a good agreement with model of half-cylindrical aggregates. The substrate symmetry axes are defined as lines connecting nearest neighbour atoms from different simple crystalline cells.

The SFM images of the structures formed by TAB molecules on hydrophilic substrates like mika show meandering stripes, which are separated by a distance slightly more than twice the length of TAB molecules, fore axample 6.0±0.5 nm on mika. Stripes did not follow consistent orientation relative to the underlying substrate lattice. The height of these aggregates determined with surface force apparatus was roughly twice the length of fully extended TAB molecule. Full cylindrical micelles model was proposed. It was supposed that cylindrical micelles may be flattened at the substrate bottom to allow a better contact area between head-groups and the surface. Flattening of the cylinders may also explains why the spacing between full cylinders is slightly higher than the spacing between half cylinders.

The adsorption of amphiphilic molecules from solution onto metals received some attention in the past as a method of controlling electrochemistry [1] at electrode surfaces and a way of limiting corrosion of metal surfaces. AFM scanning of structures formed by TAB molecules and TAOH - where the Br^- ion is substituted by OH^- group - on gold was performed[9]. It was suggested that TAB molecules form full cylindrical micelles on gold substrate, while TAOH molecules form half cylindrical micelles. This phenomenon was explained by the presence of halide ion in TAB molecule. It is well known that gold can strongly adsorb both organic molecules and halide ions from aqueous solution. It was supposed that during adsorption of TAB molecules on the gold surface

halide ions adsorb preferentially on the gold surface producing a hydrophilic surface. Then the TAB molecules can form full cylinders to bring the head groups in contact with adsorbed Br^- ions.

The SFM method provides valuable information on the shape of the adsorbed aggregates of amphiphilic molecules, but it does not provide any information either on the detailed structure i.e. the organisation of the amphiphilic molecules in these aggregates nor on the dynamic properties. There are few experimental techniques which provide information on structures adsorbed on the surface. Neutron reflection experiment provide high resolution in the direction perpendicular to the adsorbate surface but do not yield any structural information in the plane parallel to the surface. It is interesting to combine neutron reflection with SFM results because SFM on the other hand provide very good resolution in the plane of the surface but very poor resolution in the direction normal to the surface. Neutron reflection experiments were performed on the structures formed by TAB molecules on silica. It was suggested that TAB molecules form bilayers with 32±1 Å thickness, while the length of fully extended TAB molecule is 25 Å. That is why the model of a bilayer with interpenetrating tails was proposed. It was also found that about 10 % of the bilayer is occupied with water. The SFM imaging of structures formed by TAB molecules on silica showed circular structures. Hence the model of spherical aggregates was proposed on the basis of SFM data. Combining neutron reflection with SFM imaging one may propose spherical aggregates very pressed toward the surface. Experimental methods like nuclear magnetic resonance or neutron scattering provide information on bulk materials but can not determinate signal from the thin layer of amphiphilic molecules at the solid-liquid interface beyond noise.

4.2.2 **Model**

The present limitation of MD simulation is the length of simulation time. The characteristic times for aggregation of amphiphilic molecules are in the seconds time range or even longer. MD simulation allow to trace the time evolution of a system on a nanosecond range only. It is therefor impossible to see the aggregation of amphiphilic molecules from a polydispersed phase. That is why one should create these molecular systems in conformations which are closely related to experimentally established molecular structures. The SFM experiments on imaging of structures formed by TAB molecules on different substrates were taken as the starting point for computer simulation.

Four conformations were constructed and considered as starting structures for MD simulation: 1. a cylindrical micelle of TAB molecules in water environment, 2. a half cylindrical micelle on gold substrate in water environment, 3. a half cylindrical micelle on paraffin substrate in water environment and 4. a cylindrical micelle on gold substrate in water environment.

1. Cylindrical micelle of TAB molecules in water environment:

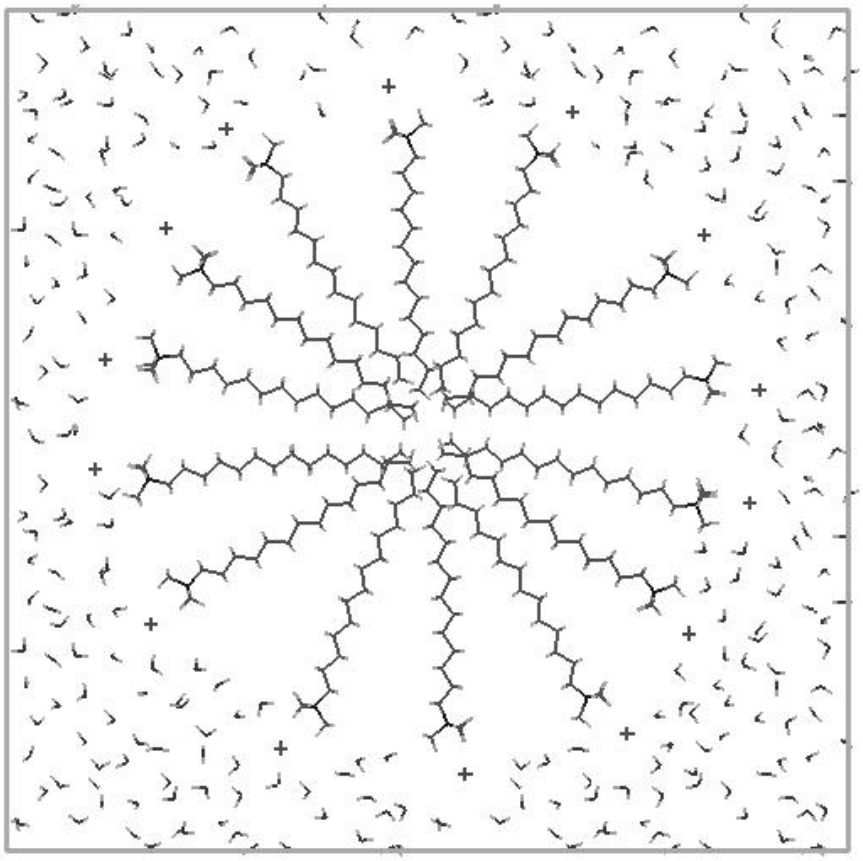

Figure 2. Starting structure for cylindrical micelle in water environmen t.

The diameter for the starting structure of a cylindrical micelle was chosen to be the same as the diameter of a half cylindrical micelle of TAB molecules on a graphite substrate[2], i.e. 4.8 nm. The head groups of TAB molecules were placed on the micelle surface, while the tails of the TAB molecules were completely stretched toward the centre of micelle. The cylindrical micelle constructed this way exhibits a low density at the periphery and a high density in the centre, due to the initially stretched tails. The average density of the TAB molecules in the micellar system was set to 0.9 g/cm^3 resulting in 0.81 g/cm^3 average density of the micelle core composed of alkyl chains. The length of cylindrical micelle was set to 25 Å with the use of periodic boundaries. The micelle was placed in water environment with distance of the micelle edge to the simulation cell border of 5 Å and with nearest distance of micellar periodic

image of 10 Å (Fig 2.). It is important to notice that during MD simulation with constant pressure condition size and hence density of the system could change. The pressure was controlled as stress with diagonal elements of stress tensor equal to pressure and zero non-diagonal elements. Cell sizes could vary independently during MD simulation.

The cylindrical micelle of TAB molecules in water environment was subjected to energy minimisation and then MD simulation was applied. For the first 100 ps of MD simulation NVT (Number of particles, Volume and Temperature were constant) conditions were chosen. It was important to choose constant volume, because it allowed to equilibrate the high density in the centre of the micelle. Constant pressure conditions has lead to an instability of MD simulation – high energy deviations. Then the structure was equilibrated at the temperature 300 K for 200 ps under NPT conditions (Number of particles, pressure and temperature were constant) and subject to simulated annealing for another 100 ps at a temperature of 500 K. A pressure was set to 1 bar. After annealing of the cylindrical micelle MD simulation was done with NPT conditions at a temperature of 300 K for 1.6 ns. In total the cylindrical micelle was simulated over 2 ns.

2. Half cylindrical micelle of TAB molecules on the gold substrate

The diameter for the starting structure of the half cylindrical micelle was set to 4.6 nm, which is the same as the experimentally established width of half cylindrical micelles formed by TAB molecules on the graphite substrate [2]. The height of the half cylindrical micelle was set to half of the value of the micelles width. The gold substrate was constructed with (111) contacting surface, and was 10 Å thick. The head groups of TAB molecules were placed on the micelle surface, while tails of TAB molecules were stretched toward the micellar centre. The average density of the amphiphils in the micelle was set to 0.9 g/sm [3]. The surface of the half cylindrical micelle, in contact with the gold substrate, was constructed as the layer of TAB molecules. The molecules were placed parallel each other and parallel to the surface of gold. Alkyl tails of TAB molecules were oriented parallel to a gold symmetry axe. The system of gold substrate and half cylindrical micelle was placed in water. Distance between the top of the micelle and periodic image of the gold surface was set to 15 Å (Fig 3.).

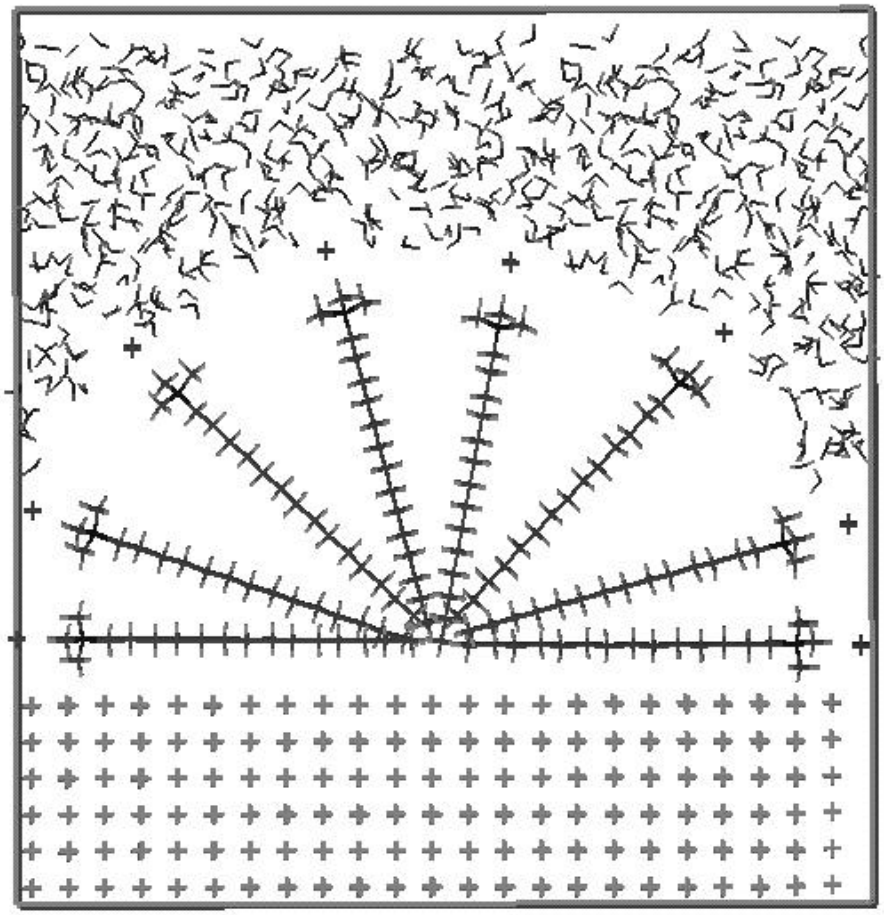

Figure 3. Starting structure for half cylindrical micelle on gold substrate in water environment.

The half cylindrical micelle on the gold substrate in a water environment was energy minimised and then a MD simulation was started. The system was equilibrated at a temperature of 300 K for 50 ps under NVT conditions and for the next 50 ps under NPT conditions. The half cylindrical micelle was then annealed for 100 ps at a temperature of 500 K. After annealing of the molecular system a MD simulation was performed with NPT conditions at a temperature of 300 K and 1 Bar pressure for 1.8 ns.

3. Half cylindrical micelle of TAB molecules on paraffin substrate

In order to save CPU time used for the equilibration of the molecular system the output structure after a 500 ps of MD simulation of the half cylindrical micelle of TAB molecules on the gold substrate was used to construct a half cylindrical micelle on a paraffin substrate. The gold substrate was replaced by paraffin substrate. The (100) crystallographic plane of paraffin was chosen to contact with the half cylindrical micelle. The paraffin substrate was placed with matching of its symmetry axe with the symmetry axe of the gold substrate. The water molecules were not changed.

The half cylindrical micelle on the paraffin substrate was energy minimised and then treated by MD simulation. The structure was first

equilibrated at a temperature of 300 K for 100 ps and then simulated annealing at 500 K temperature was done for 100 ps time. After annealing of the molecular system MD simulation with NPT conditions at the temperature 300 K was performed for 1.3 ns. Paraffin substrate was kept fixed.

4. Cylindrical micelle of TAB molecules on gold substrate in water environment.

In order to save CPU time the atomic coordinates after a 500 ps of MD simulation of the cylindrical micelle of TAB molecules in water was used to construct a cylindrical micelle on the gold substrate. For that purpose the water environment was partially removed and replaced by the gold layer with a (111) contacting crystallographic plane as contact surface. The cylindrical micelle was put about 3 Å above the gold surface. The layer of gold was constructed with 10 Å thickness. An additional layer of water of 5 Å thickness was added in between the cylindrical micelle and the periodic image of gold in order to prevent contact of cylindrical micelle with the periodic image of the gold substrate.

Cylindrical micelle on the gold substrat e in water solution was energy minimised and then treated by MD simulation. The molecular structure was equilibrated at a temperature of 300 K for 100 ps of time and then annealed at 500 K for 100 ps. After annealing the molecular system was subjected to MD simulation with NPT conditions at 300 K for 800 ps.

4.2.3 **Results**

Cylindrical micelle in water environment.

A snapshot of the structure of the cylindrical micelle of TAB molecules in water environment after 2 ns of MD simulation is presented in figure 4.

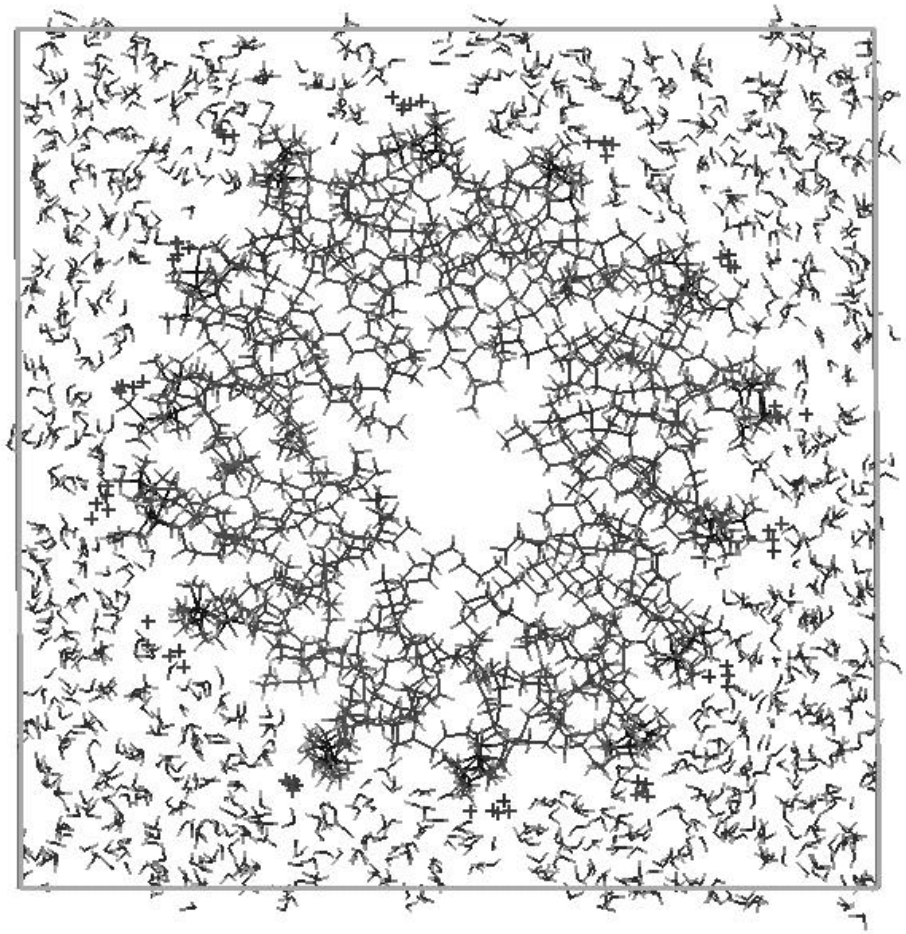

Figure 4. Cylindrical micelle in water environment after 2 ns of MD simulation.

The initial cell size of the system of was 60x60x25 Å and the micelle had a diameter of 49 Å and was 25 Å long. The length of the micelle matched with the cell size in z direction. The micelle diameter was determined by the overall distance of the bromine ions. The MD simulation did not change cell sizes significantly; the cell size fluctuated on opposite positions around initial values, and after 2 ns of MD they were 59.8x59.8x25.1 Å. The diameter of the micelle also did not change drastically; after 2 ns of MD it increased from 49 Å to 50 Å. It is easy to define the diameter for the starting structure of cylindrical micelle. However it is difficult to measure it after MD simulation since the surface roughness of the micelle is of order of several Å, and can thus lead to uncertainties of the micelle diameter in the order of 1-2 Å. Interestingly the change from 49 Å to 50 Å results in a change of the micelle core density composed of the hydrophobic alkyl chains from the initial value of 0.81 g/cm ^{3} to 0.74 g/cm^3, as compared to the density of liquid N-alkanes which is 0.63 pentane, 0.7 octane and density of amorphous polyethylene is 0.855 g/sm ^{3}. While the shape of the micelle and size did not change drastically, the micelle structure changed significantly. Initially stretched alkyl chains adopted a random orientations during the minimisation and first several hundreds pico-seconds of MD simulation. The order parameter that characterise the regularity in the structure of the micelle core will be introduced later.

The most striking feature of the structure of the MD simulated cylindrical micelle is the inhomogeneous density of the hydrophobic micelle core composed of the hydrophobic alkyl tails. The alkyl chains did not fill completely a centre region of the micelle of about 4±1 Å in diameter. A plot of the micelle core density versus the distance from the micelle centre is presented in figure 5a. The density profiles were averaged for structure snapshots made each 25 ps over the last 500 ps of MD trajectory.

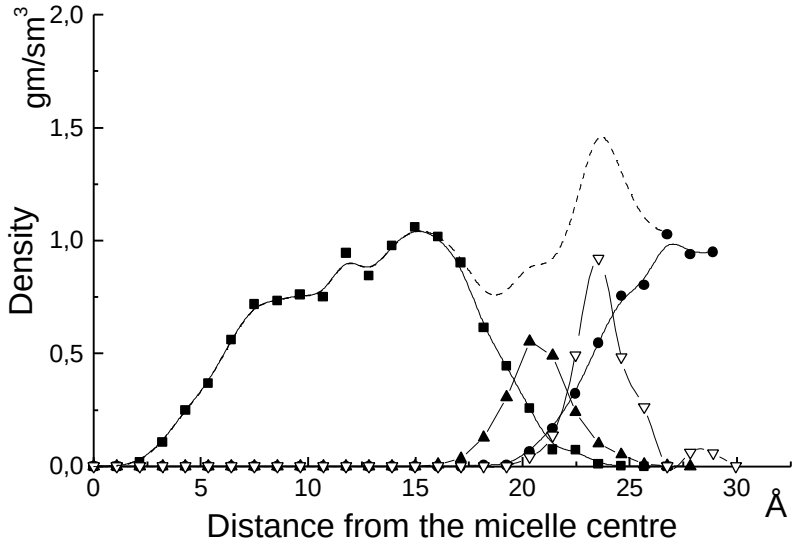

Figure 5. Density distribution functions in cylindrical micelle in water plotted vs the distance from the micelle centre: a) ¦ : density of the hydrophobic core composed of alkyl chains; b) ? : head groups ($N^{+}\left(CH_3\right)_3$), c) ∇ - density of the Br^- ions; d) ? - density of the water and e) --- - density of the total molecular system of the cylindrical micelle of TAB molecules in water.

Clearly during 2 ns of MD simulation water did not diffuse into the micelle core (Fig 5a and 5d). Instead the water formed a perfect shell around the micelle. No water tentacles or single water molecules were penetrating into the micelle core. The roughness of the water shell corresponds to the roughness of the surface of the cylindrical micelle which is roughly 2-3 Å. The head groups and Br^- ions sit between the hydrophobic core and water (Fig 5b and 5c respectively). Br^- ions stay attached to the surface of the micelle (Fig 5b and 5c).

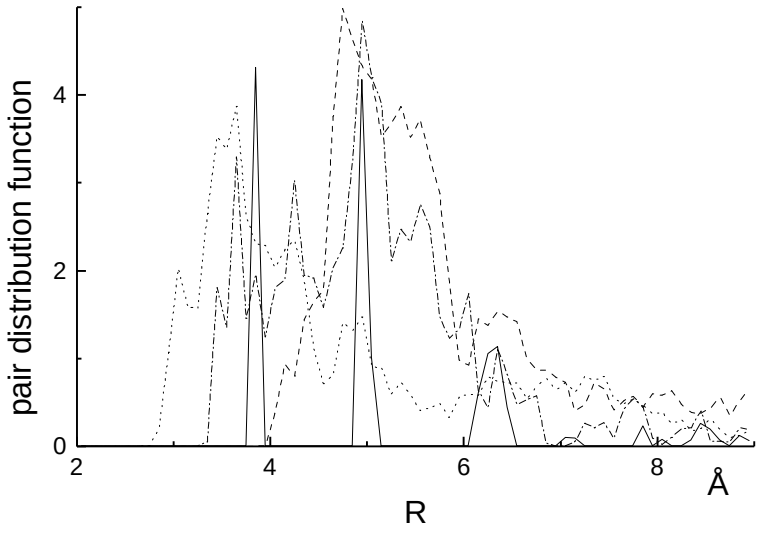

Figure 6. Pair distribution functions of the Br^- and N^+ ions in cylindrical micelle. a) solid line: pair distribution function for initial configuration of the subset of Br^- and N^+ ions (Br - Br, N - N and Br - N pair distribution functions), the first maximum is the Br - N distance in the dipole and second is the Br - Br or N - N distance, hence inter-dipole distance; b)-e) pair distribution functions after 2 ns: b) dotted line: Br - N pair distribution function; c) dashed line: N - N pair distribution function; e) dashed-dotted line: Br - Br pair distribution function.

Initially the micelle was constructed with Br^- - N^+ dipoles forming regular rows oriented along the micelle axe. After 2 ns of MD simulation the rows of Br^- - N^+ ions still can be recognised on the surface of the micelle. Figure 6 demonstrates the arrangement of Br^- - N^+ dipoles. The curve 6a presents the pair distribution functions of Br^- and N^+ ions for the initial configuration. The first maximum corresponds to the Br^- - N^+ dipole distance and the second to the inter-dipole distance in a row. The curves 6.b-e present the pair distribution functions of Br^- and N^+ ions for the micelle after 1 ns of MD simulation. We may see that both maximums can still be recognised well demonstrating the clustering of Br^+- N^- dipoles. In order to obtain the pair distribution function for the MD simulated structure, snapshots of the half cylindrical micelle on paraffin were saved every 0.5 ps and then pair distribution functions for each snapshot were averaged over the last 500 ps of the MD trajectory. Diffusion coefficient for the Br^- - N^+ ions is lower then 0.08 $Å^2$/ns. The diffusion coefficient was determined from the mean square displacements of the Br^- and N^+ ions: $6Dt = <\left(\left|\bar{r}_i(t) - \bar{r}_i(0)\right|\right)^2>$, where D is the diffusion coefficient and $\bar{r}_i$ are the spacial positions of the ions.

To compare the dynamic of alkyl chains in the micelle core from NMR measurements of fast correlation times [4], t_c^f, fast correlation times were estimated from the auto correlation functions of C-H bond orientation: $C(t) = \langle \bar{b}(0) \cdot \bar{b}(t) \rangle / \langle \bar{b}^2(0) \rangle$, where $\bar{b}$ is the vector of C-H bond orientation. From the definition of the auto-correlation function it follows directly that

$C(t) = \langle \cos(a(t)) \rangle$, where $a(t)$ is the angle between the bond vector at time zero and the bond vector at time t. For simple systems like a solvent of small molecules as for example water. The bond auto-correlation function displays a single exponential decay form $\exp\left(-\frac{t}{t}\right)$, where t is the characteristic time for the average rotational motion of water molecules. In general, $C(t)$ decays as a sum of several exponentials, where each term represents different types of motion of the C-H bonds. For example in the case of amphiphilic molecules packed into a micelle the C-H bond can loose its initial orientation: 1) due to the changing of C-C-C torsional angle in the alkyl tail (trans-gosh transitions) 2) due to the diffusion of the head groups on the surface of a micelle and the rotation of the micelle. The characteristic time for the first type of motion is in the pico-second time regime - fast correlation times, while the second type is in the nanosecond time regime - slow correlation times. Because of the large difference between slow and fast correlation times we may determine a fast correlation time by fitting the correlation function on the time of 50-100 ps using a single exponential, where A represents slow motions and is almost independent on time scale of pico-seconds.

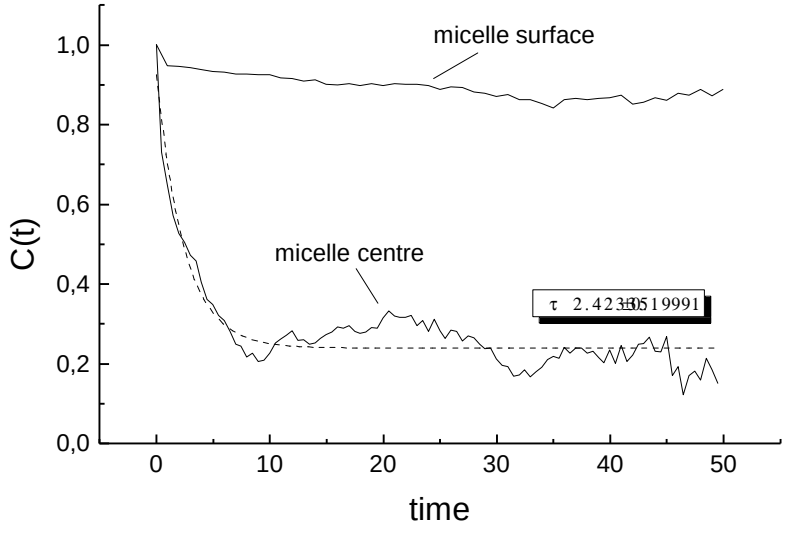

Figure 7. Correlation functions of the terminal methyl groups that are picked: a) from the centre of the micelle and b) from the micelle surface. The dashed line is the best fit of the curve a) with decay law $y = y_0 + A\exp(-x/t)$, and realxation time τ 2.4±0.2 ps.

The main problem in the interpreting fast correlation times arises because in NMR experiments fast correlation times are plotted for the different carbon atoms vs their positions in the alkyl hydrophobic tails. The motion of carbon atoms in amphiphilic molecules in a dispersed phase depends on the position of the carbon atoms with respect to the bulky head group, carbons close to the head group move slower. The motion of carbon atoms in amphiphilic molecules packed in a micelle depends not only on their position in the alkyl chain but also

on their position in the micelle. Parts of alkyl tails move faster in the centre of a micelle and slower, when they are close to the micelle surface, where their motion is hindered by the bulky head groups, which are mostly concentrated on the surface. Of course, the ends of alkyl chains have a higher probability to be in the centre of the micelle but they could be found as well on the surface of the micelle. Figure 7 presents correlation times for the carbons of the terminal methyl groups picked from the centre of the micelle 7.a and from the surface of the micelle 7.b. The position of carbon atoms in the centre or on the edge of the micelle was determined visually.

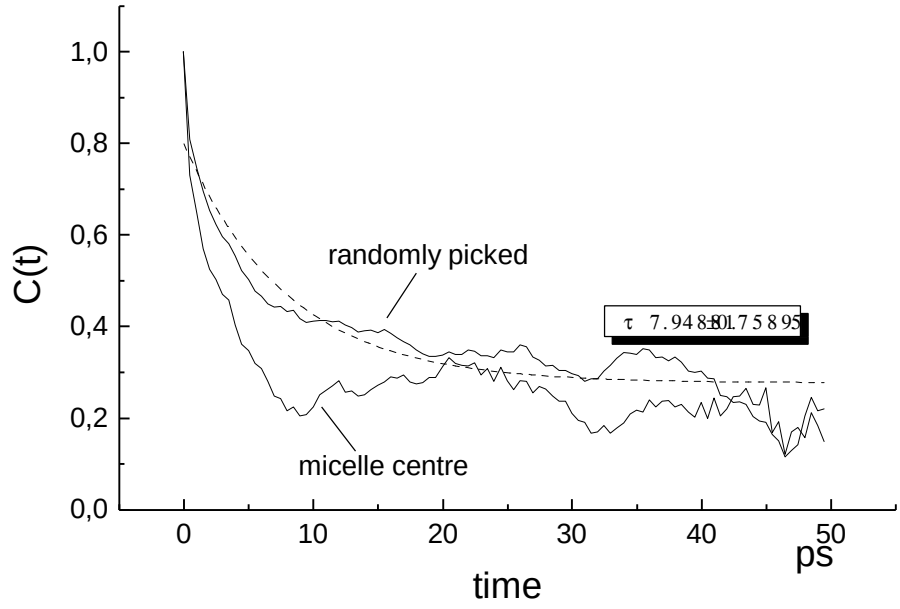

Figure 8. Correlation fun ction for the terminal methyl groups that are picked a) randomly and b) from the centre of the micelle. The dashed line is the best fit of the curve a) with single exponent and the decay term τ (relaxation time) is 7.9 ±0.8 ps.

One can observe indeed that the relaxation times for these two cases are quite different: for the carbon atoms of the alkyl tails in the micelle centre τ=2.4±0.2 ps and for the case at the micelle surface where it is difficult to determine the correlation time exactly. The relaxation time is obviously much longer than 2.4 ps. The correlation function of carbons from all terminal methyl groups *C(t)* is an integral of the correlation function *C(t,r)* over all positions *r* of the carbons in the micelle with a weight $r(r)$ given by the probability to find the carbon on the given distance from the micelle centre: $C(t) = \int_0^\infty C(t,r)r(r)dr$. It is clear that *C(t)* cannot be described just by one decay exponential. Figure 8 presents the correlation function for the terminal methyl groups picked randomly within the volume of the micelle; the correlation function for the terminal methyl groups from the centre of the micelle is drawn for comparison. The

relaxation time for the correlation function of the terminal methyl groups picked randomly is $\tau = 7.9 \pm 0.8$ ps.

NMR experiments give just one averaged relaxation time for each carbon atoms in the alkyl tail. Therefore in order to compare the MD simulation data with NMR data a single relaxation time was computed from the correlation functions by fitting it with a single exponential. Each correlation function was averaged over more than 30 randomly picked carbon atoms and averaged over the last 200 ps of the MD trajectory. The relaxation times were computed from the correlation functions by fitting them with a single exponential using the data from trajectories of 50 ps length. The correlation functions were calculated for different carbon atoms in the alkyl tails. It was possible to evaluate relaxation times just the last 5 carbon atoms in the alkyl tail, because carbon atoms close to the head group move too slow to determine their relaxation times on the time scale of the MD simulations (Fig. 9).

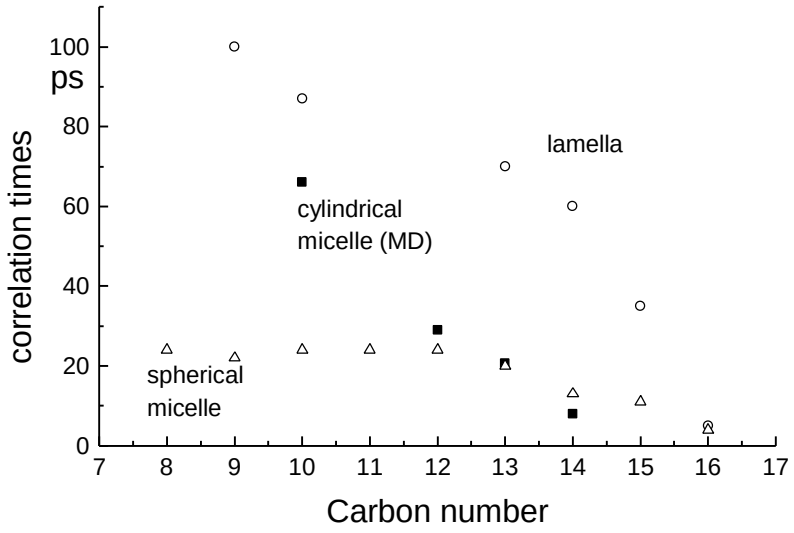

Figure 9. Relaxation times. Filled squares (¦): correlation times for MD simulated cylindrical micelle of TAB molecules. Open circles (?): experimental relaxation times for PPALM lamella ($CH_3 - \left(CH_2\right)_{14} - CO^- K^+$). Open up-triangles (?): experimental relaxation times for PPALM spherical micelle.

The order parameter of the cylindrical micelles also cou ld be compared with experimental results. The order parameter is defined as $S \equiv 0.5(3 \cdot < \cos^2(\Theta) > -1)$, where θ is the angle between the surface normal and the C-H bond vector in an alkyl chain. NMR experiments yield the dependence of the order parameter on the position of a carbon atom in the alkyl chain. The modulus of the order parameter micelle is plotted on Fig 10 for MD simulated cylindrical. Experimental order parameters for spherical micelles and lamellas are added on the same figure.

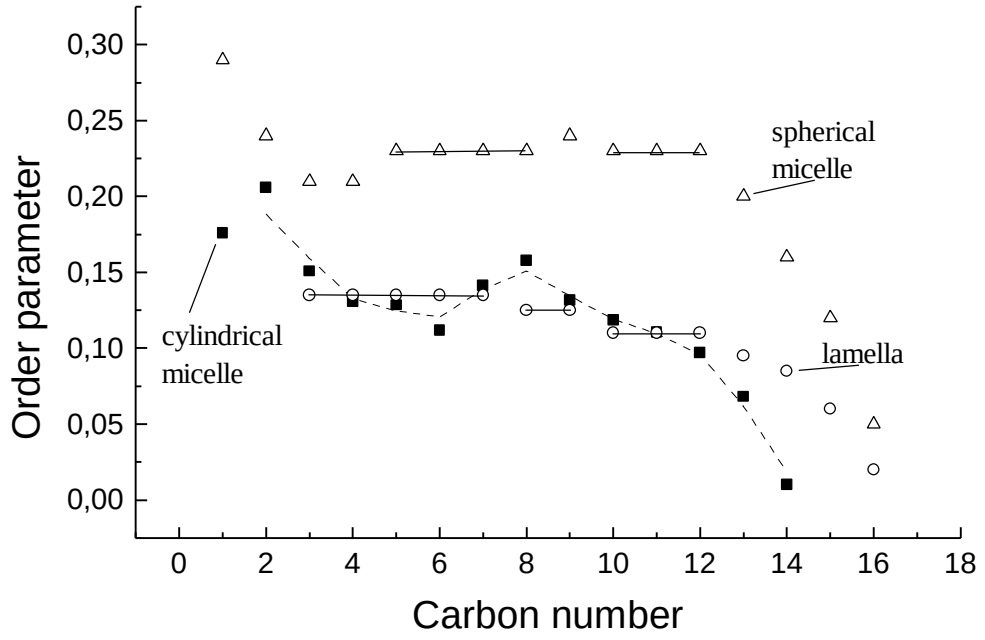

Figure 10. Order parameters S open symbols - experiments, closed symbols - simulated data. Filled squares (¦): order parameter from MD simulation of cylindrical micelle of TAB molecules. The dashed line is a line guide for eyes. Open circles (?): experimental order parameter for the lamella phase of SOBS molecules $(Na^{+}SO_3^{-}\langle\bigcirc\rangle\text{-}(CH_2)_7\text{-}CH_3)$. Open triangles (?): experimental order parameter for the micelle phase of CTAC molecules $(Cl^{-}N^{+}(CH_3)_3-(CH_2)_{15}-CH_3)$.

The dependence of the order parameter on the carbon number was calculated as on averaged over 10 snapshots of the last 300 ps of MD simulation. There are no experimental data for the order parameter of structures of amphiphilic molecules adsorbed on different substrates available. We have modified the order parameter for the MD simulated structures adsorbed on different substrates. It allows to show the influence of the substrate on the aggregated structures. The angle Q was defined as the angle between the C-H bond and the normal to the substrate surface and it was calculated as the function of the distance from the surface. Figure 11 presents the modified order parameter S_m for the cylindrical micelle in water defined for the structures adsorbed on the different substrates. The substrate surface normal was defined as a vector perpendicular to the cylinder symmetry axis. Because of the isotropy of the vector normal to the cylinder surface, the order parameter was averaged over different orientations of the vector.

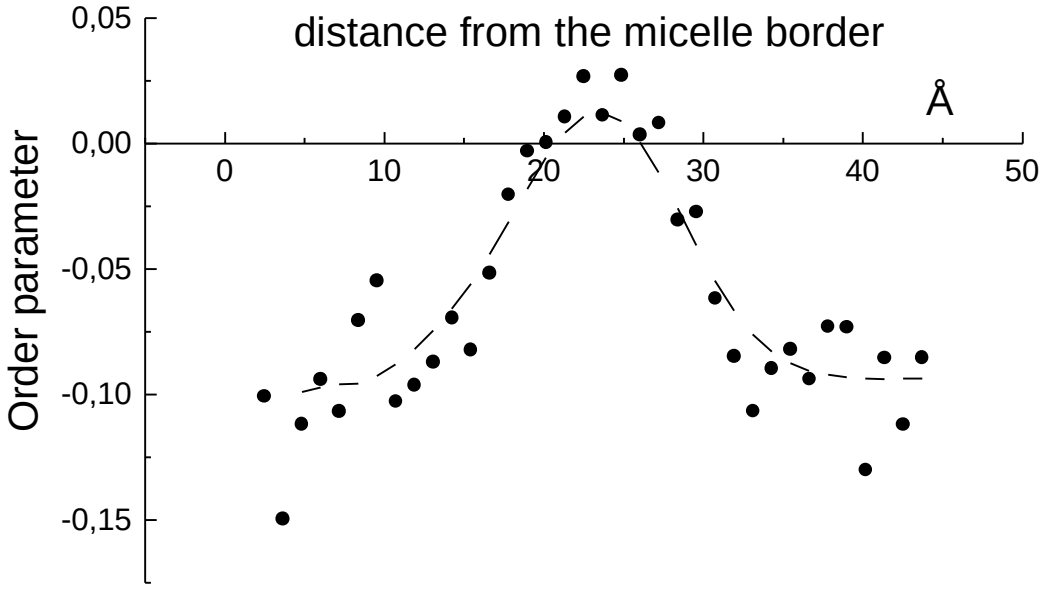

Figure 11. Modified order parameter S_m for a cylindrical micelle of TAB molecules plotted vs the distance from an edge of the micelle.

The small-angle neutron scattering technique (SANS) can provide information on the cross-section of structure of micelles in terms of a radial scattering density distribution, which is proportional to the averaged scattering lengths <b> of all elements in the volume involved in the averaging. The radial scattering density was calculated from MD simulations for cylindrical micelle by averaging of scattering lengths over atoms that fall in a volume element $\Delta V \sim \Delta r$, and then it was normalised to the volume ΔV, which is proportional to r, the distance from the micelle centre. The plot of <b> versus the distance from the centre of the micelle is displayed in figure 12, for protonated micelle (a) and deuterated micelle (b). Each curve was averaged over more than 30 snapshots from the last 500 ps of MD simulations. The difference between radial scattering densities form protonated and deuterated micelles is explained by the large difference between the scattering lengths of hydrogen and deuterium: b_H=-0.374 and b_D=0.667 . The scattering length of carbon b_C=0.665 is almost twice the scattering length of hydrogen and has the opposite sign. That is why scattering density of CH_2 groups is almost zero and the scattering density of a protonated micelle is determined mostly by distribution of the terminal methyl groups. The scattering length of deuterium is positive and the scattering density of deuterated micelle is much higher than for a protonated one and better reflects the actual micelle mass density.

	CH_2	CH_3	CD_2	CD_3
|<b>|	0.083	0.457	1.999	2.666

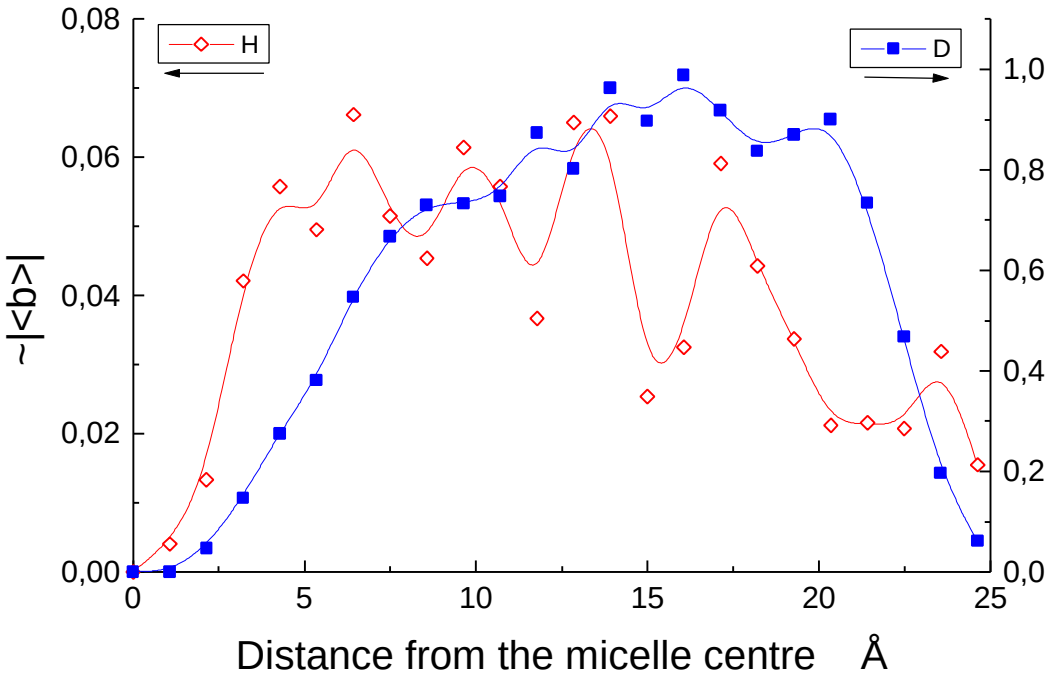

Figure 12. Radial scattering density distribution function for a cylindrical micelle of TAB molecules simulated in water. a) ? - micelle with hydrogens, b) ¦ - all hydrogens were substituted by deuteriums. Both curves where scaled so that curve b) would be unity at its maximum.

The calculated scattering density for a protonated cylindrical micelle is highly fluctuating. The reason is almost zero scattering density. In order to demonstrate that the scattering density of a protonated micelle is determined mostly by the distribution of terminal methyl groups, the scattering density of a protonated micelle and the distribution of terminal methyl groups are plotted in one figure (Fig. 13). Just one experimental paper was found where the scattering cross section of a protonated cylindrical micelle was deduced from a SANS experiment[14]. The scattering cross section of the cylindrical micelle formed by egg yolk lecithin molecules was calculated from neutron scattering intensities. The structure of the lecithin molecule is quite complicated: it has a complicated head group, two alkyl tails with C_{15} and C_{17}, which is comparable to the length of the alkyl tail in TAB molecules. The fact that lecithin molecules form cylindrical micelles allows to suggest that the structure of the hydrophobic core of the cylindrical micelle formed by TAB molecules and by lecithin molecules should be compared. That is why to figure 13 also the scattering cross section of a protonated cylindrical micelle of lecithin molecules was added.

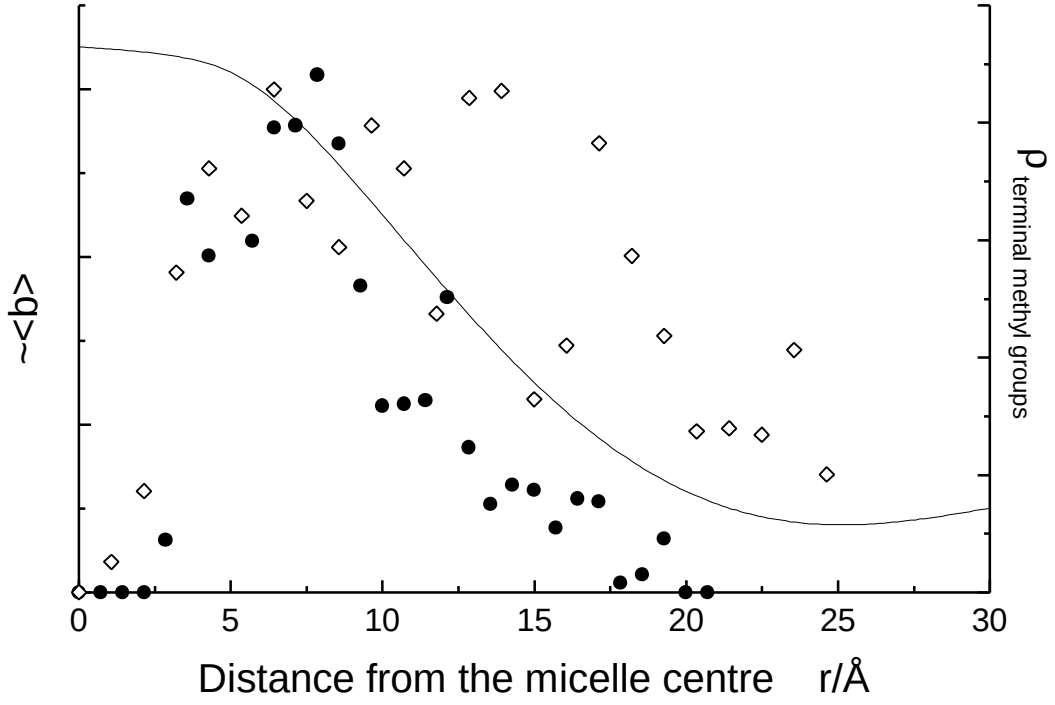

Figure 13. a) ?- radial scattering density for MD simulated cylindrical micelle, b) ? - radial distribution of the terminal methyl groups for MD simulated cylindrical micelle and c) — - radial scattering density deduced from neutron scattering from cylindrical micelles formed by egg yolk lecitin [14]. All profiles were scaled in order to fit to one graph.

It is interesting to notice that the scattering cross section of the MD simulated cylindrical micelle and the experimental scattering cross section of the cylindrical micelle formed by lecithin molecules grow from the edge of the micelle to the centre. The MD simulated scattering cross section peaks at about 5-6 Å from the micelle centre and drops to zero scattering density at the micelle centre, while the experimental scattering cross section bends at the distance 5-6 Å from the centre and has a maximum at the micelle centre.

SANS measures the distribution of terminal methyl groups in the micelle, which is defined as the probability density to find a terminal methyl group at a given distance r from the micelle centre $P(r)$. If the probability to find the terminal methyl group on the r distance from the micelle centre is $r(r)$, then the volume weighted probability density for a cylindrical micelle is $P(r)=rCr(r)$, where C is a normalisation constant. The probability density for the terminal methyl groups for a cylindrical micelle of TAB molecules calculated for a MD simulated structure is plotted in figure 14. The data were averaged over 7 snapshots from the last 800 ps of MD trajectory. Averaging over more snapshots did not make sense as the distribution of the terminal methyl groups does not change significantly over 100 ps.

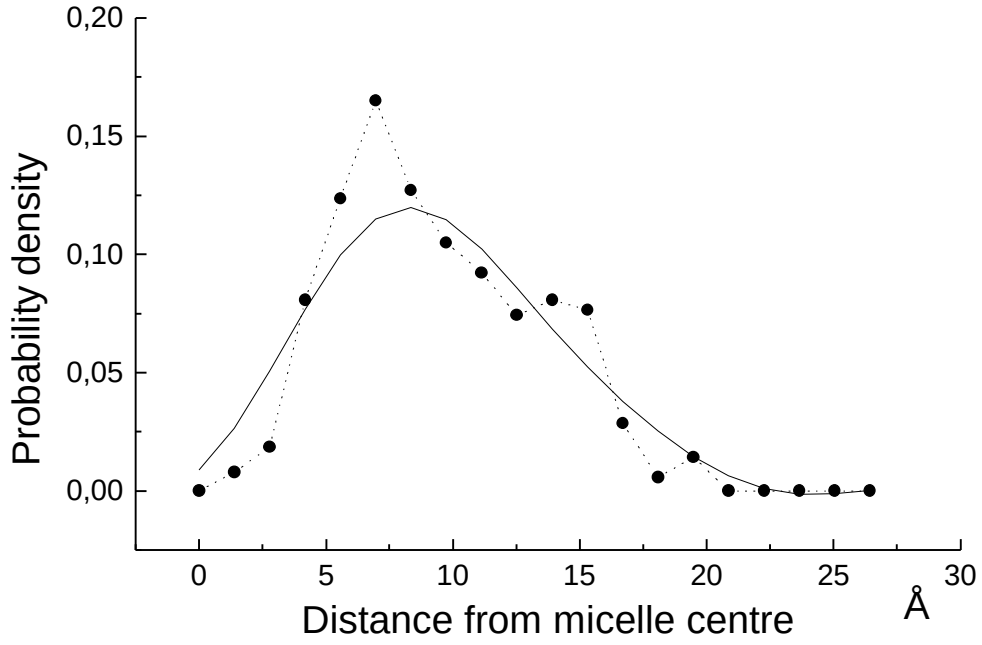

Figure 14. Volume weighted probability density P(r) versus the distance from micelle centre *r*. Full circles connected by the dotted line are the data of a MD simulation of a cylindrical micelle of TAB molecules. The solid line is the FFT smoothing.

Experimental data for *P(r)* of cylindrical micelles, could not be found, only data for spherical micelles formed by LDS molecules ($CH_3-(CH_2)_{11}-SO_4^-Li^+$) were available. The radii of a LDS micelle and a MD simulated TAB cylindrical micelle are comparable: the mean radius of LDS micelles is 18.9 Å, while the mean radius of a MD simulated cylindrical micelle is roughly 20 Å. In order to compare results of MD simulation for a cylindrical micelle with experimental results for the spherical micelles, the data of the MD simulation were corrected for the shape of the micelle and for the polydispersity of the micelle sizes in the experiment. It was established that the experimental data could be explained taking into account the polidispersity of the micelle sizes approximated by a gaussian distribution. In order to correct the distribution of terminal methyl groups of the MD simulated structure for the polydispersity of micelle sizes it was assumed that the distribution of terminal methyl groups in micelles of different sizes could be scaled as $r(r\cdot\frac{R}{R_0})$, where R_0 is the mean micelle radius and R is the current micelle radius and $r(r)$ is the distribution for the micelle with the radius R_0. Integration over all radii R with a weight given by a gaussian function $\frac{1}{\sqrt{2p}\,d}\exp-\frac{(R-R_0)^2}{2d^2}$ gives the distribution of terminal methyl groups measured with the SANS experiment. The volume weighted probability has square dependence on the distance from the micelle centre for the spherical micelle and a linear dependence for the cylindrical micelle. The data of MD

simulation with polydispersity correction were multiplied by the distance from the micelle centre to compare MD data for a cylindrical micelle with the experimental data on spherical micelles. MD simulation data of a cylindrical micelle of TAB molecules with polydispersity correction and shape correction is presented in figure 15.

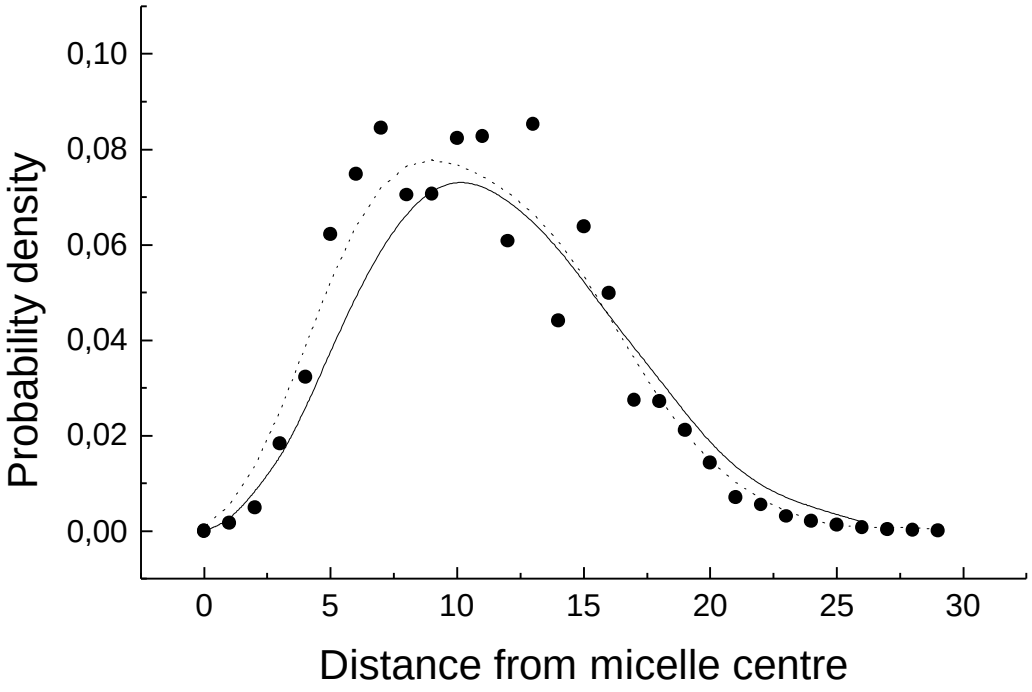

Figure 15. Volume weighted probability density *P(r)*. ? - MD data corrected to polydispersity add to shape. ···· - FFT smoothing of MD data. — - the experimental data for micelles of LDS molecules ($CH_3-(CH_2)_{11}-SO_4^-Li^+$) with the radius of the hydrophobic core 18.9 Å. (For comparison the radius of the hydrophobic core of the MD simulated cylindrical micelle is roughly 20 Å.)

Half cylindrical micelle on the gold substrate in water environment.

As mentioned above, in order to save computational time and to avoid possible artefacts the substrates were fixed. In the case of half a cylindrical micelle on gold, the substrate was involved in the MD simulation for the first 200 ps. It stayed more or less unperturbed for 100 ps and then started to form domains, where in each domain crystallographic planes of gold were slightly rotated with respect to the same crystallographic planes in the other domains. Bulk gold was simulated to compare it with the thin layer of the gold substrate. The simulation of bulk gold was carried out for 100 ps and bulk gold was obviously much more stable, hence the instability of the gold substrate was induced by the influence of the amphiphilic aggregate from one side and water from the other side. After 200 ps gold substrate was replaced with the gold from the initial configuration and kept fixed.

The initial size of the amphilic aggregates on different substrates was set as close as possible to the experimentally measured sizes. The exact matching with experimentally established size was impossible because the cell size was dictated by the substrate crystalline structure. Fixing of the substrates fixed as well the two cell size dimentions defined by substrate, yet the third dimension was not fixed. For simplicity unfixed dimension will be called the z – axis. The initial value of the z cell size of the half cylindrical micelle on gold was set to 50 Å and it did not change significantly with time, after 1.6 ns of MD simulation it was 50.1 Å. The height of the half cylindrical micelle changed from 20.6 Å to 24±1 Å, with the error bar defining the fluctuation of the micelle height. The height was defined as the distance from the micelle atom that is the closest to the gold substrate to the micelle atom that is most far from the surface. The shape of half cylindrical micelle did not change significantly.

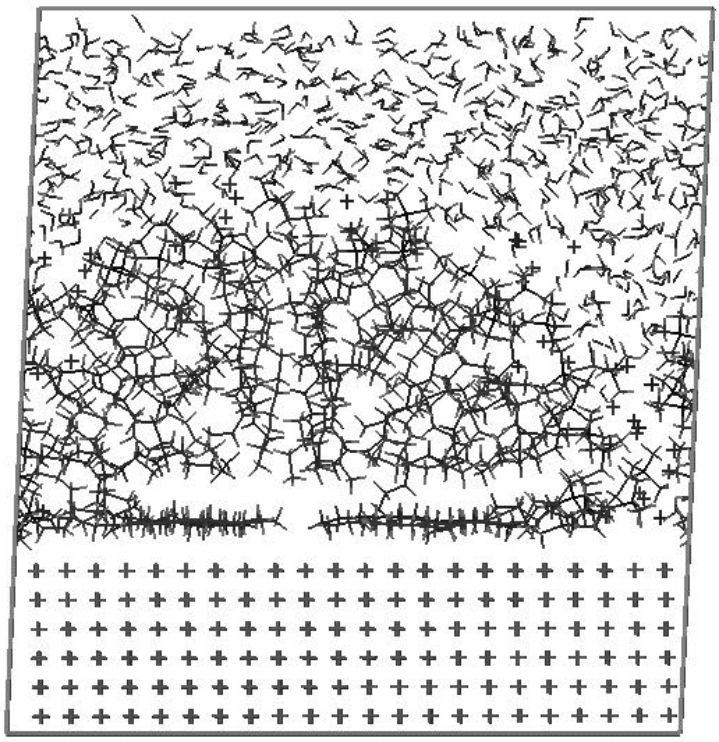

Figure 16. Snapshot of a half cylindrical micelle of TAB molecules on a gold substrate in water environment after 1.5 ns of MD simulation.

It is possible to definitely conclude that water molecules did not diffuse into the hydrophobic core of the half micelle composed of the alkyl chains, and that the alkyl chains did not leave the micelle core (Fig 17.a and 17.d). The head groups of the TAB molecules formed the surface of the half micelle (Fig 17.b) and the Br^- ions stayed attached to the surface of the micelle, i.e. they did not diffuse into the surrounding water (Fig 17.c).

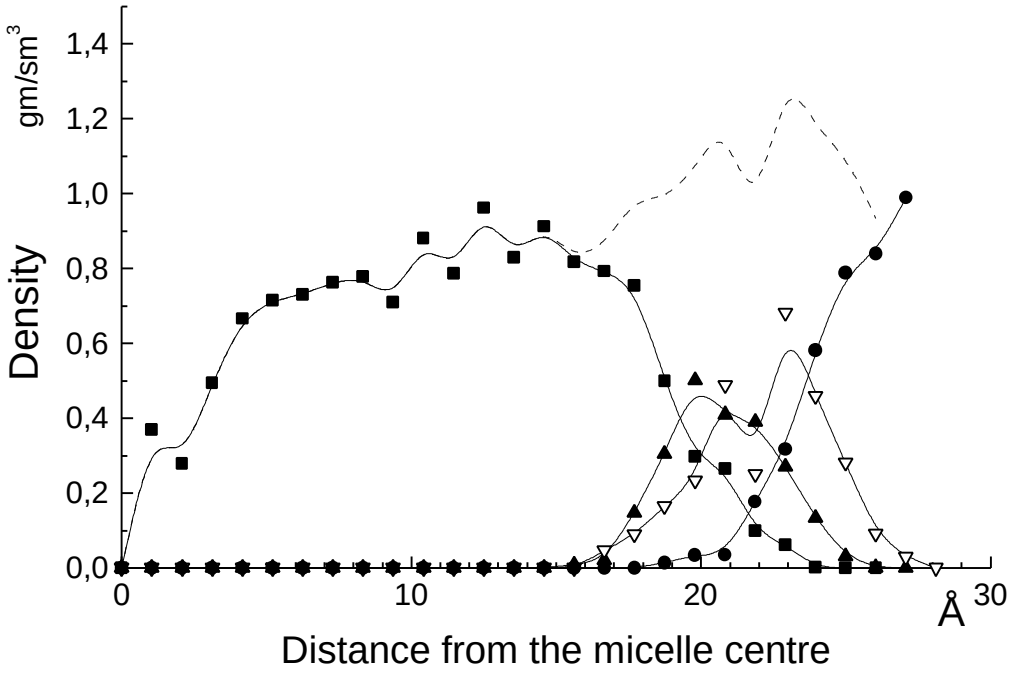

Figure 17. Density distribution functions for a half cylindrical micelle on a gold substrate plotted vs the distance from the geometrical centre of the first adsorbed layer of TAB molecules: a) ¦ - density of the hydrophobic core composed of alkyl chains, b) ? - head groups ($N^{+}\left(CH_3\right)_3$), c) ∇ - Br^{-} ions, d) ? - water and e) --- - total density of the system half cylindrical micelle of TAB molecules on gold substrate and water.

Unlike for the cylindrical micelle, Br^{-} - N^{+} dipoles randomised their positions and dipole moments. In the pair distribution function of the Br^{-} - N^{+} subset (Fig 18) the maxima that characterised inter-dipole distances and the distance between Br^{-} and N^{+} ions at the starting configuration can not be recognised at all. The curve a) presents the pair distribution function of Br^{-} and N^{+} ions for initial configuration. The curve b)-d) presents the pair distribution functions of ions for the MD simulated half cylindrical micelle. In order to obtain pair distribution function for the MD simulated structure, snapshots of the half cylindrical micelle on gold were saved every 0.5 ps and then pair distribution functions for each snapshot were averaged over the last 500 ps of the MD trajectory.

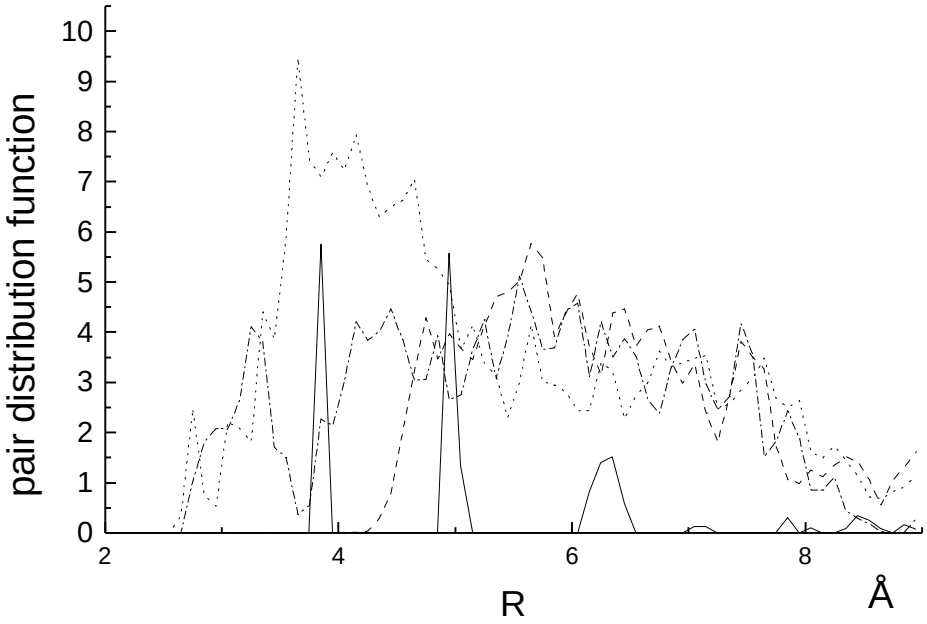

Figure 18. Pair distribution functions of Br^- and N^+ ions in half cylindrical micelle on the gold substrate. a) solid line: initial configuration of the subset of Br^- and N^+ ions (Br - Br, N - N and Br - N pair distribution functions), the first maximum reflects the Br - N distance in the dipole and the second the Br - Br or N - N distance, hence an inter-dipole distance; b) dotted line: Br - N pair distribution function; c) dashed line: N - N pair distribution function; e) dashed-dotted line: Br - Br pair distribution function.

The reason for the randomisation of the Br^- - N^+ dipole positions during 1.6 ns in the half cylindrical micelle on gold in comparison to the cylindrical micelle in water being much higher mobility of the ions in the half cylindrical micelle. The diffusion coefficient for the Br^- and N^+ ions in the half cylindrical micelle is 1.3±0.3 $Å^2$/ns. It was determined from the mean square displacements of the Br^- and N^+ ions: $6Dt = <\left(\bar{r}_i(t) - \bar{r}_i(0)\right)^2>$, where D is the diffusion coefficient and $\bar{r}_i$ are the coordinates of the ions. Here it should be noticed that it is hard to define a diffusion coefficient for the Br^- and N^+ ions in a half cylindrical micelle on the gold substrate, because of the fast motion of the whole half cylindrical micelle. The motion of Br^- and N^+ ions consists of their internal motion in the micelle and motion of the micelle itself. As the bottom of the micelle stayed attached to the gold surface, the micelle motion should not contribute to the diffusion coefficient, but highly influences the mean square displacement of the Br^- and N^+ ions.

An explanation for the high mobility of Br^- and N^+ ions could be that the Br^- ions lost their ionic bonds with the N^+ ions and instead got bound to the gold surface. Since the Br^- ions would have relative freedom along the surface of gold, and since the bulk dipoles are destroyed, the Br^- ion and the charged head group move much faster. In this case the mean square displacements of Br^- and N^+ ions would be independent for the ions close to the surface and the mean

square displacement of all ions also would be quite different. However the comparison of the mean square displacements of Br^- ions and N^+ ions show that they are almost identical. This lead to the conclusion that all ionic bonds are still active and the supposed explanation for the increased diffusion coefficient of Br^- and N^+ ions is not suitable.

The TAB molecules in the layer close to the substrate stayd moreover parallel to the surface of gold. The molecules further away from the surface of gold adopted more random configurations. It is interesting to notice that the hole in the centre of the half micelle was not formed, unlike in the cylindrical micelle in water.

In order to characterise the influence of the gold substrate on the structure of the half cylindrical micelle, the order parameter was calculated. The order parameter for the structures adsorbed on the surfaces was redefined in comparison to the order parameter for a cylindrical micelle in water. It was defined as: $S_m \equiv 0.5(3 \cdot \cos^2(\Theta) - 1)$, where the q is the angle between the C-H bonds and the normal to the substrate surface. The order parameter was calculated as a function on the distance from the substrate surface (Fig 19).

The orientation of the TAB molecules parallel to the surface does not necessarily result in the orientation of the C-H bonds parallel to the surface normal and S_m=1. The TAB molecules are forced by the substrate to orient parallel to the substrate symmetry axes and adopt ideally all trans conformations. The alkyl chains with all trans conformation can lie on the substrate either perpendicular or parallel to the surface which lead to the two possible angles between C-H bond and the substrate normal: roughly 35° and 55°. The initial conformation was constructed with a 35° angle between the C-H bonds and the surface normal resulting in an order parameter of 0.46 for the first layer of TAB molecules. This is the maximum possible order parameter for molecules which are close to the surface and oriented parallel to it. The order parameter S_m was normalised to the maximum order parameter S_{max}=0.46 for gold substrate. The order parameter was averaged by calculating order for structure snapshot every 25 ps from last 400 ps of MD trajectory. The standard deviations from the mean or fluctuations of the order parameter are shown as error bars.

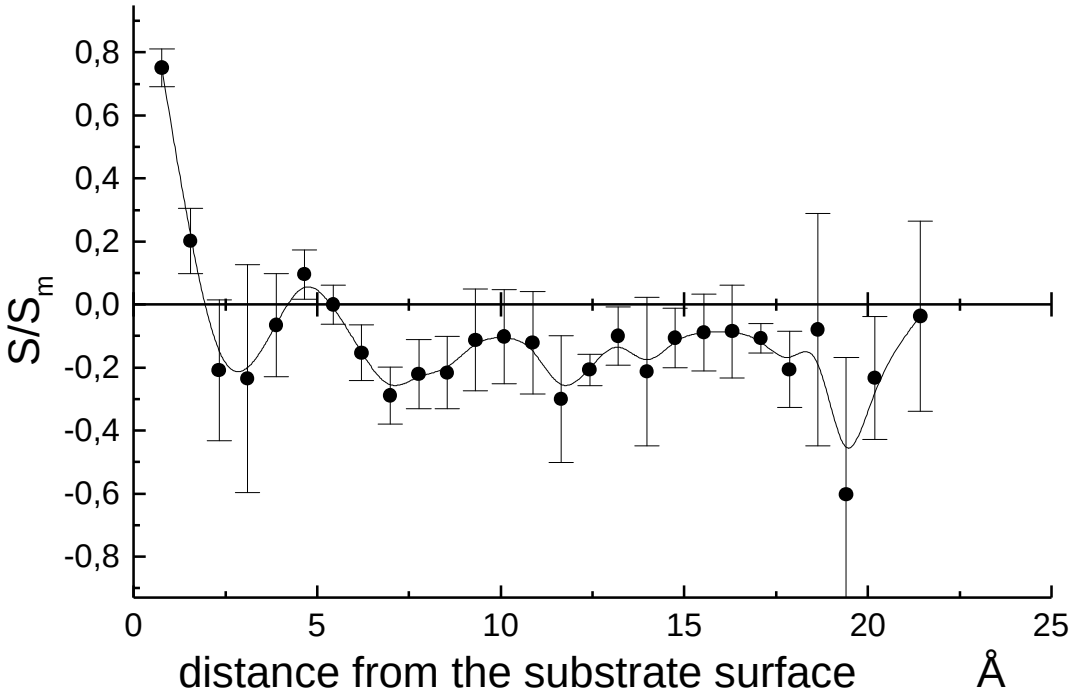

Figure 19. Order parameter S_m/S_{max} for the half cylindrical micelle of TAB molecules on the gold substrate. The error bars denote the standard deviation from the mean. It is more important to display the standard deviation instead of the standard error of the mean determination as the standard deviation defines actual fluctuations in the system. The error of the mean determination is about four times lower than the fluctuations.

A layer of well ordered molecules close to the surface of gold can be detected. High fluctuations of the order parameter at a distance of 2-4 Å away from the gold substrate indicate a spacing between the first layer and the rest of the micelle. It seems possible to define a second layer of alkyl chains at a distance about 5 Å from the gold surface.

The maximum order parameter for the molecules close to the substrate surface is not a strictly defined parameter. Molecules close to the surface did not move far from the initial configuration. That is why the maximum order parameter for the first layer of alkyl chains is determined the starting configuration taking as a reference state. In general, alkyl chains close to the substrate surface may like to adopt conformations different from the starting conformations. That is why the order parameter $S_s \equiv 0.5(3 \cdot \cos^2(\Theta) - 1)$ is introduced, where Θ is defined as the angle between the CH bonds and a substrate symmetry axis. Again, S_s depends on the starting configuration. But in the case of a half cylindrical micelle on hydrophobic substrates it was established in the SFM work that half cylindrical micelles are oriented perpendicular to the substrate symmetry axes and hence the alkyl tails of the TAB molecules are oriented parallel to the symmetry axis. That is why it is

reasonable to characterise the orientation of the alkyl chains with respect to the orientation of the substrate symmetry axes (Fig 20).

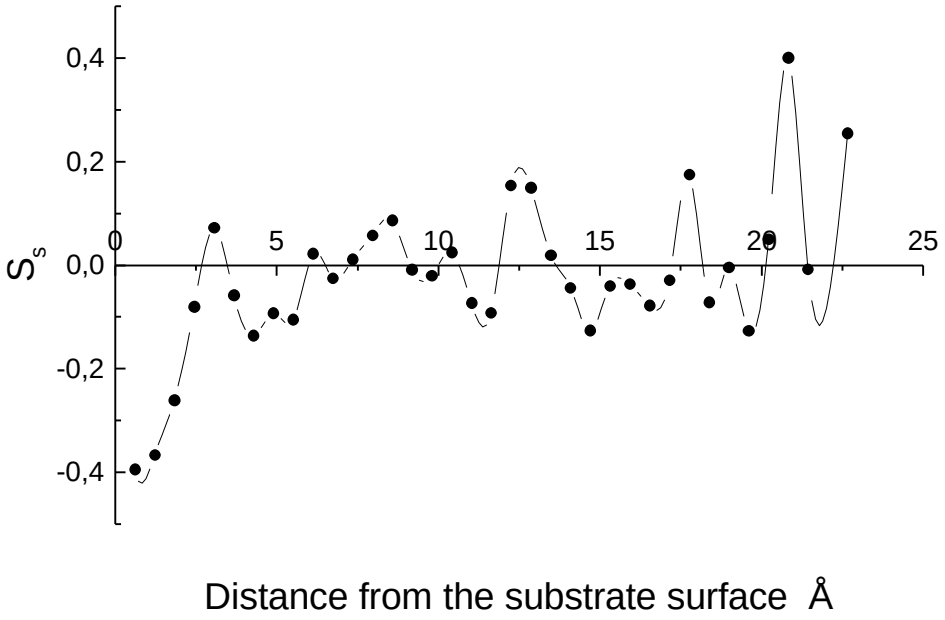

Figure 20. Order parameter S_s for a half cylindrical micelle formed by TAB molecules on a gold substrate.

The order parameter S_s for a chain oriented parallel to a substrate symmetry axis is –0.5. The order parameter for chains close to the substrate surface is –0.4 and 0.8 from the maximum order parameter. This is in excellent agreement with the S_m/S_{max} order parameter for chains close to the substrate surface. It is also important to notice that the dependence of S_s on the distance from the substrate shows the same features as the dependence of S_m/S_{max} on the distance from the substrate.

Half cylindrical micelle on paraffin substrate in water environment

Since the paraffin substrate was kept fixed, two cell dimensions of the half cylindrical micelle on gold did not change during MD simulation. The z cell dimension has changed from the initial value of 51.2 Å to 53 Å. The height of the half cylindrical micelle has changed from its starting value of 22.2 Å to 24.2±0.2 Å. The height was defined as the distance from the micelle atom that is the closest to the paraffin substrate to the micelle atom that is most far from the surface.

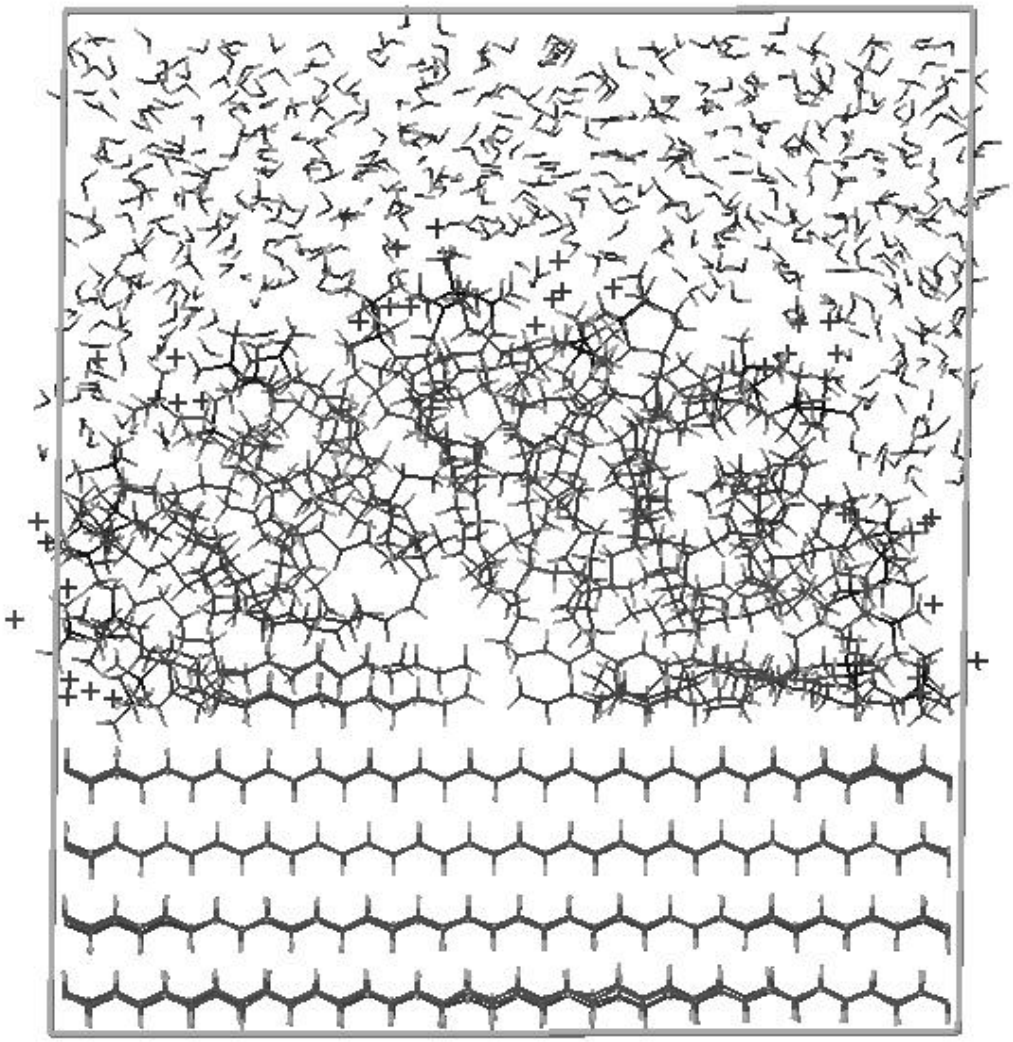

Figure 21. Snapshot of the half cylindrical micelle of TAB molecules on the paraffin substrate after 1.2 ns of MD simulation.

The structure of the half cylindrical micelle on the paraffin substrate is qualitatively the same as the structure of the half cylindrical micelle on the gold substrate. The water did not diffuse into the micelle core composed of hydrophobic alkyl tails (Fig 22 a and 22 d) . The hydrophobic tails did not leave the micelle core either. The Br^- and N^+ ions formed the surface of the half micelle. Br^- ions did not diffuse into the water surrounding (Fig 22 b and 22 c). A hole (vacuum) in the centre of the half micelle was not formed, even though the density of the micelle core is still not homogeneous (Fig 22 a). The density dependencies are plotted vs the distance from the geometrical centre of the first adsorbed layer. The densities were averaged over half spherical slices with width Δr given by the resolution of the curve. When the density of water was calculated it was taken into account that water cover half micelle partially and just parts of half spherical slices filled with water were taken into account. The layer of TAB molecules close to the paraffin surface stayed parallel to the

substrate, while alkyl tails far form the surface adopted more random configurations.

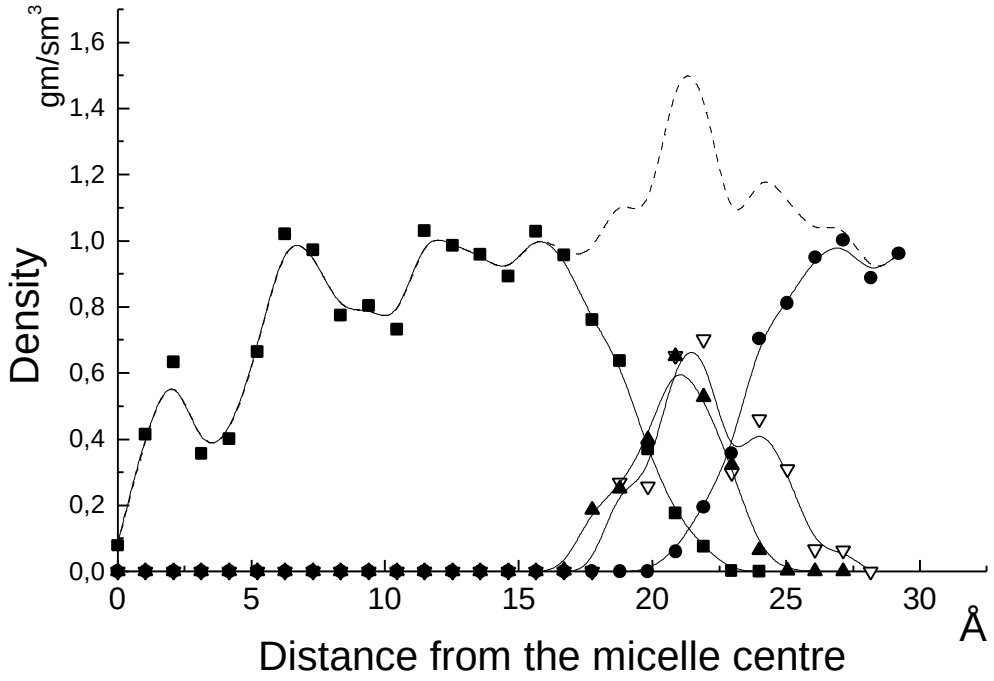

Figure 22. Density distribution functions in half cylindrical micelle on paraffin substrate plotted vs the distance from the geometrical centre of the first adsrobed layer of TAB molecules: a) ¦ - density of the hydrophobic core composed of alkyl chains, b) ? - density of the head groups ($N^{+}\left(CH_3\right)_3$), c) ? - density of the Br^- ions, d) ? - density of the water and e) --- - total density of half cylindrical micelle of TAB molecules on paraffin substrate and water.

The pair distribution function of the subset of Br^- and N^+ ions of the half cylindrical micelle on the paraffin substrate exhibit the same characteristics as the pair distribution function for the half cylindrical micelle on the gold substrate (Fig. 23). The maxima that characterise inter-dipole distances and the distance between Br^- and N^+ ions at the starting configuration are very broadened (Fig 23.b-d).

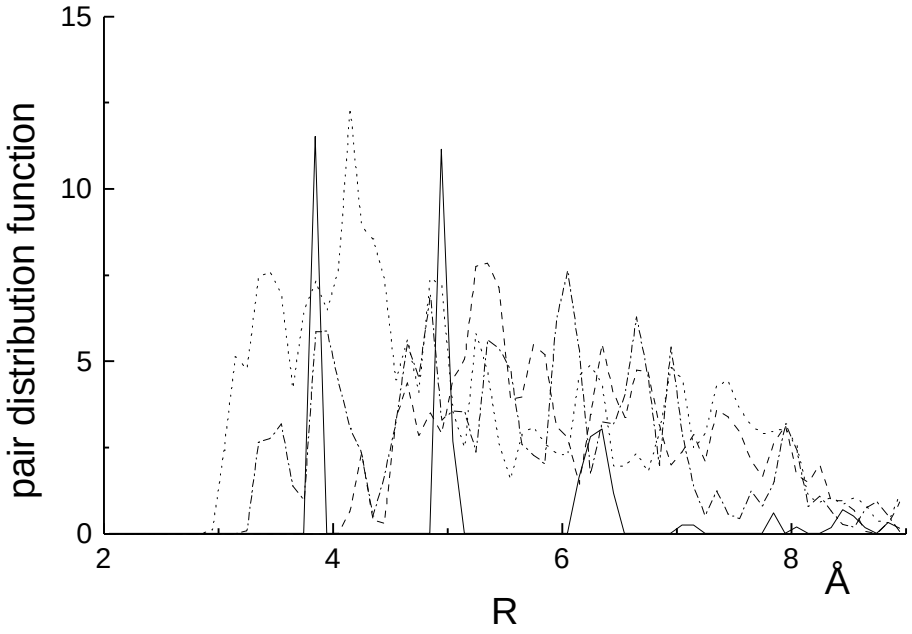

Figure 23. Pair distribution functions of the Br^- and N^+ ions in a half cylindrical micelle on a paraffin substrate. a) solid line: pair distribution function for initial configuration of the subset of Br^- and N^+ ions (Br - Br, N - N and Br - N pair distribution functions); the first maximum is the Br - N distance in the dipol and the second is the Br - Br or N - N distance, hence an inter-dipole distance; b) dotted line: Br - N pair distribution function; c) dashed line: N - N pair distribution function; e) dashed-dotted line: Br - Br pair distribution function.

In order to obtain the pair distribution function for the MD simulated structure, snapshots of the half cylindrical micelle on paraffin were saved every 0.5 ps and then the pair distribution functions for each snapshot were averaged over the last 500 ps of the MD trajectory.

The order parameter for the half cylindrical micelle on the paraffin substrate was defined exactly in the same way as the order parameter for the half cylindrical micelle on the gold substrate:

$$S_m \equiv 0.5(3 \cdot \cos^2(\Theta) - 1)$$

the q was defined as the angle between the C-H bonds and the normal to the substrate surface. The calculation of the maximum order parameter S_{max} for alkyl chains close to the paraffin substrate was based on the assumption that alkyl chains would tend to adopt a crystalline structure of paraffin (Fig 24).

It is interesting to notice that molecules close to the paraffin substrate have the same normalised order parameter as molecules on a gold substrate. However the layer of alkyl chains is smeared out as indicated by the width of the first maximum. The order of the half cylindrical micelle fluctuates highly on the paraffin substrate. The fluctuations of the order parameter are indicated with error bars. From the high fluctuations and the smearing out of the first layer on

the paraffin substrate it is reasonable to conclude that TAB molecules are relatively strongly bound to the gold substrate.

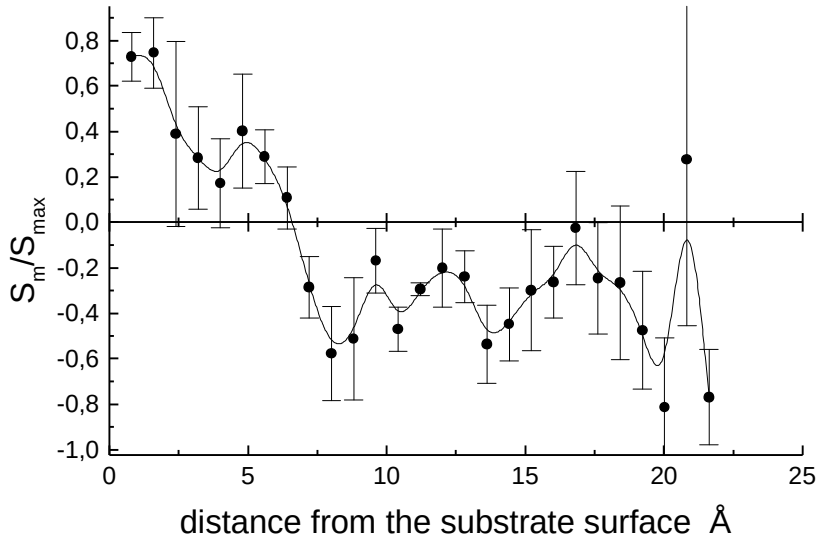

Figure 24. Ration of order parameter to the maximum order parameter for the half cylindrical micelle of TAB molecules on the paraffin substrate. The error bars show the standard deviation from the mean. The error of the mean determination is about four times lower than the deviations.

The order parameter S_s is defined exactly in the same way as for the half cylindrical micelle on the gold substrate (Fig. 25).

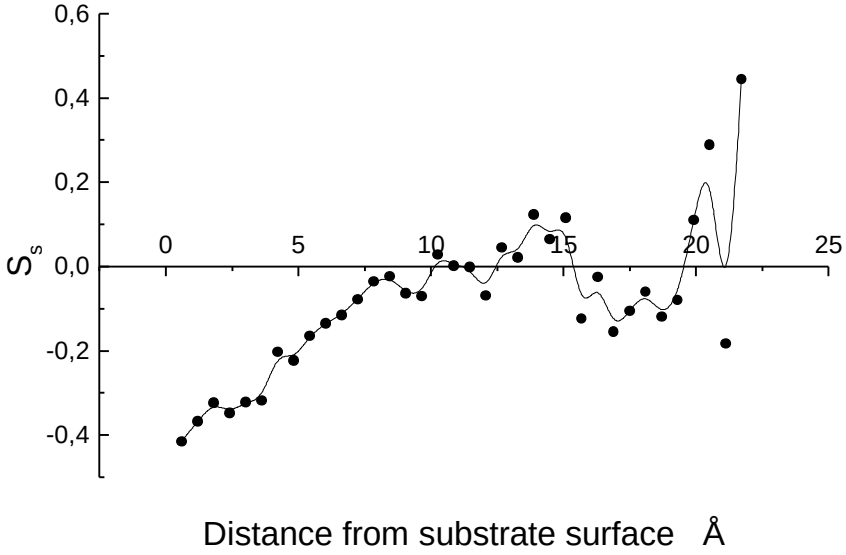

Figure 25. Order parameter S_s for half cylindrical micelle formed by TAB molecules on paraffin substrate.

It should be noticed that the order parameter S_s exhibit in general the same features as the ratio of the order parameter S_m/S_{max}. The order of alkyl chains close to the surface is –0.4 or 0.8 times the maximum order parameter –0.5. The first layer of alkyl chains is smeared out.

Cylindrical micelle on the gold substrate in water environment.

The gold substrate was kept fixed, causing that two cell dimensions of the system of a cylindrical micelle of TAB molecules on a gold substrate did not change during MD simulation. The z cell dimension has changed from the initial value of 69.7 Å to 68.1 Å. The height of the cylindrical micelle changed from 48.6 Å to 48 Å, the width changed from 49.7 Å to 51.4 Å. The height and width were defined by the positions of bromine ions.

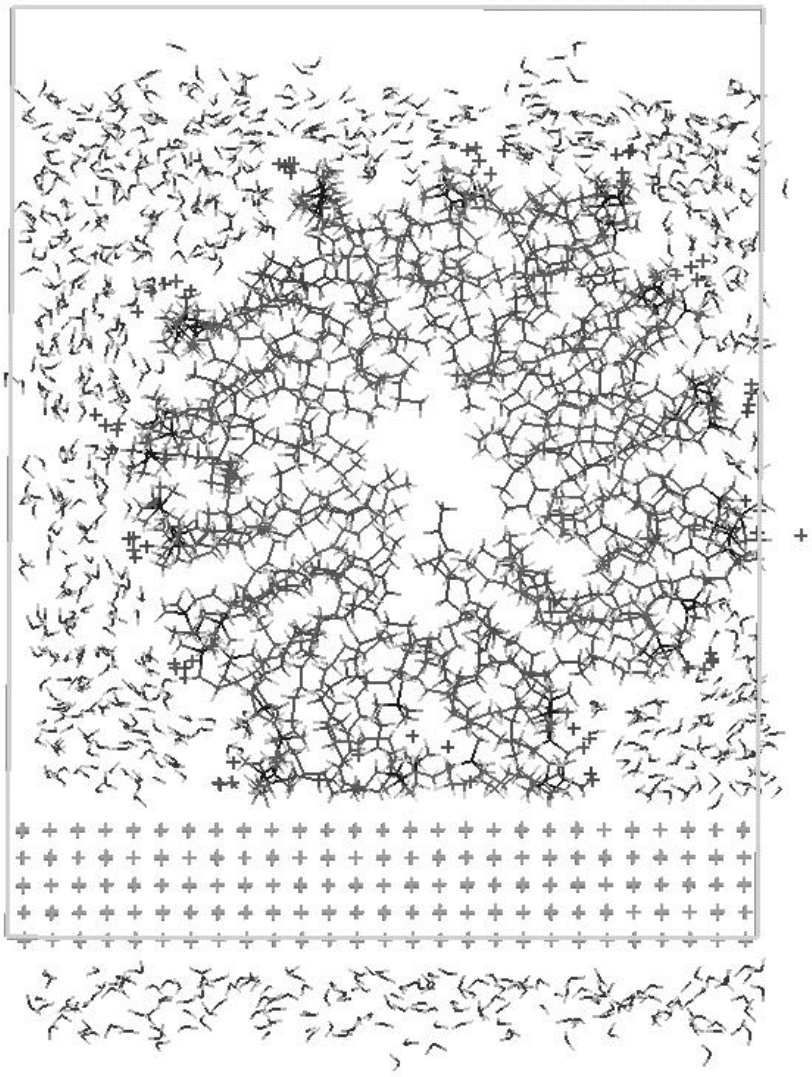

Figure 26. Snapshot of a cylindrical micelle of TAB molecules on a gold substrate in water environment after 1 ns of MD simulation.

The structure of the cylindrical micelle on the gold substrate was qualitatively the same as the structure of a cylindrical micelle in water. The water molecules did not diffuse into the hydrophobic core and the hydrophobic alkyl tails did not leave the micelle core (Fig. 27.a and d). The Br^- and N^+ ions formed the surface of the cylindrical micelle (Fig 27.b and c).

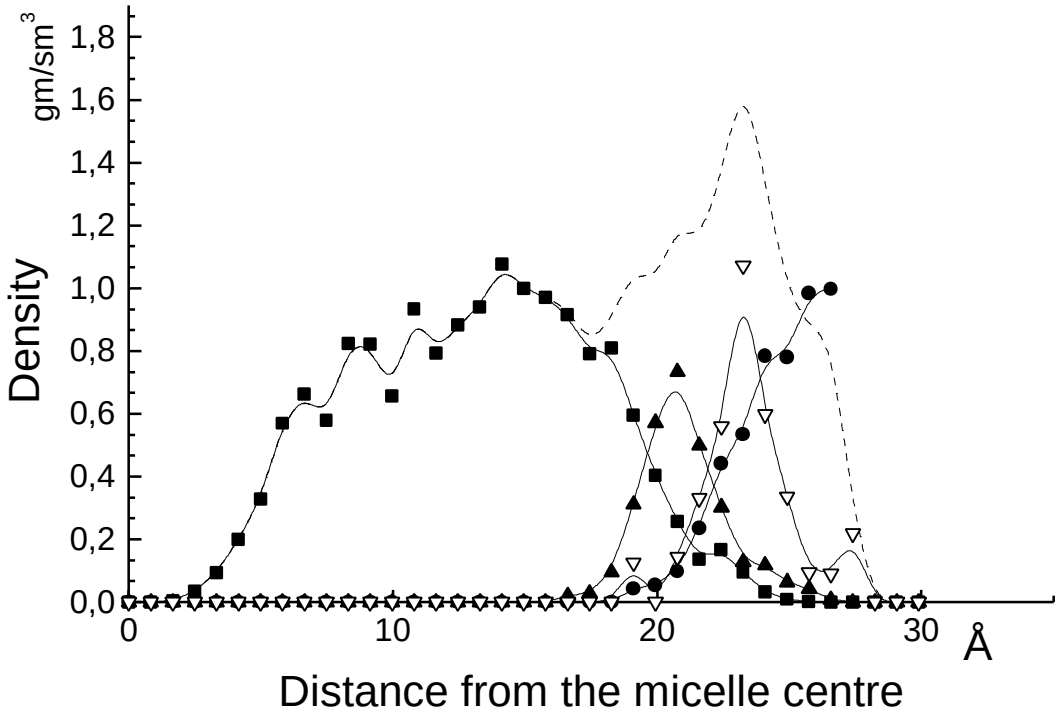

Figure 27. Density distribution functions for cylindrical micelle on a gold substrate plotted vs the distance from the micelle center of mass a) ¦ - density of the hydrophobic core composed of alkyl chains, b) ? - density of the head groups ($N^{+}\left(CH_3\right)_3$), c) ? - density of the Br^- ions, d) ? - density of the water and e) --- - total density of the system half cylindrical micelle of TAB molecules on the paraffin substrate and water.

The pair distribution function of the subset of the Br^- and N^+ ions is presented in Fig. 28. The first maximum on the pair distribution function which characterises the Br^- and N^+ distances still can be recognised (Fig. 28.b), while the N – N pair distribution function that characterise the inter-dipole distance is smeared out (Fig. 28.c).

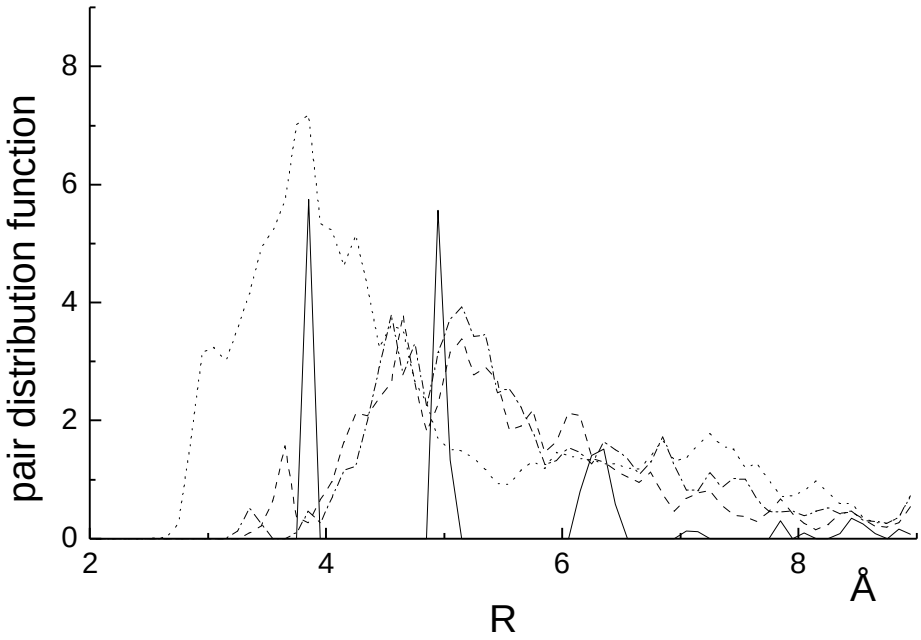

Figure 28. Pair distribution functions of the Br^- and N^+ ions in a cylindrical micelle on a gold substrate. a) solid line - pair distribution function for initial configuration of the subset of Br^- and N^+ ions (Br - Br, N - N and Br - N pair distribution functions), the first maximum is the Br - N distance in the dipol and the second is the Br - Br or N - N distance, hence inter-dipole distance; b) dotted line - Br - N pair distribution function; c) dashed line - N - N pair distribution function; e) dashed-dotted line is the Br - Br pair distribution function.

In order to obtain the pair distribution function for the MD simulated structure, snapshots of the half cylindrical micelle on paraffin were saved every 0.5 ps and then the pair distribution functions for each snapshot were averaged over the last 500 ps of the MD trajectory.

The order parameter (Fig. 29) for the cylindrical micelle on gold substrate was calculated in the same way as the order parameter for the half cylindrical micelle on the gold substrate:

$$S_m \equiv 0.5(3 \cdot \cos(\Theta) - 1)$$

where the q is the angle between the C-H bonds and the normal to the substrate surface (Fig. 29). The error burs show the standard deviations from the mean or fluctuations of order parameter.

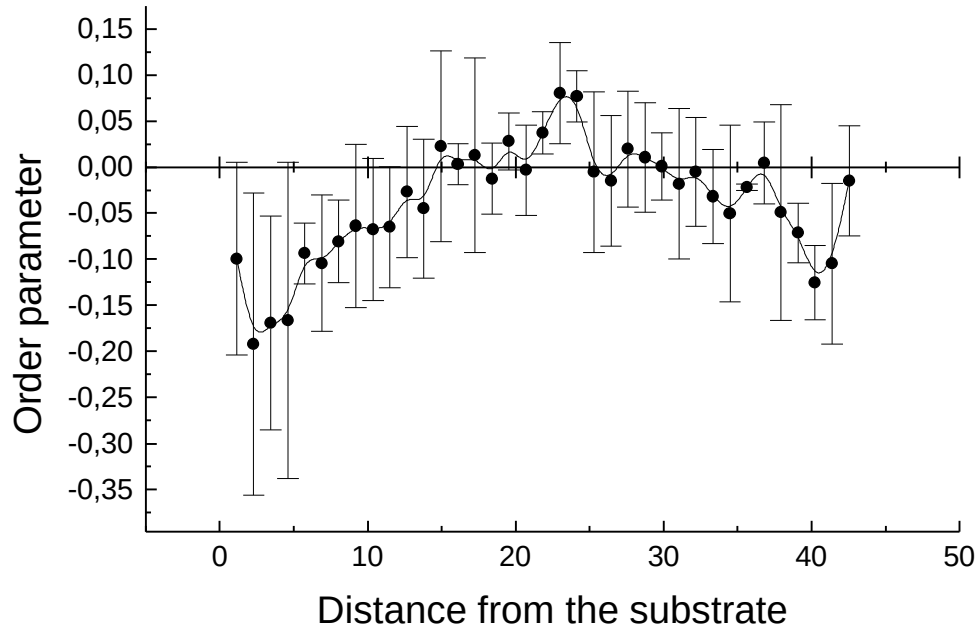

Figure 29. Order parameter for the cylindrical micelle on the gold substrate. The error bars show the standard deviation from the mean.

4.2.4 Discussion

The simulation of the cylindrical micelle of TAB molecules in water was performed in order to establish the reliability of the MD simulation of structures formed by TAB molecules. Therefore first of all the MD simulated structure of the cylindrical micelle in water shell be compared to experiments.

Qualitatively the MD simulated cylindrical micelle is in good agreement with the standard picture of the ionic micelle in aqueous solution, which was described in the introduction. From the density profiles of the alkyl tails, ions and water (Fig. 5) it is clear that the boundary between the hydrophobic core and the water is sharp. Ions and head groups sit between the hydrophobic core and water. From the same figure and from visual inspection it is clear that the alkyl chains are packed into the micelle core and do not mix with the surrounding water. The Br^- ions and the head groups are totally excluded from the micelle core. The overall density of the hydrophobic core is a little higher than the

density of n-alkanes: 0,74 and 0.62-0,7 g/cm ^{3} respectively. The conformational disorder of the alkyl tails requires, however a more quantitative comparison.

As it was described in details in the results section, the comparison of the correlation times from the MD simulation with the correlation times given by NMR experiments is questionable.

While it was not possible to find any measurements of the order parameter for cylindrical micelles, one would expect that the order parameter for a cylindrical micelle would be in-between the order parameter for the lamella case and for the spherical micelle. Indeed, the order parameter for the cylindrical micelle is in good agreement with the experimental order parameters for the spherical micelle and the lamella cases (Fig. 9). The order parameter is defined such that it gives -0.5 when the C-H bonds are oriented parallel to the micelle surface, 1. when the C-H bonds are perpendicular to the micelle surface and 0 for complete disorder. The orientation of the alkyl tails perpendicular to the micelle surface automatically means that the C-H bonds are oriented parallel to the surface, hence the order parameter is -0.5. The orientation of the alkyl tails parallel to the surface does not necessarily result in the orientation of the C-H bonds perpendicular to the surface, but the C-H bonds can be oriented randomly resulting in an order parameter 0. Fig. 9 presents the modulus of the order parameter in order to compare experiments with the MD simulation. Without taking the modulus, the sign of the order parameter is always negative indicating that the alkyl tails are oriented preferably perpendicular to the micelle surface. The parts of alkyl tails that are close to the head groups have a more pronounced orientation perpendicular to the micelle surface, while the ends of the alkyl tails are conformationally almost disordered.

The modified order parameter S_m is more helpful to explain the spatial dependence of the order parameter in the cylindrical micelle (Fig. 10). S_m for the cylindrical micelle in water varies from -0.1 at the edges to slightly positive values in the centre. The negative order parameter at the edges indicates that the alkyl chains have a slightly pronounced orientation perpendicular to the surface close to the surface of the cylindrical micelle. Random orientation of the chains in the plane parallel to the surface results in an order parameter 0, but when the alkyl chains are oriented parallel to the surface and perpendicular to the cylinder symmetry axis the C-H bonds have just two dimensional disorder resulting in an order parameter of 0.25. The slightly positive order parameter at the centre of the curve indicates this (Fig. 10).

It is interesting to compare the pair distribution functions of Br^- and N^+ ions for the cylindrical micelle in water and for different structures adsorbed on the surfaces. The main difference is the well pronounced second maximum on the pair distribution function for the cylindrical micelle and the complete

absence of the second maximum of the pair distribution functions for the adsorbed structures. Let me remind that the second maximum characterises the inter-dipole distances. It was experimentally established that TAB molecules form spherical micelles in water and cylindrical micelle in water with high salt concentration[11]. On the other hand it was also found that dimerized TAB molecules:

$$Br^{-}\left(CH_3\right)_2 N^{+} - (CH_2)_s - N^{+}\left(CH_3\right)_2 Br^{-}$$
$$\qquad\qquad\quad | \qquad\qquad\quad |$$
$$\qquad\quad C_mH_{2m+1} \qquad C_mH_{2m+1}$$

form cylindrical micelles in water for *s* equal to 2-3 and for *s*=4, and larger cylindrical micelles converge to spherical ones[12]. The chemical bond between two head groups forces the head groups to stay at on the given distance from each other. This experimentally established fact allows to suppose that the cylindrical micelle in water with a narrow distribution of inter-dipole distances is a metastable aggregation of TAB molecules.

The most striking f eature of the MD simulated cylindrical micelle in water is the hole in its centre with a radius of roughly 2-3 Å and an inhomogeneous density of the hydrophobic core. A good agreement between the simulated cylindrical micelle and the experimental data does not help to understand whether the formation of the hole is an artefact of the MD simulation or not. One of the explanations could be that the starting structure was too dense and this resulted in the formation of the shell. The simulation of the cylindrical micelle was performed under constant pressure and pressure was controlled anisotropically. This means that the length of the cylinder could change independently of its diameter and this could help to relieve the high density by elongation of the cylinder. On the other hand the process of cylinder elongation could take place on times much longer than several nanoseconds. That is why an additional simulation was performed, where the initial structure contained 7.5 % less molecules within the same dimensions of the cylindrical micelle. The hole of roughly the same size formed as well.

The overall density of the hydrophobic core of the cylindrical micelle of 0.74 g/cm^3 is in-between the density of amorphous polyethylene (0.855 g/cm^3) and the density of liquid n-alkanes 0.62 g/cm^3 for pentane and 0.7 g/cm^3 for octane. The difference in density between liquid n-alkanes and PE is caused by the high concentration of terminal methyl groups in liquid n-alkanes and almost none of them in polyethylene. The hydrophobic alkyl tails in TAB molecules are terminated just at one end by methyl groups; therefore it is reasonable that the overall density of the hydrophobic core is in-between the density of liquid n-alkanes and amorphous PE. The hole in the centre of the micelle does not affect the overall density as the hole of the radius 2 Å in the core with the radius 20 Å takes just 1% of the volume. The surprisingly inhomogeneous density can be

also explained on the basis of the distribution of the terminal methyl groups. They are mostly concentrated in the centre of the micelle, which causes a lowering of the density in the centre of the hydrophobic core. The hydrophobic core density close to the head groups should be comparable to the density of amorphous PE . Because of the high order of alkyl chains close to the head groups, the density of the hydrophobic core could be even higher than the density of amorphous PE. The densities of semi-crystalline PE lies in the range of 0.92-0.97 gm/sm^3 and the density of crystalline PE is close to 1 g/cm^3. As we can see the density of the hydrophobic core is indeed a little higher than the density of amorphous PE in the region with high order and low concentration of terminal methyl groups.

The standard picture of the ionic micel le includes a homogeneous density of the hydrophobic micelle core. It should be noticed that this means obviously a homogeneous density of electron clouds. However the mass density of the hydrophobic core is not necessarily homogeneous. It was established[17] for spherical micelles that most of the terminal methyl groups are concentrated in the centre of the micelle. It is reasonable to expect that most of the terminal methyl groups are also concentrated in the centre of a cylindrical micelle. The volume of the terminal methyl groups is roughly twice the volume of a CH_2 group and that is why a high concentration of terminal methyl groups results in low mass density. The scattering density of the hydrophobic micelle core is also not necessarily homogeneous. As it was already mentioned in the results section, the averaged neutron scattering density of CH_3 group is several times higher than the averaged scattering density of a CH_2 group. The averaged scattering density of an ionic head group of a TAB molecule is almost zero. That is why it is reasonable to expect that the scattering density of a micelle formed by TAB molecules should grow from the edge of the micelle to the micelle centre. In general, the scattering density of a micelle would depend on the chemical formula of the head group; but the scattering density of the hydrophobic core should dominate at the micelle centre. It is accepted that head groups sit outside the hydrophobic core, hence the scattering density of the hydrophobic core should not mix with the scattering density of the head groups. That is why it does not look reasonable to use a model of a homogeneous micelle to fit neutron scattering data from protonated micelles.

Despite of the large number of experimental studies it appears that it was not possible to establish experimentally the existence of the hole. SANS which is the most reliable experimental technique does not provide enough resolution to determine a hole with a radius of several angstroms in the centre of a protonated micelle[13]. On the other hand it was established that micelles formed by TAB and similar amphiphilic molecules may have a hydrophobic core with a diameter larger than the length of fully extended alkyl tails. The suggested explanation of this phenomena was a non spherical form of the micelles.

However the experimental results can be explained as well by the presence of the hole in the micelle centre. Interestingly, it should be possible to determine the inhomogeneous density in the deiteurated micelle centre, but no experimental studies on neutron scattering were found in the literature, where the scattering cross section of a completely deteriorated micelle was determined.

On the other hand it was predicted theoretically that ampiphilic molecules may tend to form micelles with a hole in the centre [15,16]. The highest possible cost of the hole formation with a volume of 54 $Å^3$ was estimated to be 109 cal/mol of chains for a spherical micelle with a hydrophobic core radius of 20.4 Å. A more realistic estimate gives only 45 cal/ mol of chains. The energy cost of hole formation was estimated as work against internal pressure in the micelle to form the hole and loss of Van-der-Waals energy by chains surrounding the hole. Different estimates of internal pressure also lead to different estimates for energy cost of hole formation. The energy of the hole formation is very small indeed: for comparison, the estimated entropic cost of micelle formation is roughly 0.6 kcal/mol of chains and the experimentally measured free energy, which C_{12} chain gain when being transferred from water to bulk n-alkane is approximately 12 kcal/mol. The formation of the hole allows to increase the aggregation number. For example, the formation of a hole with a volume of 54 $Å^3$ in a micelle with a radius of 20.4 Å allows to increase the aggregation number by 30%. On the other hand it was also argued that even small deviations away from a perfect sphere would eliminate a small hole.

The deviation from the spherical shape increases the surface area of the micelle which is energetically unfavourable. On the other hand a deviation from the spherical shape eliminates the hole in the centre of the micelle and hence gains energy equal to the cost of hole formation. As the aggregation number of the micelle does not change when it changes its form the energy cost of deviation from the spherical form is equal to the surface change multiplied by the tension of the water/n-alkane interface, i.e. 50 $mN \cdot m^{-1}$. A spherical micelle with a radius of 22 Å and a hole in its centre with a radius of 2 Å should converge to an ellipsoid with main axes equal to 20, 23.1 and 23.1 Å in order to eliminate the hole. The energy cost of the increased surface area is 23 cal/ mol of chains. Taking into account the estimated energy of the hole formation, the elliptical micelle is energetically more favourable by 2-8 kcal/mol or 3.4-13.6 kT. The estimated energy difference between a spherical micelle with the hole in its centre and an elliptical micelle is very small indeed. For example the difference between gauche and trans conformations in alkyl chains is of the order of 1 kT. Another example: during 1 ps of MD simulation of a cylindrical micelle in water the potential energy varied more than by 100 kcal/mol and the total potential energy of the system cylindrical micelle of TAB molecules in water environment was minus $2x10^5$ kcal/mol.

It should be emphasised again that estimated energy difference between a micelle with a hole and an elliptical micelle is very low. It was assumed that the elimination of the hole does not change the entropy of the micelle, which is obviously wrong. When the micelle adopts an elliptical form the alkyl chains should also adopt different conformations and this should lead to additional free energy cost. This means that a micelle with a hole could be even energetically more favourable. Let us assume that the estimated energies are close to reality. Then amphiphilic aggregates would adopt different shapes between spherical with hole and elliptical with probabilities given by the Boltzman distribution:

$$\frac{\exp(-(E(l)-E_{elips})/kT)}{\int_{elips}^{sphere}\left(\exp(-(E(l)-E_{elips})/kT\right)dl}$$

where λ denotes the path between spherical and elliptical forms. The estimate of energy cost of hole formation was performed for the spherical micelle, but one would expect that the mechanism of the hole formation in a cylindrical micelle is the same.

It is interesting to notice that when a micelles adopts different shapes from elliptical to spherical with a hole in the micelle centre and the probabilities are given by a Boltzman distribution. On average a micelle would have an inhomogeneous density in its centre.

The simulations of a cylindrical micelle and a half cylindrical micelle on gold suffers from the fact that the metallic properties of gold are not taken into account. The TAB molecules interact with the gold atoms only via Lennard-Jones potentials since the gold atoms are completely uncharged. In classical physics it is well known that charge close to the metal surface would cause the redistribution of the free electrons which would lead to the appearance of an effective mirror charge. If we leave this uncertainty it is interesting to compare how substrates with different Lennard-Jones interaction with TAB molecules would affect the adsorbed structures. For instance the Lennard-Jones interaction between gold and carbon atoms is much higher than between carbon and carbon.

The structure of a half cylindrical micelle on gold after MD simulation still exhibit a very well ordered first layer (Fig 19-20). The layer of TAB molecules close to the substrate is separated from the rest of the micelle by several angstroms with relatively low density, which causes high fluctuation of the order parameter in this part. In a half cylindrical micelle on paraffin (Fig 24-25) it is also clearly possible to define a layer of TAB molecules oriented by the paraffin substrate. But in comparison to the gold substrate the order fluctuations are higher and the first layer is smeared out indicating that the half cylindrical micelle is better bound to the gold substrate. It is interesting to notice that the

order for molecules close to the substrate surface is the same for paraffin and gold substrates.

The order parameter S_m for a cylindrical micelle on a gold substrate (Fig. 29) clearly indicates that these structure is not yet equilibrated. The deviation from the mean of the order parameter for molecules close to the surface is very high indicating that these molecules still have to adopt their equilibrium conformations. Because of the high fluctuations it is questionable to conclude a general trend in the order parameter. A lower order parameter for the molecules close to the substrate surface indicates that the molecules close to the surface tend to orient themselves perpendicular to the surface, which is consistent with the flattening of the cylindrical micelle toward the surface and with neutron reflection experiments[10], where it was shown that aggregates of TAB molecules on the substrate silica are in good agreement with the model of a bilayer.

4.3 Conclusions

MD simulations of a cylindrical micelle formed by TAB molecules in water environment, a half cylindrical micelle of TAB molecules on gold and paraffin substrates and a cylindrical micelle formed by TAB molecules on a gold substrate were performed. A good qualitative and quantitative agreement between the simulated cylindrical micelle in water and corresponding experimental results was found, except for the non-homogeneous density of the hydrophobic core. The simulated cylindrical micelle was qualitatively in good agreement with the standard picture of an ionic spherical micelle. Good quantitative agreement was found between experimentally established and MD simulated structure regarding order parameter and distribution of terminal methyl groups. It was difficult to compare relaxation times given by NMR experiments and calculated from MD trajectories. As it was argued it is not possible to give just a single relaxation time for a given carbon in the alkyl chain, rather spectra of relaxation times.

The MD simulated cylindrical micell e formes a hole (vacuum) in its centre and in addition the density of the hydrophobic core composed of alkyl chains was not homogeneous. The proposed explanation of the inhomogeneous density of the micelle core was related to the distribution of the terminal methyl groups in the micelle centre. The explanation for the hole formation in the centre of the micelle was based on the work of Gruen[15,16]. It was argued that the formation of a small hole in the micelle centre lead to sufficient increasing of micelle aggregation number, which could be energetically favourable The small deviation from the spherical form that may eliminate the hole also increases the micelle surface, hence costs additional energy.

The influence of gold and paraffin substrates on the structure of half cylindrical micelles was characterised. The ability of metals to form mirror charges was not included in the model of gold. The gold was simulated just a crystalline material formed by gold uncharged atoms. Since the model of the gold substrate used in this investigation does not include free electrons, gold and paraffin substrates were compared as two substrates with different Lennard-Jones interaction with adsorbed structures. It was found that the gold substrate induces higher order in adsorbed half cylindrical micelle than a paraffin substrate.

The time evolution of a cylindrical micelle on a gold substrate was simulated. It was found that the cylindrical micelle started to flatten on the gold substrate and the alkyl chains close to the substrate tend to orient perpendicular to the substrate plane. The flattening and the orientation of alkyl chains perpendicular to the substrate was compared favourably to the experimental established flattening of the structures formed by TAB molecules on silica.

4.4 Literature

1. Murray, R. W., Ed. Molecular Design of Electrode Surfaces; John Wiley & Sons: New York, 1992.

2. Srinivas Manne and Hermann Gaub, Science, **270,** (1995) 1480-1482.

3. Milton J. Rosen, Surfactants and Interfacial Phenomena, John Wiley & Sons: New York.

4. Harald Walderhaug, Olle Södermann and Peter Stilbs, J. Phys. Chem. **88**, (1984), 1655-1662.

5. Schatzberg P, J. Phys. Chem. **67**, (1963) 776-779.

6. Halle B, Carlström G, J. Phys. Chem. **85,** (1981), 847.

7. Wennerström H, Lindman B, J. Phys. Chem. **83,** (1979), 2931.

8. J. Israelachvili, Intermolecular and Surface forces, Second Edition, Academic Press, London.

9. M. Jaschke, H.J. Butt, H.E. Gaub and S. Manne, Langmuir, **13,** (1997) 1381-1384.

10. Giovanna Fragneto and Robert K. Thomas, Adrian R. Rennie, Jeffrey Penfold, Langmuir **12,** (1996), 6036-6043.

11. S. Ozehi, S.J. Ikeda, J. Colloid Interface Sci., **87,** (1982), 424.

12. R. Zana, Y. Talmon Nature, **362,** (1993), 228.

13. Jan Skov Pedersen and Peter Schurtenberger, J. Appl. Cryst., **29,** (1996), 646-661.

14. Jan Skov Pedersen, Stefan U. Egelhaaf, Peter Schurtenberger, J. Phys. Chem. **99,** (1995), 1299-1305.

15. D.W.R Gruen, Progr. Colloid and Polymer Sci. **70**, (1985), 6-16.

16. D.W.R. Gruen and E.H.B. de Lacey, in: Surfactants in Solution, **Vol 1**, (1984), 279-307.

17. D. Bendedouch, Sow-Hsin Chen and W.C. Koehler, J. Phys. Chem, **87**, (1983), 153-159.

18. S. M. Gruen, J. Phys. Chem, **93,** (1989), 7562-7570

5. Summary

The key-parts of the work are:

(1) **Molecular dynamic (MD) simulation of the Polyethylene (PE) – isotactic Polypropylene (iPP) interfaces.**

(2) **MD simulation of the cylindrical micelle formed by tetradecyltrimethylammonium bromid (TAB) molecules in water environment.**

(3) **Influence of the substrate on the structure of the half-cylindrical and cylindrical micelles formed by TAB molecules.**

(1) The starting structures of the interfaces were chosen close to those suggested in the experiments on the epitaxial crystallisation of PE on iPP and several reference interfaces. While it is possible in the experiment to establish the orientation of the crystallographic axes of PE and iPP at the interface, it is not possible to establish whether PE crystallises preferably on the iPP surface with high or low density of methyl groups. In comparing adhesion energies computed from MD simulation of different interfaces it was found that the lowest adhesion energy corresponds to the interface with the low concentration of methyl groups on the iPP surface. Hence it was suggested that PE crystallises on the iPP surface with low density of methyl groups.

It was also found that the entire layer of orthorhombic crystalline PE in the simulated system with the strongest adhesion has transformed to the monoclinic form. This phenomena was critically discussed. It was argued that while the transformation from the monoclinic to the orthorhombic form could be due to some general shortcoming of the MD simulation, it is also possible that indeed the thin layer of PE close to the iPP surface transformed to monoclinic form, while bulk PE is still in the orthorhombic crystalline form.

(2) The purpose of the simulation of the cylindrical micelle in water was first to check the reliability of the simulation because there are many experimental results for the cylindrical micelles. Second, up to now there was not any detailed computer simulation of large spherical or cylindrical micelles. The advantage of the simulation of the cylindrical micelle over the simulation of the spherical micelle is that applying periodic boundary conditions allows to simulate virtually infinite cylindrical micelles by simulation of a rather small part of the cylindrical micelle, while for a spherical micelle the entire micelle should be simulated.

A good agreement between experimental results and the MD simulated cylindrical micelle was found. Nevertheless the MD simulated cylindrical micelle does not exhibit a homogeneous micelle core density, while the commonly accepted point of view is a homogeneous liquid like micelle core. It was argued that the micelle core could be considered just in a first approach as

homogeneous. The order in the micelle core is induced by the fact that the head groups sit on the micelle surface. The non-uniform distribution of the terminal methyl groups produces the non-homogeneous density of the micelle core.

(3) Half cylindrical micelles formed by TAB molecules on the gold and paraffin substrates were simulated. It was found that the gold substrate induces much higher order in the half cylindrical micelle than the paraffin substrate.

Also a cylindrical micelle formed by TAB molecules on a gold substrate was simulated. It was found that the cylindrical micelle started to flatten on the gold substrate and the alkyl chains tended to orient perpendicular to the substrate plane. The flattening and the reorientation of the alkyl chains was compared favourably to experimentally established flattening of the structures formed by TAB molecules on silica.

Zusammenfassung:

Die Schwerpunkte der Arbeit sind:

(1) **MD Simulation der Grenzfläche zwischen Polyethylen (PE) und isotaktischem Polypropylen (iPP)**

(2) **MD Simulation einer zylindrischen Mizelle aus Tetradecyltrimethylammoniumbromid (TAB) in einer wässerigen Umgebung.**

(3) **Der Einfluß des Substrats auf die Struktur einer halbzylindrischen und einer zylindrischen Mizelle aus TAB – Molekülen.**

(1) Die durch Experimente zur epitaxialen Kristallisation von PE auf iPP vorgeschlagenen Grenzflächenstrukturen sowie andere Referenzgrenzflächen waren Ausgangspunkt für die MD – Simulation. Während es experimentell gelingt, die kristallographischen Achsen von PE und iPP an ihrer Grenzfläche zu bestimmen, ist es nicht möglich festzustellen, ob PE an dieser Grenzfläche bevorzugt mit hoher oder geringer Methylgruppendichte kristallisiert. Ein Vergleich der durch MD – Simulation bestimmten Adhäsionsenergien verschiedener Grenzflächen ergibt, daß die niedrigste Energie derjenigen Grenzfläche zugeordnet werden kann, die die niedrigste Konzentration von Methylgruppen auf der iPP – Oberfläche aufweist. Daher ist zu vermuten, daß PE auf der iPP Oberfläche mit geringer Methylgruppendichte kristallisiert.

Ebenso konnte herausgestellt werden, daß sich die gesamte orthorombische Schicht kristallinen PEs, die im simulierten System die stärkste Adhäsion aufweist, in die monokline Form umwandelt. Dieses Phänomen wurde kritisch diskutiert. Es wurde argumentiert, daß die Transformation von der monoklinen Form hin zur orthorombischen aufgrund gewisser Fehler in der MD

– Simulation vollzogen wird und dies möglicherweise lediglich einen Artefakt darstellt. Denkbar ist aber auch, daß sich tatsächlich eine dünne Lage PE unmittelbar an der iPP – Oberfläche in die monokline Form umwandelt, während PE sonst aber bevorzugt in der orthorombischen Form vorliegt.

(2) Das Ziel der Simulation einer zylindrischen Mizelle in Wasser bestand zunächst darin, die Zuverlässigkeit der Simulationsergebnisse zu überprüfen. Hierzu konnte auf experimentelle Arbeiten zurückgegriffen werden. Außerdem gibt es bis heute keine detaillierten Ergebnisse von Computersimulationen für große kugelförmige oder zylindrische Mizellen. Der Vorteil der Simulation einer zylindrischen Mizelle gegenüber der einer kugelförmigen liegt in der Möglichkeit der Anwendung periodischer Randbedingungen. Folglich muß für die zylindrische Mizelle lediglich ein kleiner Ausschnitt simuliert werden, das System wird aber trotzdem als virtuell unendlich betrachtet.

Zwischen Experiment und simulierter zylindrischer Mizelle wurde eine gute Übereinstimmung gefunden. Ungeachtet dessen weist die simulierte Mizelle keine homogene Dichte im Kern auf. Die allgemein herrschende Auffassung geht hingegen von einem homogenen, flüssigkeitsähnlichen Mizellkern aus. Es wird argumentiert, daß der Mizellkern ohnehin nur in erster Näherung als homogen betrachtet werden kann. Die Ordnung des Mizellkerns wird dadurch bestimmt, daß die Kopfgruppen an der Mizelloberfläche sitzen. Die nicht uniforme Verteilung der terminalen Methylgruppen wird hierbei für die nichthomogene Dichte im Kern verantwortlich sein.

(3) Hier wurden halbzylindrische Mizellen aus TAB – Molekülen auf einer Goldoberfläche simuliert. Es konnte gezeigt werden, daß die Goldoberfläche eine wesentlich höhere Ordnung in der halbzylindrischen Mizelle hervorruft als das Paraffinsubstrat. Ebenso wurde eine zylindrische Mizelle aus TAB –

Molekülen auf einem Goldsubstrat mit Hilfe der MD – Simulation studiert. Hierbei flachte die zylindrische Mizelle ab, wobei die Alkylketten zu einer senkrechten Ausrichtung bezüglich der Substratebene tendierten. Dieses Abflachen und die Reorientierung der Alkylketten wurde mit entsprechenden Experimenten auf Silizium verglichen, wobei auch hier eine gute Übereinstimmung gefunden werden konnte.

Lebenslauf

Persönliche Angaben:

Name:	Severin
Vorname:	Nikolai
Anschrift:	Schulstr. 57 14169 Berlin Tel.: (030) 46606788
Geburtsdatum:	04.01.1971
Geburtsdatum:	Moskau (Rußland)
Familienstand:	verheiratet
Staatsangehörigkeit:	russisch

Schulbildung:

1977-1987	Allgemeine Schule

Studium:

1987-1993	Studium der Physik an der Moskauer Lomonosow Universitäat
01/93	Abschluß: Diplom in Physik
1993-1995	Wissenschaftlicher Mitarbeiter an der Moskauer Lomonosow Universität
1995-1998	Doktorand
1998-	Wissenschaftlicher Mitarbeiter an der Humboldt Universität

Berlin, den 1.12.1998

Selbständigkeitserklärung

Hiermit versichere ich, die vorliegende Arbeit selbständig angefertigt zu haben und keine weiteren als die Hilfsmittel verwendet zu haben.